



UNIVERSIDADE DE SÃO PAULO

FACULDADE DE CIÊNCIAS FARMACÊUTICAS DE RIBEIRÃO PRETO

Controle Redox em *Neospora caninum*: investigação de enzimas do sistema antioxidante

Jade Cabestre Venancio Brochi

**Ribeirão Preto
2021**

UNIVERSIDADE DE SÃO PAULO
FACULDADE DE CIÊNCIAS FARMACÊUTICAS DE RIBEIRÃO PRETO

Controle Redox em *Neospora caninum*: investigação de enzimas do sistema antioxidante

Tese de Doutorado apresentada ao Programa de Pós-Graduação em Biociências e Biotecnologia da Faculdade de Ciências Farmacêuticas de Ribeirão Preto para obtenção do Título de Doutor em Ciências

Área de Concentração: Bioagentes e Biotecnologia Aplicados à Farmácia.

Orientador(a): Prof^a Dra. Ana Patrícia Yatsuda Natsui

Orientado(a): Jade Cabestre Venancio Brochi

Versão corrigida da Tese de Doutorado apresentada ao Programa de Pós-graduação em Biociências e Biotecnologia em 21/02/2022. A versão original encontra-se disponível na Faculdade de Ciências Farmacêuticas de Ribeirão Preto/USP.

Ribeirão Preto

2021

FICHA CATALOGRÁFICA

AUTORIZO A REPRODUÇÃO E DIVULGAÇÃO TOTAL OU PARCIAL DESTE TRABALHO, POR QUALQUER MEIO CONVENCIONAL OU ELETRÔNICO, PARA FINS DE ESTUDO E PESQUISA, DESDE QUE CITADA A FONTE.

Venancio-Brochi, Jade Cabestre

Controle Redox em *Neospora caninum*: investigação de enzimas do sistema antioxidante. Ribeirão Preto, 2021.

148p. : il. ; 30cm.

Tese de Doutorado, apresentada à Faculdade de Ciências Farmacêuticas de Ribeirão Preto, Universidade de São Paulo para obtenção do título de doutor em Ciências, Área de concentração: Bioagentes e Biotecnologia Aplicados à Farmácia.

Orientador: Yatsuda, Ana Patrícia

1. *Neospora caninum*. 2. Apicomplexa. 3. Protozoário. 4. Estresse Oxidativo. 5. Peroxirredoxina. 6. Glutathione redutase.

FOLHA DE APROVAÇÃO

Candidato: Jade Cabestre Venancio Brochi

Controle Redox em *Neospora caninum*: investigação de enzimas do sistema antioxidante.

Tese de Doutorado apresentada ao Programa de Pós-Graduação em Biociências e Biotecnologia da Faculdade de Ciências Farmacêuticas de Ribeirão Preto para obtenção do Título de Doutor em Ciências

Área de Concentração: Bioagentes e Biotecnologia Aplicados à Farmácia.

Orientador(a): Prof^a Dra. Ana Patrícia Yatsuda

Aprovado em:

Banca Examinadora

Prof. Dr. _____

Instituição: _____ Assinatura: _____

Prof. Dr. _____

Instituição: _____ Assinatura: _____

Prof. Dr. _____

Instituição: _____ Assinatura: _____

Prof. Dr. _____

Instituição: _____ Assinatura: _____

Dedico este trabalho aos meus pais, Maria
Cristina Cabestre e Jair da Luz Venancio;
ao meu amado esposo Matheus Garcia
Brochi; e à minha tia, Luciane Venancio.

AGRADECIMENTOS

A Deus, por me alcançar com sua graça e amor incondicional. A Ele sou grata por cada experimento realizado, relatório, projeto, bolsa, oportunidades, pelas alegrias e ensinamentos e pelas pessoas que passaram pela minha vida ao longo desse doutorado.

À minha orientadora, Ana Patrícia Yatsuda, agradeço imensamente por me receber em seu grupo de pesquisa de forma não planejada, rs, pela generosidade, pelo tempo, disponibilidade, apoio e incentivo constantes mesmo quando as condições não eram muito favoráveis; por sempre apontar os melhores caminhos e por facilitar tantos processos ao longo do doutorado!

Aos colaboradores do grupo de pesquisa do Laboratório de Parasitologia Molecular que ajudaram ativamente na elaboração e nos experimentos dessa tese: Ao Luís Miguel Pereira (Buda), pela paciência, por dividir tanto conhecimento e por colaborar com suas ideias mirabolantes! Luciana Baroni, pela paciência constante, criatividade e por me mostrar tantos truques para realizar os experimentos! Ao Péricles Gama Abreu-Filho, pelas parcerias científicas, pelas inúmeras ajudas e por trazer alegria ao nosso laboratório! À Maraísa Palhão Verri, pela amizade, almoços, pelas células, soluções e placas (hehe) e por sempre me socorrer no laboratório. À Letícia Pollo de Oliveira, não só pela tese de doutorado que me auxiliou em vários experimentos, como também pelas excelentes e divertidas aulas de inglês!! Foi muito bom passar esses anos com vocês!

À Prof^a Cristina Nonato, por compartilhar sua experiência e conhecimento colaborando com caracterização da NcGR. Ao Felipe Calil, por me ajudar com precisão na padronização e análise dos ensaios enzimáticos. À Olivia Teixeira, por toda dedicação e persistência na realização dos experimentos envolvendo a NcGR.

Ao Prof^o Gilberto Úbida Leite Braga pela parceria e por fornecer os compostos fenotiazínicos.

A todos meus familiares que estiveram na torcida por mim. Em especial: aos meus pais, Maria Cristina Cabestre e Jair da Luz Venancio, pelos sacrifícios, encorajamento e todas as oportunidades que me deram de buscar uma boa formação mesmo em meio às dificuldades financeiras e familiares. Ao meu amado esposo, Matheus Garcia Brochi, por me fazer feliz, cuidar de mim e sempre mostrar o valor da eternidade em meio ao dia a dia, me trazendo equilíbrio para lidar com as dificuldades. Aos meus sogros Marco e Flávia Brochi, por todo suporte e carinho. À minha tia Luciane Venancio, por demonstrar amor e carinho sempre.

À Igreja Bíblica dos Irmãos pelas orações por essa tese e pela calorosa comunhão que ajudaram a atravessar esse período. Ao pastor Rafael Simões e Aline Simões pelo aconselhamento ao longo desses anos.

Aos professores e funcionários do programa de Pós-graduação em Biociências e Biotecnologia! Em especial, a Ana Lúcia Turatti e Rosana Florêncio, pela excelente assistência!

À Fundação de Amparo à Pesquisa do Estado de São Paulo (FAPESP) pela bolsa de doutorado (nº de Processo: 2019/05758-5).

O presente trabalho foi realizado com apoio da Coordenação de Aperfeiçoamento de Pessoal de Nível Superior - Brasil (CAPES) - Código de Financiamento 001.

RESUMO

VENANCIO-BROCHI, J. C. **Controle redox em *Neospora caninum*: investigação de enzimas do sistema antioxidante**. 2021. 148 p. Tese (Doutorado). Faculdade de Ciências Farmacêuticas de Ribeirão Preto- Universidade de São Paulo, Ribeirão Preto, 2021.

Neospora caninum é um parasita Apicomplexa e agente etiológico da neosporose, uma doença que resulta em sintomas neurológicos em cachorros e abortos em gado bovino. A neosporose está disseminada em todo o mundo e não possui tratamento eficaz aprovado. A sobrevivência e replicação de *N. caninum* dependem de sua capacidade de defesa do estresse oxidativo dentro da célula hospedeira. Nesse sentido, a elucidação de novas moléculas e mecanismos relacionados ao controle redox de *N. caninum* pode contribuir com o desenvolvimento de tratamentos para a neosporose. Portanto, neste trabalho descrevemos duas enzimas do Sistema redox: Peroxirredoxina (NcPrx, Capítulo 1) e Glutaciona redutase (NcGR, Capítulo 2), bem como investigamos os efeitos das formas recombinantes de NcGR (rNcGR) e NcPrx (rNcPrx), e do H₂O₂ na invasão e proliferação do taquizoíta na célula Vero (Capítulo 3). As sequências de aminoácidos de NcPrx e NcGR apresentaram alta identidade e similaridade comparadas com os representantes homólogos do filo Apicomplexa. rNcPrx e rNcGR foram clonadas e expressas em *Escherichia coli* (BL21) com massa molecular predita (22 kDa e 52kDa, respectivamente) e a identidade das formas monoméricas e diméricas foram confirmadas por espectrometria de massas. A análise de imunofluorescência revelou que NcPrx e NcGR estão localizadas no citosol do taquizoíta. NcPrx e NcGR nativas e recombinantes foram detectadas por ELISA e western blot, utilizando os soros policlonais anti-rNcPrx e anti-rNcGR. rNcPrx apresentou atividade peroxidase e antioxidante *in vitro*. Além disso, H₂O₂ aumentou a dimerização de NcPrx em taquizoítas intracelulares e extracelulares. A atividade *in vitro* de rNcGR (875 nM) foi verificada avaliando a absorbância do NADPH (340nm). rNcGR apresentou perfil enzimático Michaeliano ($K_m(\text{GSSG}): 0.10 \pm 0.02 \text{ mM}$; $k_{\text{cat}}(\text{GSSG}): 0.076 \pm 0.003 \text{ s}^{-1}$; $K_m(\text{NADPH}): 0.006 \pm 0.001 \text{ mM}$; $k_{\text{cat}}(\text{NADPH}): 0.080 \pm 0.003 \text{ s}^{-1}$). Além disso, rNcGR foi inibida pelos corantes fenotiazínicos (IC_{50} (azul de metileno): $2.1 \pm 0.2 \mu\text{M}$, IC_{50} (1,9-dimetil-azul-de-metileno): $11 \pm 2 \mu\text{M}$, IC_{50} (novo azul de metileno): $0.7 \pm 0.1 \mu\text{M}$, e IC_{50} (azul de toluidina): $0.9 \pm 0.2 \mu\text{M}$). No capítulo 3, foi demonstrado que rNcPrx interfere na invasão de *N. caninum* de forma dependente do estado redox. rNcPrx oxidada inibiu a invasão e proliferação de *N. caninum* em células Vero. Por outro lado, a menor concentração de H₂O₂ (10 μM) estimulou a invasão de *N. caninum*, o que foi revertido em altas doses (> 100 μM). H₂O₂ inibiu a proliferação do parasita em uma menor concentração (IC_{50} : 320 μM) quando comparado com a citotoxicidade em células Vero (CC_{50} : 586 μM), resultando em um índice de seletividade positivo (1.8). Finalmente, nossos resultados demonstraram a importância de NcPrx e NcGR na biologia de *N. caninum* e em mecanismos antioxidantes. Nossos dados sugerem que NcGR é um importante alvo dos corantes fenotiazínicos na inibição da proliferação de *N. caninum* e que NcPrx atua no *clearance* de H₂O₂ e como um sensor deste peróxido no parasita. Além disso, mostramos que o desenvolvimento intracelular de *N. caninum* é influenciado por alterações redox em seu meio, contribuindo com a elucidação de mecanismos relacionados a propagação e controle deste parasita.

Palavras-chave: *Neospora caninum*, Apicomplexa, antioxidante, sistema redox, peroxirredoxina, glutaciona redutase.

ABSTRACT

VENANCIO-BROCHI, J. C. **Redox control in *Neospora caninum*: investigation of antioxidant system enzymes.** 2021. 148 p. Thesis (Doctorate). Faculdade de Ciências Farmacêuticas de Ribeirão Preto- Universidade de São Paulo, Ribeirão Preto, 2021.

Neospora caninum, an apicomplexan parasite, is the etiological agent of neosporosis, a disease that leads to neurological symptoms in dogs and abortion in cattle. Vaccine or drug treatments for neosporosis remain to be determined. The development of the parasite inside host cells is characterized by the active secretion of proteins, allied to the tight control of the redox status. In this sense, the elucidation of new molecules and mechanisms related to redox control of *N. caninum* may contribute to the development of neosporosis treatments. Therefore, here it was described two enzymes of redox system: Peroxiredoxin (NcPrx, Chapter 1) and Glutathione reductase (NcGR, Chapter 2), as well it was investigated the effects of the recombinant forms of NcGR and NcPrx, and H₂O₂ in the tachyzoite invasion and proliferation in Vero cell (Chapter 3). Both NcPrx and NcGR amino-acid sequence showed high identity and similarity compared to homologues representatives of the Apicomplexa phylum. The recombinant NcPrx (rNcPrx) and recombinant NcGR (rNcGR) were cloned and expressed in *Escherichia coli* (BL21) with the predicted molecular weight (22 kDa and 52kDa, respectively) and the identity of monomer and dimer forms of rNcPrx and rNcGR were confirmed by mass spectrometry. Immunofluorescence analysis showed that NcPrx and NcGR are located in tachyzoite's cytosol. Native and recombinant NcPrx and NcGR were detected by ELISA and western blot, using the polyclonal anti-rNcPrx and anti-rNcGR sera. rNcPrx demonstrated peroxidase and antioxidant activity *in vitro*. Moreover, H₂O₂ increased the NcPrx dimerization in intracellular and extracellular tachyzoites. We verified the *in vitro* activity of rNcGR (875 nM) following NADPH absorbance at 340. rNcGR exhibited a Michaelian behavior ($K_m(\text{GSSG}): 0.10 \pm 0.02 \text{ mM}$; $k_{\text{cat}}(\text{GSSG}): 0.076 \pm 0.003 \text{ s}^{-1}$; $K_m(\text{NADPH}): 0.006 \pm 0.001 \text{ mM}$; $k_{\text{cat}}(\text{NADPH}): 0.080 \pm 0.003 \text{ s}^{-1}$). Furthermore, rNcGR was inhibited by phenothiazinium dyes ($\text{IC}_{50}(\text{Methylene blue}): 2.1 \pm 0.2 \text{ }\mu\text{M}$, $\text{IC}_{50}(1,9\text{-dimethyl methylene blue}): 11 \pm 2 \text{ }\mu\text{M}$, $\text{IC}_{50}(\text{new methylene blue}): 0.7 \pm 0.1 \text{ }\mu\text{M}$, e $\text{IC}_{50}(\text{toluidine blue O}): 0.9 \pm 0.2 \text{ }\mu\text{M}$). In chapter 3, it was demonstrated that rNcPrx interfered in the *N. caninum* invasion in a redox state manner. Oxidized rNcPrx inhibited the *N. caninum* invasion and proliferation with no toxic effects observed in Vero cells. In contrast, lower concentrations of H₂O₂ (10 μM) stimulated the *N. caninum* invasion, which was reverted in higher doses (> 100 μM). H₂O₂ inhibited the parasite proliferation in lower concentrations ($\text{IC}_{50}: 320 \text{ }\mu\text{M}$) compared to the cytotoxicity in host cells ($\text{IC}_{50}: 586 \text{ }\mu\text{M}$), resulting in a positive selectivity index (1.8). Finally, our results suggest the importance of NcPrx and NcGR in *N. caninum* biology and antioxidant mechanisms. Data presented here strongly suggest that NcGR is an important target of phenothiazinium dyes in *N. caninum* proliferation inhibition and that NcPrx is enrolled in H₂O₂ clearance and sensing in the parasite. Besides, we showed a connection between the *N. caninum* development and the redox state, contributing to the elucidation of mechanisms related to parasite propagation and control.

Key words: *Neospora caninum*, Apicomplexa, antioxidant, redox system, peroxiredoxin, glutathione reductase.

SUMÁRIO

RESUMO	iii
ABSTRACT	iv
1.INTRODUÇÃO	1
1.1 Neosporose	2
1.2 Transmissão	4
1.3 Epidemiologia	6
1.4 Neosporose: prejuízos e controle	8
1.5 Estresse oxidativo e defesas antioxidantes	10
1.6 Sistema Glutathiona	12
1.7 Peroxirredoxinas	14
1.8 O controle redox em parasitas Apicomplexas	17
1.9 Justificativa e relação entre os capítulos da Tese	19
2. OBJETIVOS	20
CAPÍTULO I	21
CAPÍTULO II	50
CAPÍTULO III	92
3. DISCUSSÃO FINAL	105
4. CONCLUSÕES	110
5. REFERÊNCIAS BIBLIOGRÁFICAS	111
6. ANEXOS	138

1. INTRODUÇÃO

1. INTRODUÇÃO

1.1 Neosporose

A neosporose foi descrita primeiramente como uma doença causadora de paralisia em cães domésticos associada com um protozoário formador de cisto e excluiu-se a hipótese de ser causada por outros apicomplexas como *Toxoplasma* e *Hammondia* (BJERKÅS; MOHN; PRESTHUS, 1984). Posteriormente o agente causador da neosporose, *Neospora caninum*, foi identificado como uma nova espécie por Dubey et al. (1988), um parasita intracelular obrigatório do filo Apicomplexa. Os autores demonstraram associação entre a infecção por *N. caninum* e meningoencefalomielite e miosite em cachorro. A partir disso, percebeu-se que a infecção por *N. caninum* vinha sendo erroneamente identificada como uma doença causada por *Toxoplasma gondii* em cachorros, já que os parasitas apresentam similaridades morfológicas e de desenvolvimento. Além disso, as características do oocisto de *N. caninum* são similares aos oocistos de *Hammondia heydorni* (fezes de cães) e de *T. gondii* e *Hammondia hammondi* de fezes de gato (DUBEY et al., 1988; LINDSAY; UPTON; DUBEY, 1999).

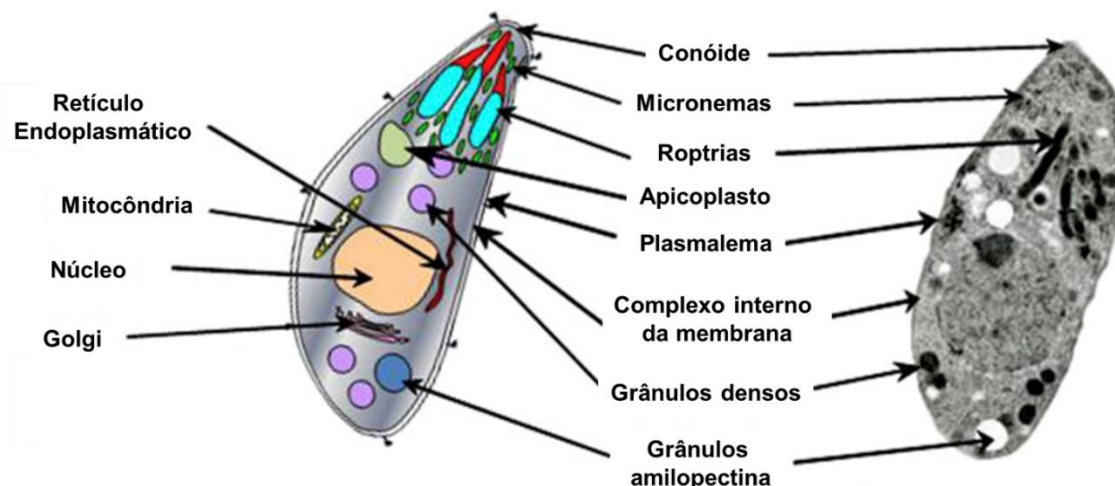
Neospora caninum é um parasita heteroxênico, ou seja, necessita de dois hospedeiros diferentes para completar seu ciclo de vida (BAKER et al., 1995; LINDSAY et al., 1996; MCALLISTER et al., 1998; UGGLA et al., 1998). Inicialmente foi descrito que cães experimentalmente infectados por cistos teciduais de *N. caninum* de camundongos eliminavam fezes contendo oocistos não esporulados (os oocistos esporularam dentro de 3 dias, resultando em 2 esporocistos, cada um com 4 esporozoítos), confirmando serem hospedeiros definitivos do parasita (MCALLISTER et al., 1998). O coyote (*Canis latrans*) foi o segundo hospedeiro definitivo descrito de *N. caninum* (GONDIM et al., 2004a). Posteriormente, mostrou-se que o lobo cinza (*Canis lupus*) e o dingo (*Canis lupus dingo*) são importantes hospedeiros definitivos no ciclo silvestre do parasita (KING et al., 2010; DUBEY et al., 2011). A prevalência da neosporose canina foi estimada em 17,14% na população de cachorros domésticos em todo mundo (ANVARI et al., 2020).

Enquanto a reprodução sexuada do parasita restringe-se aos animais da família Canidae, a reprodução assexuada pode ocorrer em uma gama de hospedeiros intermediários de sangue quente. O mais estudado é o bovino, porém outros animais são importantes na epidemiologia da doença, por exemplo: galinhas (COSTA et al., 2008) e pardais (GONDIM et al., 2010), raposas (ALMERÍA et al., 2002) e a gazela da cauda

branca (VIANNA et al., 2005). Aves podem ser predadas por canídeos contribuindo para continuidade do ciclo de vida do parasita. Por outro lado, carcaças de animais de caça infectados evisceradas no campo, como raposas e gazelas, podem ter um papel na transmissão para canídeos (VIANNA et al., 2005). Apesar da neosporose não ser considerada uma doença zoonótica, baixos títulos de anticorpos para *N. caninum* já foram detectados em seres humanos assintomáticos (TRANAS et al., 1999). Além disso, Duarte et al. (2020) detectaram cordões umbilicais de humanos soropositivos para *N. caninum*, e isso esteve associado significativamente com a presença de cachorros ou animais domésticos em casa, porém não houve dano no desenvolvimento fetal.

N. caninum pode estar em 3 estágios ao longo de seu ciclo de vida: taquizoíta, bradizoíta ou esporozoíta. Os componentes celulares comuns aos três estágios que caracterizam parasitas do filo Apicomplexa são os conóides, o complexo de membrana interno, apicoplasto, micronemas, roptrias e grânulos densos (Figura 1) (MARUGAN-HERNANDEZ, 2017). A forma taquizoíta é a principal forma de *N. caninum* que causa infecção aguda no hospedeiro intermediário e locomove-se por meio do *gliding*, um modo de locomoção exclusivo de apicomplexas (FRÉNAL et al., 2017). O *gliding* resulta da ação do sistema actinmiosina, abaixo da membrana plasmática e permite a migração do parasita entre diferentes tecidos, a invasão e o egresso da célula hospedeira (DUBEY; SCHARES, 2011). *N. caninum* se estabelece na célula hospedeira a partir de um processo ativo de invasão. Graças à polaridade do parasita, seu complexo apical é repleto de organelas que auxiliam no processo coordenado da invasão celular. Inicialmente, a porção apical do parasita realiza um contato de baixa afinidade com a superfície da célula seguido de adesão na célula hospedeira e da formação de uma junção de movimento (KHAN et al., 2020). A junção de movimento consiste na união íntima entre a membrana do parasita e do hospedeiro, formando um anel que percorre o parasita permitindo sua entrada na célula (BESTEIRO; DUBREMETZ; LEBRUN, 2011).

Figura 1. Principais estruturas e componentes celulares da forma taquizoíta de *N.caninum*



Modificado de: MARUGAN-HERNANDEZ, 2017.

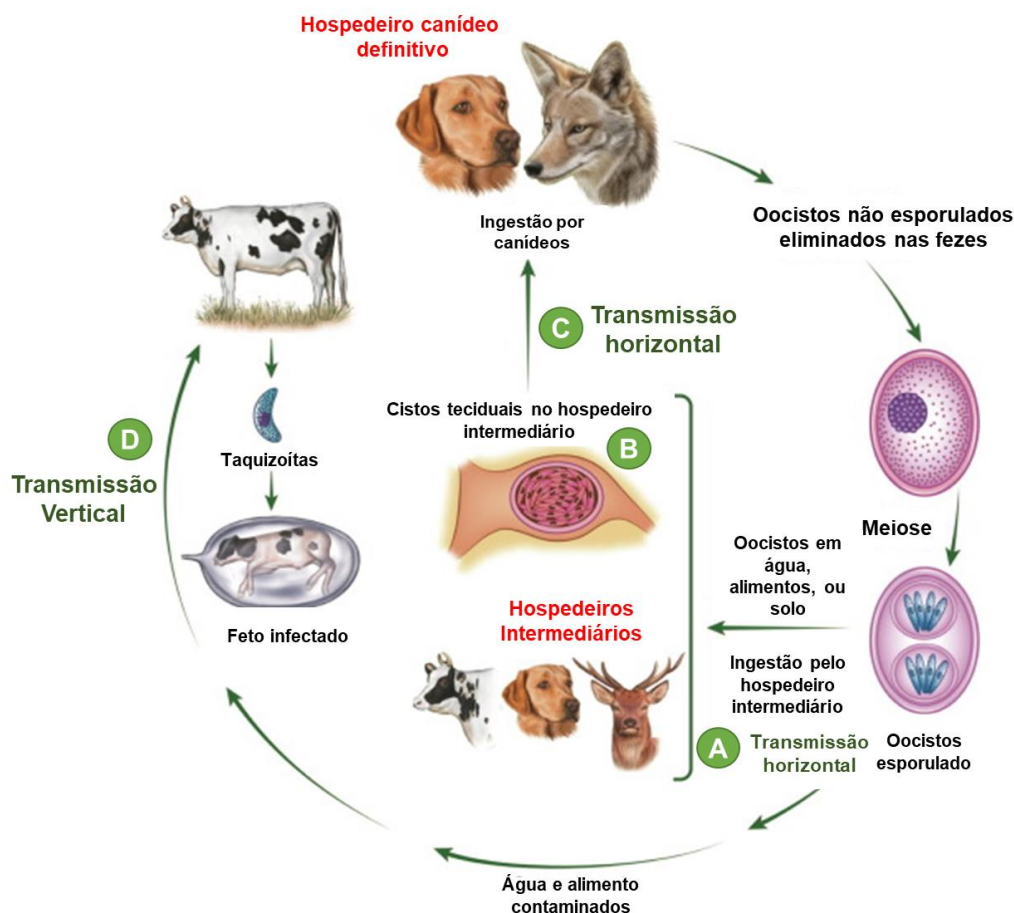
A secreção do conteúdo dos micronemas, dependente de cálcio, libera adesinas responsáveis pela ligação entre membrana do parasita e receptores de membrana do hospedeiro (NAGULESWARAN et al., 2001; LI et al., 2015; WANG et al., 2021). Por outro lado, as proteínas do pescoço das roptrias (RON) são secretadas durante a invasão auxiliando na entrada do parasita dentro da célula hospedeira por meio da formação da junção de movimento e eliminação de componentes da membrana da célula hospedeira (MARUGÁN-HERNÁNDEZ et al., 2011). Ademais, proteínas do corpo das roptrias e dos grânulos densos são secretadas no vacúolo parasitóforo (VP) e atuam como sinalizadores no núcleo da célula hospedeira (BRADLEY; SIBLEY, 2007).

1.2 Transmissão

A transmissão horizontal ocorre pela ingestão de oocistos esporulados liberados pelas fezes de canídeos infectados que podem contaminar pastos ou água (REICHEL et al., 2014) (Figura 2. A e C). Em seguida, no intestino dos hospedeiros intermediários, os oocistos liberam os esporozoítas que se diferenciam em taquizoítas capazes de invadir a parede intestinal (FEREIG; NISHIKAWA, 2020) e se disseminam pelo organismo, infectando o cérebro, músculo, fígado e pulmões (DUBEY et al., 2002). Os taquizoítas são a forma de proliferação rápida de *N. caninum*, capazes de invadir diferentes tipos de células, reproduzindo-se assexuadamente por endodiogenia (FEREIG; NISHIKAWA, 2020; KHAN et al., 2020). Após vários ciclos de endodiogenia, os parasitas egressam da célula hospedeira para reinfectar novas células ou podem converter-se em bradizoítas,

que são formas de resistência ao sistema imune do hospedeiro e aos estímulos ambientais (KHAN et al., 2020) (Figura 2.B). O bradizoíta é um estágio semi-dormente de crescimento lento, formando os cistos teciduais com grossas camadas, que podem persistir por toda a vida do hospedeiro (Figura 1.B)(DUBEY; SCHARES; ORTEGA-MORA, 2007).

Figura 2. Ciclo de vida heteroxênico de *N. caninum*.



Fonte: adaptado de KHAN et al. (2020).

Além da transmissão horizontal, a transmissão vertical transplacentária de *N. caninum* é uma rota bastante relevante e eficiente no gado bovino (Figura 2.D), podendo ocorrer por via exógena ou endógena (TREES; WILLIAMS, 2005). A via exógena ocorre quando a fêmea se infecta com oocistos de *N. caninum* durante o período da gestação (DUBEY et al., 1992; GONDIM et al., 2004b). A via endógena decorre da gestação de uma fêmea que já apresenta uma infecção latente (crônica) por *N. caninum* pré-existente

e em virtude das mudanças da resposta imunológica no período da gestação o parasita pode ser reativado.

O parasita converte-se novamente para sua forma taquizoíta, podendo atravessar a barreira transplacentária e afetar o desenvolvimento fetal de diferentes maneiras (ANDERSON et al., 1997; DIJKSTRA et al., 2008). *N. caninum* causa danos na placenta aumentando a resposta inflamatória, podendo induzir à luteólise e ao aborto (DUBEY; BUXTON; WOUDA, 2006). Além disso, multiplica-se no feto danificando tecidos ou causando inanição e hipóxia neste, decorrente de danos na placenta. Os fetos infectados podem morrer no útero seguido de reabsorção ou nascerem mortos, ou nascerem vivos com sinais clínicos ou nascerem normais sem sinais clínicos (FEREIG; NISHIKAWA, 2020). O resultado da infecção dependerá do tipo de transmissão, mês da gestação em que houve transmissão e da resposta imunológica da fêmea grávida e do feto. Taquizoítas de *N. caninum* apresentam afinidade por tecidos cerebrais, placenta e tecidos fetais possivelmente pela alta afinidade por sulfatos de condroitinas (NAGULESWARAN et al., 2002).

A transmissão vertical (Figura 2. D) é a maior rota de infecção por *N. caninum* apresentando alta taxa de eficiência (80%) (BJÖRKMAN et al., 1996, 2003; PARÉ; THURMOND; HIETALA, 1996; SCHARES et al., 1998). Esse tipo de transmissão contribui para a persistência da infecção no rebanho bovino por várias gerações, aumentando as taxas de aborto, sem que ocorra a passagem do parasita pelo hospedeiro definitivo (MCALLISTER et al., 2000; DUBEY; BUXTON; WOUDA, 2006; DUBEY; SCHARES; ORTEGA-MORA, 2007).

1.3 Epidemiologia

Estima-se que a neosporose esteja associada com aproximadamente 20% dos abortos em rebanhos bovinos na Califórnia, Nova Zelândia, Países baixos e no Canadá (ANDERSON; BARR; HOFFMAN, 1990; ANDERSON; ANDRIANARIVO; CONRAD, 2000; WILSON et al., 2016). Em Pernambuco, no Brasil, a prevalência da neosporose em fêmeas bubalinas foi de 35,4% sendo que 100% das propriedades apresentam ao menos um animal soropositivo. A soroprevalência da neosporose no gado bovino entre os continentes é de 0,5-27,7% na Europa (IMRE et al., 2012), 10,7-21,5% na África (GHALMI et al., 2012; SEMANGO et al., 2019), 4,1-43% na Ásia (KOIWA

et al., 2006; NAZIR et al., 2013), 10,2% na Oceania (NEVERAUSKAS; NASIR; REICHEL, 2015) e entre 7,6-41% na América (LLANO et al., 2018; MARBÁN-CASTRO; MATTAR; GONZÁLEZ TOUS, 2019).

A neosporose está associada com padrões de surtos de abortos endêmicos e epidêmicos em rebanhos bovinos (DUBEY, 1999; DUBEY; SCHARES, 2011). Surtos de aborto em 4 rebanhos leiteiros nos Países Baixos, durante 1992 e 1994, estiveram associados com 78% de infecção por *N. caninum* nos fetos abortados (MOEN et al., 1998) e foi mostrado que o risco de aborto é de duas a três vezes maior em vacas soropositivas para *N. caninum* do que para soronegativas (MOEN et al., 1998). Na Austrália, após 15 meses de um surto de abortos em rebanhos leiteiros detectou-se 31% de soroprevalência de *N. caninum*, com lesões fetais consistentes com neosporose (ATKINSON et al., 2000). Waldener et al. (WALDNER et al., 1999) mostraram em gado de corte que vacas soropositivas foram 6,2 vezes mais propensas a não emprenharem e demonstrou-se a transmissão da vaca para o feto em 82% das vacas soropositivas.

Jenkins et al. (JENKINS et al., 2000) investigaram a associação de um surto de abortos em rebanhos bovinos leiteiros no sudeste dos Estados Unidos com a neosporose. Nesse rebanho 80% das vacas apresentaram anticorpos para *N. caninum*, 40% das fêmeas em estágio intermediário da gestação abortaram e exames imunohistoquímicos dos cérebros dos fetos confirmaram a infecção por *N. caninum* (JENKINS et al., 2000). Surto de abortos em rebanhos de vacas leiteiras na Nova Zelândia, em 1997, foram significativamente associados com o nível de soropositividade para *N. caninum* (SCHARES; CONRATHS; REICHEL, 1999).

Por outro lado, McAllister et al. (MCALLISTER et al., 2000) mostraram que vacas previamente infectadas por *N. caninum* apresentaram menor probabilidade de abortar ou dar à luz prematuramente durante o surto de abortos do que vacas com infecções primárias por *N. caninum*, demonstrando que organismo pode desenvolver imunidade protetora prévia contra neosporose. Além disso, foi demonstrado que a avidéz de anticorpos IgG contra antígenos de *N. caninum* aumenta significativamente durante o curso da infecção por *N. caninum*, atingindo um pico quando a infecção se torna crônica (MCALLISTER et al., 2000; BJÖRKMAN et al., 2003). Não obstante ao aumento das taxas de abortos, a neosporose também pode diminuir a produção de leite pela vaca infectada (HERNANDEZ; RISCO; DONOVAN, 2001; HOBSON et al., 2002), reduzir o

ganho de peso após o desmame em gado de corte (BARLING et al., 2000) e provocar o abate prematuro (THURMOND; HIETALA, 1996).

1.4 Neosporose: prejuízos e controle

A neosporose é uma doença distribuída mundialmente representando uma grande preocupação dado ao impacto financeiro causado na indústria bovina de carne e leite. A maior parte das perdas ocorre na indústria de leite, uma vez que o risco de aborto é maior em gado de leite (14,3%) do que no gado para corte (9,1%) (REICHEL et al., 2013). Ademais, em relação ao prejuízo econômico global causado pela neosporose, a maior parte das perdas encontra-se no Norte (65,7%), e Sul (18,5%) da América e na Australásia (10,6%), já na Holanda, Espanha e Reino Unido são estimados em 5,3% (REICHEL et al., 2013). Assim, países da América latina e do Norte são alvos primários para vacinas contra a neosporose (REICHEL et al., 2013). Estima-se que o prejuízo médio global causado pela neosporose seja de 1,3 bilhões de dólares por ano (variando de 633,4 milhões a 2,4 bilhões) (REICHEL et al., 2013), tornando imprescindível desenvolvimento drogas ou vacinas que atuem no combate da doença.

Estratégias para controlar a neosporose incluem a testagem em massa dos animais e abate dos animais soropositivos (*test-and-culling*); a reprodução selecionada, descontinuando os filhotes de mães soropositivas ou inseminação artificial de fêmeas soropositivas, o uso de vacina ou o uso de medicamentos. Por meio de modelos matemáticos, Liu et al., (LIU; REICHEL; LO, 2020) aponta que em rebanhos nos quais a prevalência da neosporose está acima de 30% a vacina pode trazer melhor custo-benefício como medida de controle. Já em rebanhos com prevalência menor que 10% é possível combinar todas as estratégias para controlar a transmissão e os prejuízos causados pela doença.

Medicamentos para o tratamento da neosporose têm sido testados *in vitro* e *in vivo* (QIAN et al., 2015; MÜLLER; HEMPHILL, 2016; PEREIRA et al., 2018, 2020; MÜLLER et al., 2020). Dentre os 390 compostos antimaláricos (MMV, Medicines for Malaria Venture) do Malaria Box, 5 apresentaram potencial para estudos *in vivo* (MÜLLER et al., 2020). Além desses, corantes fenotiazínicos isolados e em combinação mostraram potencial eficácia no tratamento da neosporose tanto em testes *in vitro* como em modelo de camundongos (PEREIRA et al., 2020). A miltefosina apresentou efeitos

parasitostático (10h de tratamento) e efeito parasiticida (20h de tratamento) sobre *N. caninum* em cultura de fibroblasto e diminuiu a disseminação do parasita no sistema nervoso central de camundongos (DEBACHE; HEMPHILL, 2012). O efeito inibitório da Artemisinina sobre a proliferação de *N. caninum in vitro* já foi demonstrado (KIM et al., 2002; PEREIRA et al., 2018), porém seu uso combinado com a Pirimetamina e Azul de metileno é capaz de aumentar o *clearance* de parasitas *in vitro* (PEREIRA et al., 2018). Uma triagem clínica foi realizada em bovinos para testar os efeitos preventivos da monesina em ruminantes infectados experimentalmente por *N. caninum*, porém os resultados foram inconclusivos (VANLEEUEWEN et al., 2011). Toltrazuril não foi efetivo em cordeiros infectados congenitamente por *N. caninum* (SYED-HUSSAIN et al., 2015). O tratamento com Ponazuril em bezerros experimentalmente infectados por *N. caninum* apresentou eficácia, porém não foi conclusivo já que bezerros apresentam baixa susceptibilidade à infecção experimental por *N. caninum* (KRITZNER et al., 2002). Inibidores de proteína quinase 1 dependentes de cálcio, BKI-1517 e BKI-1553 diminuíram a proliferação de taquizoítas de *N. caninum in vitro* (MÜLLER et al., 2017). No modelo *in vivo*, ambos inibidores reduziram a parasitemia cerebral em camundongos infectados após 6 dias de tratamento (MÜLLER et al., 2017). BKI-1517 inibiu a transmissão vertical de *N. caninum* para a prole e aumentou a sobrevivência da ninhada (MÜLLER et al., 2017). Além disso, o uso de drogas para tratar a neosporose tem suas limitações pela possibilidade de deixarem resíduos na carne ou no leite produzido pelo animal tratado.

A vacinação seria uma medida de controle interessante do ponto de vista econômico para evitar a infecção e transmissão da neosporose em rebanhos bovinos leiteiros e em gado de corte. Embora até o momento da escrita desta tese não haja nenhuma vacina licenciada sendo comercializada, vários tipos de vacina para neosporose já foram testados. Por exemplo, a vacina com a fração solúvel do extrato do taquizoíta (sNcAg/AVEC; adjuvante: lectina de soja) mostrou-se uma vacina segura, induziu alta imunogenicidade em novilhas grávidas imunizadas no primeiro trimestre da gestação (MANSILLA et al., 2015). Esta vacina aplicada em novilhas não prenhes estimulou a resposta imune capaz de controlar a infecção por *N. caninum* (MANSILLA et al., 2013). Vacina apresentando taquizoítas vivos isolados da linhagem Nc-6 Argentina aplicadas em novilhas antes do acasalamento reduziu parcialmente a transmissão vertical da neosporose (novilhas desafiadas com *N. caninum* nas fases iniciais da gestação)

(HECKER et al., 2013). Vacinação de novilhas com a linhagem naturalmente atenuada Nc-Nowra viva antes do acasalamento reduziu a taxa de aborto (WEBER et al., 2013). Apesar da eficácia demonstrada por vacinas utilizando *N. caninum* vivo, há o obstáculo da preservação e manejo desse tipo de vacina para que ela se torne comerciável e o potencial de reversão da virulência da linhagem atenuada (WEBER et al., 2013). Além disso, é necessário desenvolver uma linhagem de Nc atenuada mais estável, minimizando as possibilidades de reversão da virulência e assegurar que a vacina induza uma resposta imune segura durante a gravidez (WEBER et al., 2013).

Além dessas vacinas, já foram investigadas vacinas contendo rNcGRA7, rNcSAG1, rNcHSP20, porém essas vacinas não foram efetivas em prevenir a infecção em novilhas prenhes (HECKER et al., 2014). Por outro lado, vacina contendo rNcGRA7 dentro de lipossomas contendo manotriose (M3-NcGRA7) pode induzir resposta imune protetora, induzindo a formação de anticorpos específicos e reduzindo a quantidade de parasitas no cérebro de bovino (NISHIMURA et al., 2013).

A única vacina já comercializada contra neosporose foi a Bovilis-Neoguard (Intervet International B.V., Boxmeer, The Netherlands), composta por taquizoítas de *N. caninum* inativados, mas foi retirada do mercado anos depois devido à baixa efetividade (20%) na prevenção da doença, demonstrada em estudos na Costa Rica e na Nova Zelândia (ROMERO; PÉREZ; FRANKENA, 2004; WESTON; HEUER; WILLIAMSON, 2012; REICHEL et al., 2014; HEMPHILL; AGUADO-MARTÍNEZ; MÜLLER, 2016).

1.5 Estresse oxidativo e defesas antioxidantes

Espécies reativas de oxigênio (EROs) são moléculas instáveis que contêm um ou mais elétrons não pareados (CHEESEMAN; SLATER, 1993) podendo danificar estruturas celulares ou atuarem como moléculas sinalizadoras de modo dependente da concentração (WEIDINGER; KOZLOV, 2015). EROs compreendem tanto radicais livres derivados do oxigênio como também os seus derivados: ânion superóxido ($O_2^{\cdot-}$), peróxido de hidrogênio (H_2O_2) e radicais hidroxil ($\cdot OH$) (CHEESEMAN; SLATER, 1993; WEIDINGER; KOZLOV, 2015). A produção de EROs ocorre pelo metabolismo aeróbico, pela ação de macrófagos do hospedeiro, decomposição de grupos heme ou em resposta a determinadas drogas (GUEVARA-FLORES et al., 2017).

À medida que o oxigênio molecular é reduzido na cadeia transportadora de elétrons da mitocôndria ocorre a produção de radical superóxido, que sofre dismutação resultando em peróxido de hidrogênio (H_2O_2) e água (SIES, 1997). A reação de metais de transição com $O_2^{\cdot-}$ e H_2O_2 , como por exemplo, a reação de Fenton, também resulta em HO^{\cdot} que gera radicais alquils e peroxils quando atuam em ácidos graxos (SIES, 1997). $O_2^{\cdot-}$ pode reagir com óxido nítrico (NO^{\cdot}) gerando peroxinitrito ($ONOO^{\cdot-}$) (SIES, 1997; WEIDINGER; KOZLOV, 2015). Além disso, EROs podem ser gerados como produtos da catálise de enzimas, como por exemplo a xantina oxidase, NADPH oxidases, citocromos P450, óxido nítrico sintase (NOS), lipoxigenase e cicloxigenase (CAI; HARRISON, 2000).

O aumento da geração de oxidantes e diminuição dos níveis de antioxidantes podem causar estresse oxidativo, tendo forte associação com condições patológicas e envelhecimento (NORDBERG; ARNÉR, 2001). O estresse oxidativo promove danos a proteínas, lipídeos, carboidratos, ácidos nucleicos trazendo grandes prejuízos para as funções e sinalização fisiológicas (BOKOV; CHAUDHURI; RICHARDSON, 2004). Dessa forma, a concentração de EROs é finamente regulada nos compartimentos celulares, uma vez que afetam as funções das organelas, a expressão de genes e proteínas, o equilíbrio de cálcio, a bioenergética e o metabolismo de substratos (DEY; SIDOR; O'ROURKE, 2016). Essa regulação é realizada pelo sistema redox composto de enzimas antioxidantes e moléculas antioxidantes de baixo peso molecular (GUEVARA-FLORES et al., 2017). A enzima superóxido dismutase converte $O_2^{\cdot-}$ em O_2 e H_2O_2 , enquanto a enzima glutathiona peroxidase (GPx), a catalase e peroxirredoxinas (Prx) decompõem o H_2O_2 evitando a formação do radical HO^{\cdot} . Além disso, as enzimas tiorredoxina redutase e glutathiona redutase, flavoenzimas diméricas, atuam mantendo níveis adequados de tiorredoxina e glutathiona reduzidas, essenciais para o equilíbrio redox da célula. Estas moléculas atuam na desativação dos EROs ou no transporte de EROs para compartimentos menos susceptíveis ao dano oxidativo (SIES, 1997).

A glutathiona reduzida é um importante antioxidante das células de mamíferos, agindo na eliminação de EROs, na reciclagem das enzimas glutarredoxinas, glutathiona peroxidase e algumas peroxirredoxinas e mantendo o estado reduzido da vitamina C e vitamina E (FERNANDEZ-MARCOS; NÓBREGA-PEREIRA, 2016). Além disso, as enzimas glutarredoxinas (Grx) utilizam GSH/GSSG como receptor/doador de elétrons

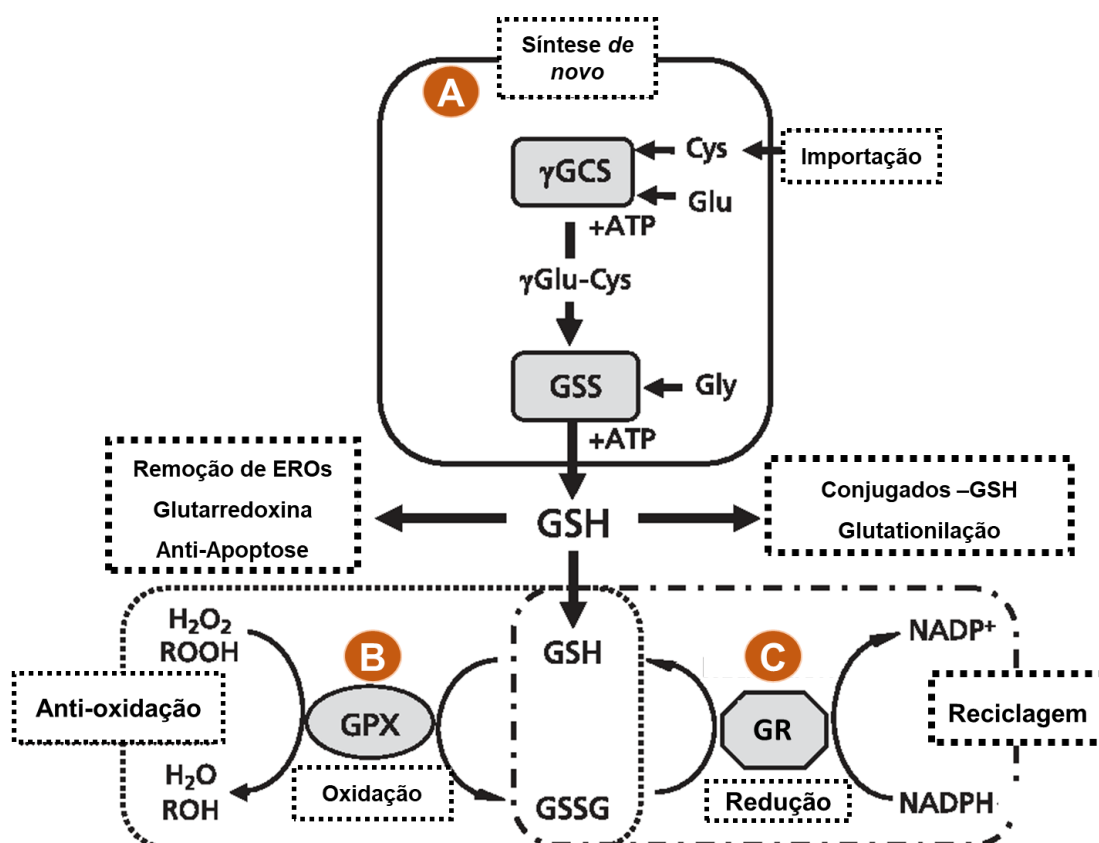
para atuar como redutores ditiol de proteínas, que restaura o estado reduzido de proteínas oxidadas com grupo sulfidrilal evitando sua remoção da célula (JORTZIK; BECKER, 2012). As tiorredoxinas (Trx) são pequenas proteínas que, por meio da redução de grupos tióis em proteínas-alvo, atuam como antioxidantes ou regulam proteínas-chave de sinalização. Trx contém um sítio ativo conservado de duas cisteínas (CXXC, sendo X qualquer aminoácido) onde ocorrem trocas de dissulfeto de ditiol(LU; HOLMGREN, 2014). Os estados redox da glutathiona e tiorredoxina são definidos pela redução ou oxidação de seus centros ativos (motivo CXXC) e suas formas oxidadas podem ser recicladas pelas enzimas Glutathiona redutase (GR) e Tiorredoxina redutase (TrxR), respectivamente, com consumo de NADPH(JORTZIK; BECKER, 2012).

Portanto, tanto a glutathiona como a tiorredoxina são altamente suscetíveis ao estado redox celular e seus níveis refletem a perturbação no *pool* tiol/dissulfeto ou da razão NADPH/NADP, influenciando uma variedade de alvos moleculares e vias de sinalização (COMINI, 2016).

1.6 Sistema Glutathiona

O sistema glutathiona é um dos sistemas chave na defesa antioxidante e na detoxificação de EROS e espécies reativas de nitrogênio (ERN), garantindo a sobrevivência e manutenção da célula (JORTZIK; BECKER, 2012). O sistema glutathiona é formado pela forma reduzida (GSH) e oxidada (GSS) da glutathiona, bem como pelas enzimas que participam de sua síntese, manutenção e metabolismo: γ glutamil-cisteína-sintase, glutathiona sintetase, glutathiona s-transferase, glutathiona peroxidase, glutathiona redutase e glutarredoxinas (Figura 3)(FUJII et al., 2011). A glutathiona é um tripeptídeo produzido em duas etapas dependentes de ATP. Esse processo envolve a ação da enzima γ glutamil-cisteína sintase, na primeira etapa, na qual forma-se a ligação peptídica entre o ácido L-glutâmico e L-cisteína, e da enzima glutathiona sintetase, que adiciona a glicina na porção C-terminal da L-cisteína (Figura 3.A)(FUJII et al., 2011). A concentração de glutathiona é duas vezes maior no ambiente intracelular do que no ambiente extracelular, sendo predominante em sua forma reduzida (GSH), exceto no retículo endoplasmático (MORRIS et al., 2014). A glutathiona age como um antioxidante à medida que atua como um doador de hidrogênio para a eliminação de radicais livres contribuindo para regeneração de outros antioxidantes como alfa-tocoferol, ascorbato e ubiquinonas (MORRIS et al., 2014).

Figura 3. Representação esquemática do Sistema glutatona. γ GCS e GSS coordenam a síntese de GSH a partir dos aminoácidos: Cys, Glu e Gly. GPX reduz peróxidos utilizando elétrons de GSH. A oxidação de GSH produz GSSG, o qual é reduzido novamente para GSH (reciclagem) pela enzima GR. GSH desempenha diversos papéis na defesa redox: remoção de EROs, evita a apoptose, participa de reações juntamente com a glutarredoxina, forma conjugados com outras moléculas, participa da glutathionilização. γ -GCS: γ -glutamilcisteína sintetase; GR: glutathione redutase; GS: glutathione sintetase; GSH: glutathione reduzida; GSSG: glutathione oxidada dissulfídica; +ATP: etapa dependente de adenosina trifosfato; NADPH: Fosfato de dinucleótido de nicotinamida e adenina; GPX: glutathione peroxidase;



Fonte: adaptada de FUJII et al. (2011).

A enzima glutathione peroxidase utiliza GSH como substrato para remover peróxidos orgânicos e inorgânicos (Figura 3.B)(JORTZIK; BECKER, 2012; MORRIS et al., 2014). O GSSG formado a partir da oxidação de GSH pode ser excretado da célula ou reduzido a GSH novamente pela ação da enzima glutathione redutase (GR) dependente de NADPH (Figura 3.C)(BERKHOLZ et al., 2008). Glutathione S-Transferases conjugam moléculas genotóxicas ou carcinogênicas com a glutathione, reduzindo a reatividade dos eletrófilos e aumentando a solubilidade desses compostos em água, o que por sua vez

favorece a eliminação da célula e reduz as interações com ácidos nucleicos e proteínas (JORTZIK; BECKER, 2012; MORRIS et al., 2014).

Já as glutarredoxinas (GRXs) são enzimas redox que utilizam o poder redutor da glutatona para catalisar reações dissulfídicas. GRXs atuam em trocas dissulfetos mistos envolvendo proteínas: $GSH + \text{Proteína-SSG} = GSSG + \text{proteína-SH}$. (LILLIG; BERNDT; HOLMGREN, 2008) A reação de proteínas-SH com ROS pode produzir proteínas-SSG e a exposição de cisteínas ao ROS também pode dar origem à ácidos sulfênicos, que são altamente instáveis e podem reagir com a glutatona para produzir uma proteína-SSG (XIAO et al., 2019). Dessa forma a oxidação de resíduos de cisteínas pode atuar como um sensor redox para célula ou para inativação de proteínas cujo grupo tiol está envolvido com a sua função (LILLIG; BERNDT; HOLMGREN, 2008).

Os ácidos sulfênicos podem ser reduzidos pela ação de uma variedade de redutases ou quando a célula se encontra em uma mudança favorável do estado oxidativo. Além das redutases, o dano oxidativo em proteínas com grupos tióis pode ser revertido pela adição de uma glutatona em sua estrutura, em um processo conhecido como S-glutationilização (JORTZIK; BECKER, 2012; MÜLLER, 2015). As glutarredoxinas catalisam tanto glutatiolinização com cisteína, ácido sulfênico ou outros motivos sulfidril, como a deglutationilização, dependendo dos níveis de GSH, GSSG, proteína-SH e proteína-SSH na célula (LILLIG; BERNDT; HOLMGREN, 2008). Esse processo pode regular a ação de proteínas, sendo de especial relevância em proteínas do citoesqueleto, quinases, proteínas de sinalização e proteínas envolvidas na produção de energia e homeostase do cálcio. Assim, através da glutationilização ou deglutationilização, a glutatona previne o dano oxidativo irreversível em proteínas com grupo tiol e auxilia na regulação redox da sinalização celular (XIAO et al., 2019).

1.7 Peroxirredoxinas

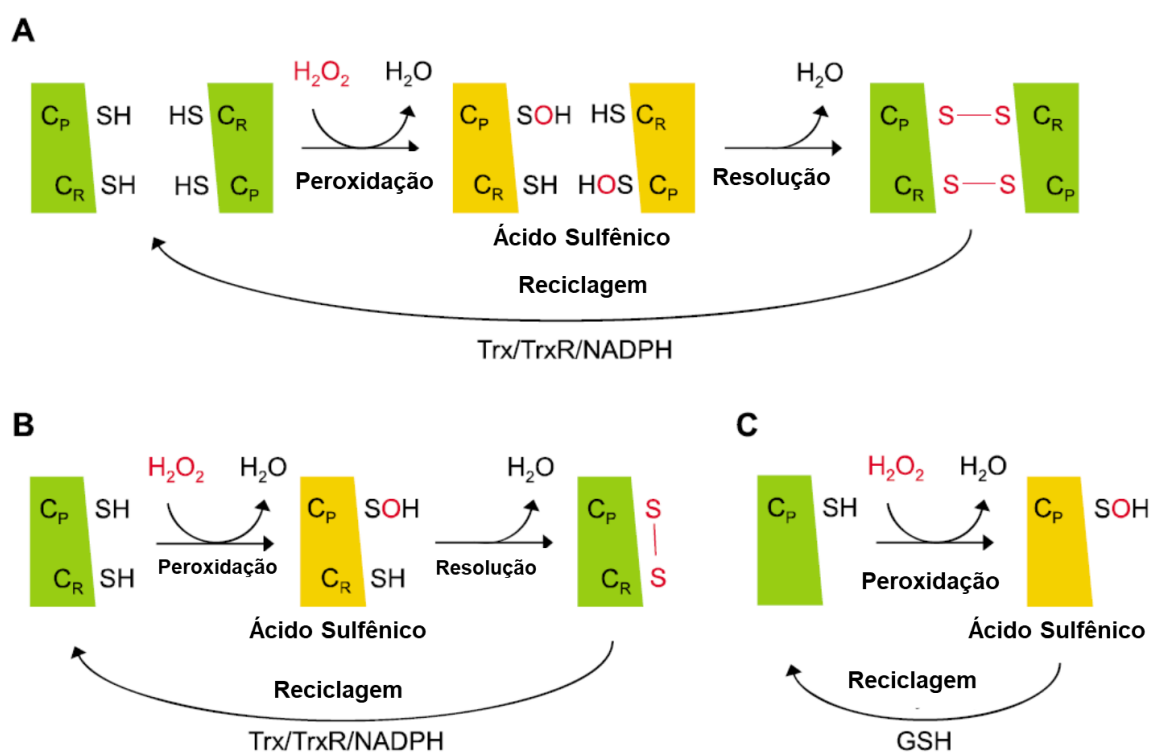
Peroxirredoxinas (Prx) são enzimas peroxidases multifuncionais abundantemente expressas em organismos de todos os reinos (RHEE et al., 2001). Além de removerem H_2O_2 , participam da sinalização redox e podem funcionar como chaperonas moleculares dependendo dos níveis de H_2O_2 (PERKINS et al., 2015). Prxs regulam uma variedade de processos fisiológicos como: crescimento celular, diferenciação, apoptose, resposta imune e metabolismo. Além disso, as Prxs têm sido correlacionadas com a carcinogênese

de diferentes tipos de cânceres em humanos, sendo que a superexpressão de Prx é relacionada com um prognóstico ruim nos pacientes (ISHII; WARABI; YANAGAWA, 2012; KIM; JANG, 2019).

As diferentes isoformas de Prx podem apresentar um ou dois resíduos de cisteínas (Cys), cisteína peroxidática (C_P) e a cisteína de resolução (C_R) (RHEE, 2016). Prx podem ser classificadas em 3 tipos, de acordo com os números e a posição dos resíduos de Cys e de acordo com o tipo de ligação dissulfídica catalisado: 2-Cys Prx típicas, 2-Cys atípicas, e 1-Cys Prx (Figura 4) (RHEE et al., 2012a).

A oxidação de C_P -SH pelo H_2O_2 em Prx 2-Cys típicas produz um ácido sulfênico intermediário (C_P -SOH), sendo seguida da formação de uma ligação dissulfídica intermolecular entre C_R de uma subunidade e C_P da segunda subunidade, inativando a enzima (Figura 4.A) (WOOD et al., 2003; RHEE, 2016). A reativação de Prx ocorre pela redução da ligação dissulfídica pela ação de equivalentes redutores. Já em Prx 2-Cys atípicas a formação da ponte dissulfídica ocorre entre C_R e C_P da mesma subunidade monomérica (intramolecular, Figura 4.B) (WOOD et al., 2003; KIM; JANG, 2019). Tanto 2-Cys Prx típicas como 2-Cys atípicas são recicladas pelo sistema tiorredoxina. A classe 1-Cys Prx caracteriza-se pela ausência de C_R , de forma que após a formação do ácido sulfênico em C_R , ocorre a reciclagem da Prx ativa que é reduzida pela glutathiona (GSH) (Figura 4.C) (WOOD et al., 2003).

Figura 4. Ciclo catalítico de diferentes classes de Prx: (A) 2-Cys Prx típicas: oxidação pelo H_2O_2 produz ácido sulfênico em C_P seguido pela forma da ponte dissulfídica (S-S) entre C_P e C_R intermolecular (B) 2-Cys atípicas: oxidação pelo H_2O_2 produz ácido sulfênico em C_P seguido pela forma da ponte dissulfídica (S-S) entre C_P e C_R intramolecular. Tanto em (A) e (B), a forma ativa de Prx é reciclada pelo sistema tiorredoxina (tiorredoxina Trx, tiorredoxina redutase TrxR, NADPH); (C) 1-Cys Prx.: oxidação pelo H_2O_2 produz ácido sulfênico em C_P seguido pela regeneração de Prx ativa pela glutathiona (GSH). C_P : cisteína peroxidática; C_R : cisteína de resolução.



Fonte: modificado de KIM;JANG (2019).

Na literatura, é descrito que altos níveis de H_2O_2 podem induzir a hiperoxidação do grupo tiol da cisteína peroxidática de Prx para ácido sulfínico (C_P -SO₂H-), resultando em Prx enzimaticamente inativa, na formação de estruturas de alta massa molecular (decâmeros ou dodecâmeros) e no acúmulo de H_2O_2 na célula (BOLDUC et al., 2018; CALABRESE et al., 2019). A forma hiperoxidada (C_P -SO₂H-) de Prx é lentamente reciclada para a forma monomérica na presença da enzima sulfirredoxina (BOLDUC et al., 2018; COLLINS et al., 2019). No entanto, em determinadas condições Prx pode ser novamente hiperoxidada à ácido sulfônico de forma irreversível (Cys - C_P O₃H) (BOLDUC et al., 2018; COLLINS et al., 2019).

O estudo da hiperoxidação de Prx de humanos e levedura sugere um importante papel fisiológico para a regulação da célula (BOLDUC et al., 2018; CALABRESE et al., 2019; COLLINS et al., 2019). Bolduc et al., (BOLDUC et al., 2018)propõem que este é um mecanismo pelo qual a célula diferencia entre níveis de H₂O₂ que indicam estresse ou não, dessa forma regulando a ativação de vias específicas de sinalização. Calabrese et al. (CALABRESE et al., 2019)sugerem que a hiperoxidação de Prx1 em levedura representa um mecanismo de proteção para reduzir a oxidação do pool de glutathiona na matriz mitocondrial em situação de aumento agudo dos níveis mitocondriais, e dessa forma influencia outras vias redox e de sinalização na célula. Em *Schizosaccharomyces pombe*, a inativação de Prx preserva tiorredoxina reduzida na célula, favorecendo a ação desta em outros substratos; como a metionina sulfóxido redutase (Mxr1), que repara proteínas oxidadas vitais para a sobrevivência da célula (DAY et al., 2012).

1.8 O controle redox em parasitas Apicomplexas

O estresse oxidativo tem um importante papel na patogênese de doenças causadas por parasitas Apicomplexas, como *N. caninum*, *T. gondii* e *Plasmodium* spp (PERCÁRIO et al., 2012; TONIN et al., 2014a; GLOMBOWSKY et al., 2017a; MOTA et al., 2020; SZEWCZYK-GOLEC et al., 2021). A multiplicação intracelular desses parasitas no interior da célula hospedeira resulta em morte e lise celular e consequente atração de células inflamatórias do hospedeiro, como macrófagos e neutrófilos. Essas células, por sua vez, produzem grandes quantidades de EROs que são tóxicos para o parasita(ALINE; BOUT; DIMIER-POISSON, 2002), mas em contrapartida podem provocar sérios danos aos tecidos do organismo hospedeiro (TONIN et al., 2014a; GLOMBOWSKY et al., 2017a).

O desafio do parasita de sobreviver em um ambiente redox desfavorável e potencialmente danoso às estruturas celulares e à sua proliferação dentro da célula (ALINE; BOUT; DIMIER-POISSON, 2002; WEIDINGER; KOZLOV, 2015) é contrabalanceado pela presença do sistema redox, que elimina o excesso de EROs produzido pelo hospedeiro e é essencial para o sucesso da infecção (GUEVARA-FLORES et al., 2017). Interessantemente, *Plasmodium falciparum*, além de usar suas próprias defesas antioxidantes, é capaz de importar a enzima peroxirredoxina 2 do hospedeiro, beneficiando-se do aparato antioxidante deste para reagir ao estresse oxidativo (KONCAREVIC et al., 2009).

O sistema redox de parasitas Apicomplexas tem sido amplamente estudado em *Plasmodium* e *T. gondii*, nos quais já foram descritas diversas moléculas e enzimas antioxidantes, como por exemplo: peroxirredoxinas (AKERMAN; MÜLLER, 2003; BOUCHER et al., 2006), tiorredoxina redutase (MCCARTY et al., 2015; XUE et al., 2017), tioredoxina (JORTZIK; BECKER, 2012; BIDDAU et al., 2018) e glutathione redutase (SARMA et al., 2003; HASSAN et al., 2014). Em *Neospora caninum*, porém, apenas as enzimas SOD1 e Glutarredoxina 1 (CHO et al., 2004a; SONG et al., 2020) haviam sido descritas antes do presente trabalho, existindo ainda uma ampla gama de moléculas antioxidantes a serem investigadas nesse parasita. Evidências de estudos em *Plasmodium* e *T. gondii* e *N. caninum* mostram que o balanço entre defesas antioxidantes e o estresse oxidativo influenciam diretamente na infecção do organismo hospedeiro. Em *T. gondii*, a capacidade de invadir e proliferar é reduzida em cepas nocaute para a enzima tiorredoxina redutase (XUE et al., 2017). Em *Plasmodium*, a tiorredoxina redutase é essencial para a sobrevivência do parasita nos estágios eritrocitários (KRNAJSKI et al., 2002) e a enzima 2-cys peroxirredoxina é essencial para a resistência ao estresse de temperatura pelo parasita (KIMURA et al., 2013). A deleção do gene da glutarredoxina 1 em *N. caninum* comprometeu o crescimento *in vitro* e induziu ao aumento do estresse oxidativo no parasita (SONG et al., 2020). Além disso, o estresse oxidativo gerado pelo tratamento com corantes fenotiazínicos em células infectadas com *N. caninum* foi associado com a atividade inibitória destes compostos na proliferação do parasita (PEREIRA et al., 2020).

1.9 Justificativa e relação entre os capítulos da Tese

Mundialmente, a neosporose representa uma das principais causas de aborto parasitário em bovinos, sendo responsável por surtos em série em rebanhos. A infecção por *N. caninum* é altamente prevalente no Brasil e estima-se que essa doença aumenta em 10% o risco de aborto em rebanhos leiteiros em nosso país, gerando altos custos para os produtores (NICOLINO et al., 2015; CERQUEIRA-CÉZAR et al., 2017). Além disso, o prejuízo global causado pela neosporose é avaliado em bilhões de dólares (REICHEL et al., 2013). No entanto, medidas preventivas e medicamentosas no combate à neosporose têm se mostrado ineficazes, tornando fundamental pesquisar novos alvos terapêuticos em *Neospora caninum*. Assim, tendo em vista que mecanismos de defesa antioxidante podem ser importantes fatores de virulência em parasitas Apicomplexas; e que o sistema redox de *N. caninum* é muito pouco conhecido e estudado até o presente momento, neste trabalho buscamos elucidar aspectos do controle redox de *N. caninum*.

O estudo de Oliveira et al.(2013) identificou no proteoma de *Neospora caninum* uma abundante expressão das enzimas peroxirredoxina dependente de tioredoxina (NcLIV_062630 = NcPrx) e da glutathiona redutase (NcLIV_063590 = NcGR), despertando o interesse em estudá-las no parasita. No capítulo 1, a enzima peroxirredoxina (NcPrx) foi caracterizada molecular e funcionalmente, bem como, foi localizada no parasita e seu comportamento redox foi avaliado frente ao tratamento com peróxido de hidrogênio. No capítulo 2, caracterizamos molecular e funcionalmente a enzima glutathiona redutase (NcGR) levantando aspectos de sua estrutura molecular tridimensional. Além disso, determinamos se NcGR é um alvo de inibição dos corantes fenotiazínicos. Finalmente, no capítulo 3, buscamos avaliar a proliferação e invasão de *N. caninum* em condições antioxidantes: tratando com as enzimas recombinantes peroxirredoxina e glutathiona redutase (descritas no capítulo 1 e 2, respectivamente); bem como em uma condição oxidante: tratando com diferentes concentrações de peróxido de hidrogênio.

2. OBJETIVOS

2.1 Caracterizar NcPrx molecular e funcionalmente e investigar seu papel como sensor redox em *N. caninum*.

2.2 Caracterizar NcGR molecular e funcionalmente e investigar os corantes fenotiazínicos como potenciais inibidores da sua atividade enzimática.

2.3 Determinar a ação do H₂O₂ e das enzimas recombinantes NcGR e NcPrx sobre a proliferação e invasão *N. caninum*.

CAPÍTULO I

Characterization of the *Neospora caninum* Peroxiredoxin: a novel peroxidase and antioxidant enzyme.

Jade Cabestre Venancio Brochi¹; Luiz Miguel Pereira¹; Luciana Baroni¹; Péricles Gama Abreu-Filho¹ and Ana Patrícia Yatsuda^{1*}

Submitted to: *Parasitology Research*.

¹ Faculdade de Ciências Farmacêuticas de Ribeirão Preto, Universidade de São Paulo, Av do Café, sn/n, 14040-903, Ribeirão Preto, SP, Brazil.

* **Author for correspondence:** Ana Patrícia Yatsuda, ORCID: 0000-0001-7957-2279, e-mail: ayatsuda@fcfrp.usp.br.

ABSTRACT

Neospora caninum, an apicomplexan parasite, is the etiological agent of neosporosis, a disease that leads to neurological symptoms in dogs and abortion in cattle. Vaccine or drug treatments for neosporosis remain to be determined. Therefore, it is of undeniable relevance to investigate new molecules involved in the parasite's successful survival within the host cell. The aim of this study was to characterize the *N. caninum* peroxiredoxin (NcPrx), an enzyme involved in the redox system of the parasite. The NcPrx amino-acid sequence showed high identity and similarity compared to homologues representatives of Apicomplexa phylum. The recombinant NcPrx (rNcPrx) was cloned and expressed in *Escherichia coli* (BL21) with the predicted molecular weight (22 kDa) and the identity of monomer and dimer forms of rNcPrx were confirmed by mass spectrometry. Native and recombinant NcPrx were detected by ELISA and western blot, using the polyclonal anti-rNcPrx serum. Multiphoton analysis showed that NcPrx is localized in tachyzoite cytosol. H₂O₂ treatment increased the rNcPrx dimerization *in vitro* and associated with the *in-silico* data we suggest that NcPrx belongs to typical 2-Cys Prx group (AhpC/Prx1 family). rNcPrx also increased the H₂O₂ clearance and protected plasmidial DNA under oxidative conditions. Finally, H₂O₂ increased the NcPrx dimerization in intracellular and extracellular tachyzoites suggesting that it is enrolled in H₂O₂ clearance and sensing in *N. caninum*.

Key words: Apicomplexan, *Neospora caninum*, Peroxiredoxin, antioxidant, peroxidase, recombinant protein.

Introduction

The Apicomplexa phylum comprises protozoan parasites of medical and veterinary importance, such as *Plasmodium* sp., *Toxoplasma gondii*, and *Neospora caninum*, the etiological agents of malaria, toxoplasmosis, and neosporosis, respectively (DUBEY et al., 1988). *N. caninum* might induce neuromuscular degeneration in dogs and abortion, infertility, and neonatal mortality in cattle (DUBEY, 1999; DUBEY; SCHARES, 2011).

Neosporosis in livestock is an important problem in milk and beef production, leading to global financial losses estimated at US \$1,3 billion per annum (REICHEL et al., 2013). As there is no effective vaccine and no licensed drug for bovine neosporosis, the control is based on biosecurity and the withdrawal of infected animals from livestock. Therefore, there is an intense investigation of *N. caninum* biology focused on the development of new treatments or vaccines.

The apicomplexans are obligate intracellular parasites conditioned to oxidative stress balance/resistance for successful survival in host cells (BOSCH et al., 2015; COUTO; WOOD; BARBER, 2016; GUEVARA-FLORES et al., 2017). The apicomplexan antioxidant enzymes have been investigated remarkably to elucidate drug resistance mechanisms and for the screening of new drug targets. The parasite redox system consists of a repertoire of antioxidant enzymes and thiol/disulfide pairs. The superoxide dismutase, catalase, and peroxiredoxin are antioxidant enzymes that act directly in pro-oxidant agents (GUEVARA-FLORES et al., 2017) whereas glutathione reductase and thioredoxin act in low weight thiol/disulfide pairs to control the antioxidant capacity of the cell (COUTO; WOOD; BARBER, 2016).

Peroxiredoxin enzymes eliminate hydrogen peroxide, organic peroxides, and peroxynitrites compounds (ONOO) through one (1-Cys-Prx) or two (2-Cys-Prx) catalytically active cysteine residues present on its molecular structures (WOOD et al., 2003). The peroxiredoxin sequence is highly conserved among prokaryotic and eukaryotic cells. In mammalian cells, Prx act as a local regulator of H₂O₂ levels, once different types of Prx are present in cytosol, mitochondria, and endoplasmic reticulum (RHEE, 2016). Furthermore, peroxiredoxin has been described as a chaperone in stressful conditions and, particularly, the Prx6 showed phospholipase activity in acidic

pH and by phosphorylation (RHEE et al., 2012a; FISHER, 2018; TEIXEIRA et al., 2019). In helminths, Prx was correlated with regulating immune responses being recognized as antigens by the immune system (DONNELLY et al., 2008).

In *T. gondii*, *P. falciparum*, and *Babesia microti*, the peroxiredoxin enzyme (Prx) was connected to the detoxification of hydroperoxides (KAWAZU et al., 2001). Moreover, the oxidative stress induced by monesin increased the peroxiredoxin transcripts levels of Prx2 in intracellular *T. gondii* (Charvat and Arrizabalaga 2016), showing that Prx2 is involved in the antioxidant stress response in this parasite. Immunization with the recombinant enzyme (rPrx1) decreased the mortality in *T. gondii* infected mice, suggesting Prx1 has the potential to become a new vaccine antigen against toxoplasmosis (Fereig et al., 2017).

Significant peroxiredoxin (NcLIV_062630) abundance in *N. caninum* excreted-secreted antigens (ESA) was observed by proteomic analysis (OLIVEIRA, 2013). This protein, unexplored in this parasite so far, has a potential role against oxidative stress that may support mechanisms of proliferation and survival. Therefore, we performed a molecular and functional characterization of the *N. caninum* peroxiredoxin (NcPrx) to provide new insights into *N. caninum* redox defense.

Materials and methods

In silico analysis of NcPrx sequence

The NcPrx sequence (NcLIV_062630) obtained from the ToxoDB database (version 46.0) was submitted to BLASTp 2.0. From the BLASTp results, the closer Prx homolog *Homo sapiens* (Hs_PrX; NP_005800.3), *Toxoplasma gondii* (Tg_PrX1; AF305718_1), *Plasmodium berghei* (Pb_PrX1; XP_022713514.1) and *Besnoitia besnoiti* (Bb_PrX1, FH38369.1) were selected and aligned with NcPrx (XP_003885863.1) by MegAlign software using hierarchical clustering method (Clustal W algorithm). The identity and similarity predictions were calculated by Genedoc software, and the alignment image was generated by Multalin software (Multiple sequence alignment by Florence Corpet). The presence of signal peptide was analyzed in SignalP 3.0 and domains at Pfam 3 (FINN et al., 2016).

***Neospora caninum* cultivation and tachyzoite protein extract**

N. caninum Nc-1 (DUBEY et al., 1988) tachyzoites were cultured in monolayers of Vero cell in RPMI-1640 at 37°C, 5% CO₂. The Vero cells were propagated in RPMI-1640 supplemented with 5% fetal bovine serum (FBS) under the same conditions. The parasites were purified after lysis of Vero cells using a needle (0,45x13mm) followed by syringe filtration at 5 µm (syringe filter). Next, the suspension was centrifuged at 5,000 g for 3 minutes at 4°C and the pellet was suspended in PBS. *N. caninum* tachyzoites were counted in a hemocytometer and normalized to 2×10⁸ tachyzoites/ml. The *N. caninum* tachyzoite protein extract and Vero protein extract (control) were obtained by lysis of the tachyzoites (1×10⁸/ml) or the Vero cells (2×10⁶/ml) in 8 M urea described by Pereira et al (PEREIRA et al., 2011).

***N. caninum* RNA extraction**

Total RNA was obtained from purified *N. caninum* tachyzoites using Trizol™ reagent (Thermo Fisher Scientific, Massachusetts, USA) following the manufacturer's instructions. Briefly, the RNA was recovered from the inorganic phase by precipitation in absolute isopropyl alcohol. The pellets containing RNA were washed with 75% ethanol and air-dried. The samples were diluted in nuclease-free water and quantified by capillary UV spectrophotometry (Genequant, GE Healthcare, USA). RNA Samples with the appropriate degree of purity (260/280nm ratio of between 1.6 and 2.0) were selected for cDNA synthesis.

Synthesis of cDNA, amplification and NcPrx ligation in pET28

The single complementary strand DNA (cDNA) was generated from total *N. caninum* RNA (1.5 µg) using the GoScript™ Reverse Transcription System (Promega, Wisconsin, USA), following the manufacturer's instructions. The NcPrx (NcLIV_062630) coding sequence was amplified (Expand™ High Fidelity PCR System, Roche) using the primers forward PrxForEco (5' TTTGAATTCGCCCCGACGGTGTCTCAG 3') and reverse PrxRevHind (5' TTTAAGCTTGTTGGCCGGGCAGACTTC 3'), flanked by the EcoRI and HindIII restriction sites (underlined). Next, the fragment of NcPrx was purified and inserted into the pGEM-T-easy cloning vector (Promega, Wisconsin, USA), transformed into

Escherichia coli electrocompetent bacteria (Top 10, Invitrogen, CA, USA) by electroporation (XCELL™, MICROPULSER™, BioRad, Hercules, CA, USA), and selected with 50 µg/ml Ampicillin. Subsequently, the pGEM-NcPrx vector was treated with restriction enzymes (EcoRI and HindIII) and ligated in a previously prepared pET28a(+) plasmid, using a T4 ligase (Thermo Fisher Scientific, MA, USA). The pET28-NcPrx plasmid was transformed by electroporation into *E. coli* BL21 (DE3) and selected with kanamycin (50 µg/ml).

Expression and purification of rNcPrx

The colonies of transformed *E. coli* BL21 (DE3) containing pET28a (+)-NcPrx were incubated in LB medium (Luria-Bertani) with kanamycin (50 µg/ml) for 18 hours, 37°C, 150 rpm, then the suspensions were inoculated (1:100) in LB with kanamycin (50 µg/ml) and incubated in 37°C, 150 rpm for 3 hours. Next, the cultures were cooled down by ice incubation for 30 minutes and the expression of recombinant thioredoxin-dependent peroxide reductase (rNcPrx) was induced by isopropyl β-D-1-thiogalactopyranoside (IPTG, 0.25 mM) at 18° C for 16h, 150 rpm. After centrifugation (15,000 g, 15 minutes), the supernatant was discarded and the bacterial pellet sonicated (15 cycles of 30 seconds at 70% amplitude; QSonica, Q500-110, CT, USA). Sonication was performed with different lysis buffer for immunization (denaturant lysis buffer: 8 M urea, 20 mM Sodium phosphate 500 mM NaCl, pH 8.0) or enzymatic assays (native lysis buffer: 50 mM Tris HCl, 0.3 mM β-mercaptoethanol, 5% v/v glycerol, 0.2% TritonX-100). After sonication, samples were centrifuged (10000 g, 15 minutes, 4°C) and the supernatant filtered in a 0.22 µm syringe filter (Millipore, MA, USA). The protein purification was carried out on a nickel column (packed GE PD-10 columns, NiSephrose, GE, USA). NcPrx purification under native conditions was performed with elution buffer (50 mM Tris HCl, 0.3 mM β-mercaptoethanol, 5% glycerol, 0.05% TritonX-100) containing 250 mM imidazole followed by desalting in Sephadex G-25 PD-10 column (GE Healthcare, UK) in reaction buffer (50 mM Tris, 0.05% Triton and 5% glycerol). The purified protein was concentrated in Pierce™ Centrifuge Column (Thermo Fisher, MA, USA). For immunization procedures, NcPrx was purified under denaturant conditions in a pH gradient (8.0 – 4.0) of urea buffer (8 M Urea, 20 mM sodium phosphate, 500 mM NaCl). Finally, the integrity and the purity of the recombinant proteins were confirmed by SDS-PAGE, followed by Coomassie Brilliant Blue staining.

Bradford assay was used for the estimation of protein concentration (BRADFORD, 1976).

Mass spectrometry

rNcPrx was separated by SDS-PAGE and the predominant bands were excised and submitted to trypsin digestion (Oliveira, 2013). The samples were diluted in 1:1 proportion in an alpha-cyano-4-hydroxycinnamic acid matrix (10 mg/mL in 50% acetonitrile and 0.1% TFA) and spotted in MALDI plates. Polyethylene glycol (PEG) was used as a calibrator diluted in a matrix solution (1:1). The identification was performed in a MALDI-TOF-TOF-MS equipment (Axima Performance, Kratos-Shimadzu, UK-Protein Chemistry Center- FMRP-USP). The results were searched against the protein data bank of *N. caninum* ToxoDB (versão 46), using the Mascot software (version 2.6.1, Matrix Science, London, UK, <http://www.matrixscience.com>). Carbamidomethylation was chosen as a fixed modification in the analysis for the identification of peptides. Oxidation of methionine was set to variable modification. Peptide and ion tolerance were established at 50 ppm and 0.6 Da, respectively, allowing the loss of two cleavages. Protein and peptide identifications with a probability higher than 95% were accepted.

Effect of H₂O₂ on rNcPrx dimerization

The purified rNcPrx (62 μ M in 10 mM DTT) was incubated with a range of H₂O₂ concentrations (0, 0.2, 2, 20 mM) for 10 minutes in buffer (1.5 M Tris-HCl, pH 8.0, 10% SDS, EDTA 20 mM, 0.05% bromophenol blue, 40% glycerol). In parallel, an identical assay was performed without DTT. Next, the samples were boiled at 95°C for 5 minutes and separated by SDS-PAGE (12.5%) followed by Coomassie Brilliant Blue staining. The band intensity, measured by the ImageJ software, was calculated for rNcPrx dimers and monomer in each condition in relation to control (rNcPrx in reaction buffer without an oxidizing or reducing agent).

Production of anti-rNcPrx serum

Male BALB/c mice (6–8 weeks of age) were housed under controlled temperatures (23°C \pm 2°C) with 12-hour light/dark cycles and were supplied with food and water *ad libitum*. The animals were acquired from the vivarium of the campus of the University of Sao Paulo at Ribeirao Preto, Sao Paulo, Brazil and housed in the animal facility of the School of Pharmaceutical Sciences of Ribeirao Preto, University of Sao

Paulo. Mice were immunized by subcutaneous injection with 50 µg of rNcPrx protein (1 µg/µl, experimental groups) or 50 µl of urea 8 M (negative control) in aluminum hydroxide (1:1, 2% Alhydrogel, Brenntag, Biosector A/S, Denmark) as an adjuvant at the weeks 0, 3, 5 and 7. Ten days after the last immunization, animals were anesthetized with ketamine (80 mg/kg) and xylazine (8 mg/kg) (KAWAI et al., 2011) by the intraperitoneal route. The euthanasia was performed by exsanguination (cardiac puncture), followed by the collection of the hyperimmune serum. All animal experimental procedures were conducted in accordance with the Animal Research Ethics Committee of the School of Pharmaceutical Sciences of Ribeirao Preto, University of Sao Paulo (CEUA-FCFRP, process 17.5.278.60.8). The authors assert that all procedures contributing to this work comply with the ethical standards of the relevant national and institutional guides on the care and use of laboratory animals.

Enzyme-Linked Immunosorbent Assay (ELISA)

The recombinant protein NcPrx (1.25 µg/ml) or the *N. caninum* protein extract (5 µg/ml) were diluted in coating buffer (60 mM Na₂CO₃) and immobilized in a 96-well plate (ELISA-Plate, Microlon, flat-bottom, Greiner Bio-One, Austria) for 18 hours at room temperature. The blocking occurred for one hour with 0.5% gelatin (Sigma-Aldrich, St. Louis, USA) diluted in PBS-T (0.5% Tween-20, in PBS). Subsequently, the serum anti-rNcPrx (1:500, 1:1000, 1:2000, and 1:4000) or serum anti-urea (1:500, negative control) diluted in PBT-T with 0.05% gelatin were added and incubated for one hour at 37°C. As secondary antibody, peroxidase-conjugated rabbit anti-mouse antibodies (IgG – whole molecule – Peroxidase, Sigma-Aldrich- USA) were incubated at 37°C for one hour. Washes (3X) were performed with PBS-T between every incubation step. The TMB chromogen solution (3,3',5,5'-Tetramethylbenzidine; Invitrogen, USA) was added and the plate was incubated for 15 minutes at room temperature, in the dark. The reaction was interrupted by the addition of HCl (2 M). The absorbance was measured at 450 nm in the ELISA reader (Synergy H1, Biotek, USA).

Western blot analysis

N. caninum tachyzoite protein extract, recombinant rNcPrx, and Vero cell extract (control) were diluted in sample buffer (0.5 M Tris HCl pH 6.8, 10% glycerol, 2% SDS; 0.01% bromophenol blue) and separated by SDS-PAGE (12.5%). After the

electrophoresis, the proteins were electrically transferred to a PVDF membrane (Immobilon™-P, Millipore, USA) for 75 minutes. Subsequently, the membranes were blocked with 0.8% PBS-GT (0.8% swine gelatin, in PBS-T) for 1 h followed by a 16 h incubation with the anti-rNcPrx polyclonal antiserum (1:5000) at room temperature. Anti-mouse IgG conjugated to peroxidase (1:10000, Sigma, USA) was used as a secondary antibody. Finally, membranes were incubated with Luminol (SuperSignal West Pico Chemiluminescent Substrate, Thermo Fisher Scientific, MA, USA) for 5 min, exposed to radiographic film and documented with a densitometric scanner (Image Scanner, GE Healthcare, UK) using the LabScan v 5.0 software.

Localization of native NcPrx by multi-photon microscopy

The localization of native NcPrx in the *N. caninum* was performed using microscopic analysis as described previously (PEREIRA et al., 2020), with few modifications. Briefly, Vero cell monolayers, previously cultured over coverslips in 24-well plates (Corning, NY, USA), were inoculated with *N. caninum* (2×10^5 tachyzoites/well) and incubated during 72 h, 37°C, 5% CO₂ for invasion and proliferation. Next, Mitotracker (400 nM, Red CMXRos, Life Technologies) and was incubated for 20 minutes for incorporation of the dye (37 °C, 5% CO₂). The cells were fixed with 3.6% formaldehyde (Sigma-Aldrich, USA) in PBS for 1 h at 25 °C, followed by permeabilization with 0.2% Triton X-100 and blocking (3% bovine serum albumin, 20 mM glycine in PBS) for 45 minutes at 25°C. The cells were incubated with anti-rNcPrx serum (1:2000) in 0.3% BSA and 2 mM glycine (in PBS) for 45 minutes. Subsequently, the samples were incubated with the secondary antibody (anti-mouse) conjugated to AlexaFluor® 488 (1:500, Molecular Probes®, USA) for 45 minutes. DAPI (4',6'-diamino-2-fenil-indol) was used to detect the nucleus. The experiments were carried out in a multiphoton microscope (LSM 780, Carl Zeiss, Axio Observer, Cellular and Tissue Image Center, Multi-photon Microscopy Multi-User Laboratory, FMRP-USP). The image capture was performed using the 63× objective with a 4× optical zoom in oil immersion. The 490/525 nm, 358/461 nm, and 579/599 nm excitation/emission wavelengths were applied for the detection of Alexa Fluor 488, DAPI, and Mitotracker, respectively. The captured images were processed in ImageJ 1.46r (National Institute of Health, USA).

Antioxidant activity of NcPrx

The antioxidant activity of rNcPrx was evaluated using the mixed-function oxidation (MFO) assay (PRIYATHILAKA et al., 2016). The test determines the ability of rNcPrx to protect DNA from damage under oxidative conditions. In a final volume of 100 μ l, 30 μ l of MFO mix reaction buffer (40 μ M FeCl₃, 10 mM DTT, 20 mM EDTA, 25 mM HEPES, pH 7) was mixed with 60 μ l of rNcPrx dilutions (610, 305, 152.5, 76.2, 38.1 μ g/ml) or PBS (control). The reaction was incubated at 37°C for one hour, followed by the addition of 500 ng of pGEM-t-easy plasmid DNA (10 μ L). The samples were incubated at 37°C for 2 hours and analyzed on an agarose gel electrophoresis (0.8%) stained with ethidium bromide.

Evaluation of rNcPrx peroxidase activity

The rNcPrx peroxidase activity was evaluated by a method described in (PUSHPAMALI et al., 2008). rNcPrx (25,50,100 μ g/mL) was incubated in reaction buffer (HEPES 50mM, pH 7,0 and DTT 10mM) for 30 minutes. Subsequently, hydrogen peroxide (H₂O₂, 67 μ M- 50 μ L) was added and the reaction was interrupted by trichloroacetic acid 26%(v/v) (volume of 40 μ L) after 0, 150, 300, 450 and 600 seconds. Finally, 40 μ l of (NH₄)₂Fe(SO₄)₂ (10mM) and 20 μ L of potassium thiocyanate (KSCN) (2.5M) were added, resulting in purple red complex with intensity proportional to the hydrogen peroxide concentration. The remaining H₂O₂ were evaluated by absorbance measure at 475nm. The H₂O₂ were calculated by equation: % H₂O₂ clearance = [(A₀ - A_x)/A₀] x 100%, A₀: absorbance at 0 seconds and A_x: absorbance at x seconds (where x can be 150, 300, 450 or 600 seconds). Two independent assays were performed, in duplicate.

NcPrx dimerization assay evaluation by Western blot analysis

Because of the catalytic cycle of typical 2-Cys peroxiredoxin, the oxidative status of the enzyme may be evaluated by SDS-PAGE or western blot analysis (COX; WINTERBOURN; HAMPTON, 2010) once the monomer and dimer represent the reduced and the oxidized forms of the enzyme, respectively. The protocol was performed as described by Cox et al. (2010) with modifications. Extracellular or intracellular tachyzoites (cultivated in Vero cell for 48 hours), were incubated with different concentrations of H₂O₂ (10-500 μ M) or PBS, reduced and non-reduced control (PBS R and PBS NR, respectively), in different time intervals (15 and 75 minutes). Afterwards, the treatments were removed through centrifugation (5 min, 8000g) and the cells were

alkylated in N-ethylmaleimide (NEM-Sigma) 100 mM for 10 min (PBS, NEM 100mM, protease inhibitor (ROCHE), catalase 20ug/mL (Sigma)) and lysed in Triton-X-100 1%. After the removal of the insoluble material, samples were quantified by BCA (Sigma) and concentration adjusted (10 ug/sample) for the western blot. All samples were diluted in SDS loading buffer 5× (0.5 M Tris HCl pH 6.8, 10% glycerol, 2% SDS; 0.01% bromophenol blue), except the reduced PBS group that was diluted in SDS loading buffer 5x containing DTT (50mM) and boiled at 95°C for 5 minutes. The samples were separated by SDS-PAGE (12,5%). Next, the proteins were transferred to PVDF membrane (Immobilon™-P, Millipore, USA) in semi-dry system at 60 mA for 75 minutes. The membranes were blocked in 0,8% swine gelatin in PBS-GT for 1 hour followed by incubation with mouse polyclonal serum anti-rNcPrx (1:2500) or mouse monoclonal serum anti-β-actin (1:2000, Santa Cruz Biotechnology) at room temperature for 16 hours. After washing steps, the membranes were incubated in rabbit secondary antibody anti-mouse IgG (Sigma-Aldrich, 1:5000 for NcPrx and 1:10000 for β-actin). Finally, the membranes were incubated with Luminol (SuperSignal West Pico Chemiluminescent Substrate, Thermo Fisher Scientific, USA) for 5 minutes and images were acquired by ChemiDoc Touch Imaging System (Multi-User Nucleic Acid Sequencing Laboratory (LMSeq)- FCFRP). Band intensity analyses were performed by ImageJ software. The signal intensity (SI) of each group was corrected concerning the β-actin protein expression and normalized using the non-treated control. The dimerization percentage was defined by the following equation: $(SI \text{ Dimer} / (SI \text{ dimer} + SI \text{ monomer})) * 100$.

Statistical analysis

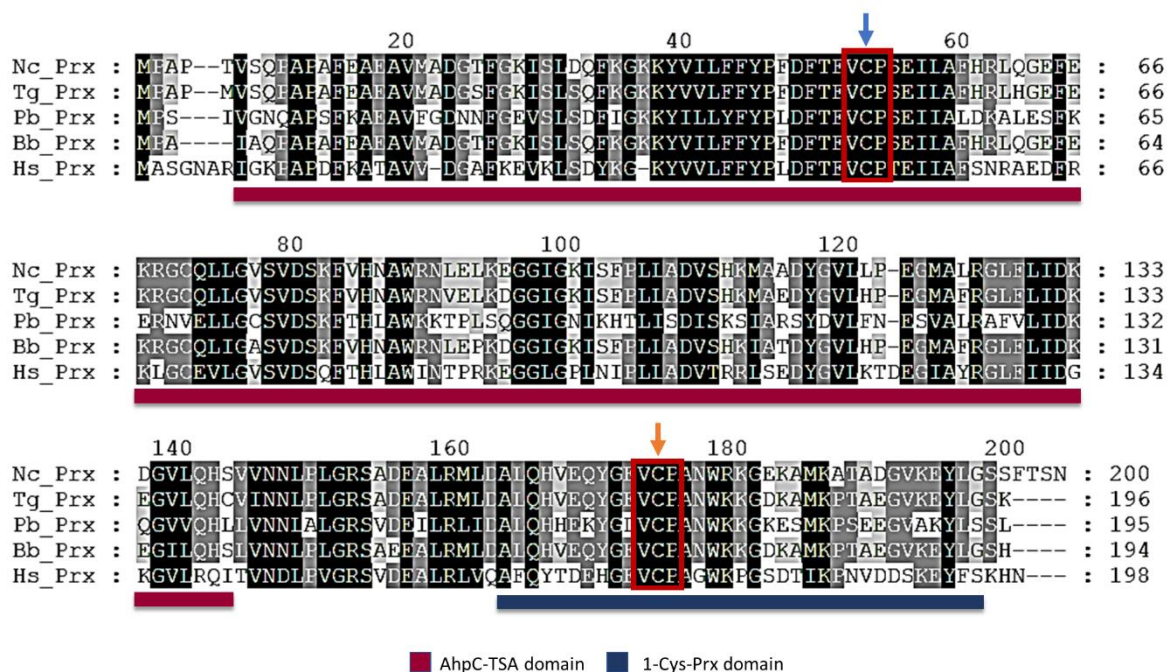
The ELISA assays were analyzed by the software GraphPad Prism 8.0 (Graph Pad, USA). The results were expressed as mean ± standard error, followed by the One-way analysis of variance ANOVA, Bonferroni post-test. The statistical significance was considered when the level of statistical error was lower than 5% (or $p \leq 0.05$).

Results

In silico analysis of *Neospora caninum* thioredoxin-dependent peroxide reductase

The *N. caninum* thioredoxin-dependent peroxide reductase (NcPrx) protein sequence revealed homology with the peroxiredoxin of *Besnoitia besnoiti*; *Plasmodium berghei* ANKA and *Toxoplasma gondii*, *Homo sapiens* with identity/similarity values (I/S%) of 87/93%, 54/73%, 89/94%, 51/70% respectively. The predicted isoelectric point and molecular weight of NcPrx were 6.35 and 22.02 kDa, respectively (ToxoDB). NcPrx has the domains Ahp C-TSA (PF07992) and 1-cysPrx-C (PF10417.8) that belong to the family of alkyl-reductase hydroperoxide (AhpC) and thiol-specific antioxidant (TSA) (AhpC/TSA family; PF00578) and to the thioredoxin-like superfamily (TRX; Clan CL0172) (Fig. 1). Moreover, two Val-Cys-Pro (VCP) motifs, conserved in peroxiredoxins, were identified in NcPrx (Fig.1, red boxes). The redox-active amino acid (peroxidatic cysteine, C_P) and the resolving cysteine (C_R), at positions 51 and 171, respectively, were also predicted for NcPrx (Fig.1, arrows).

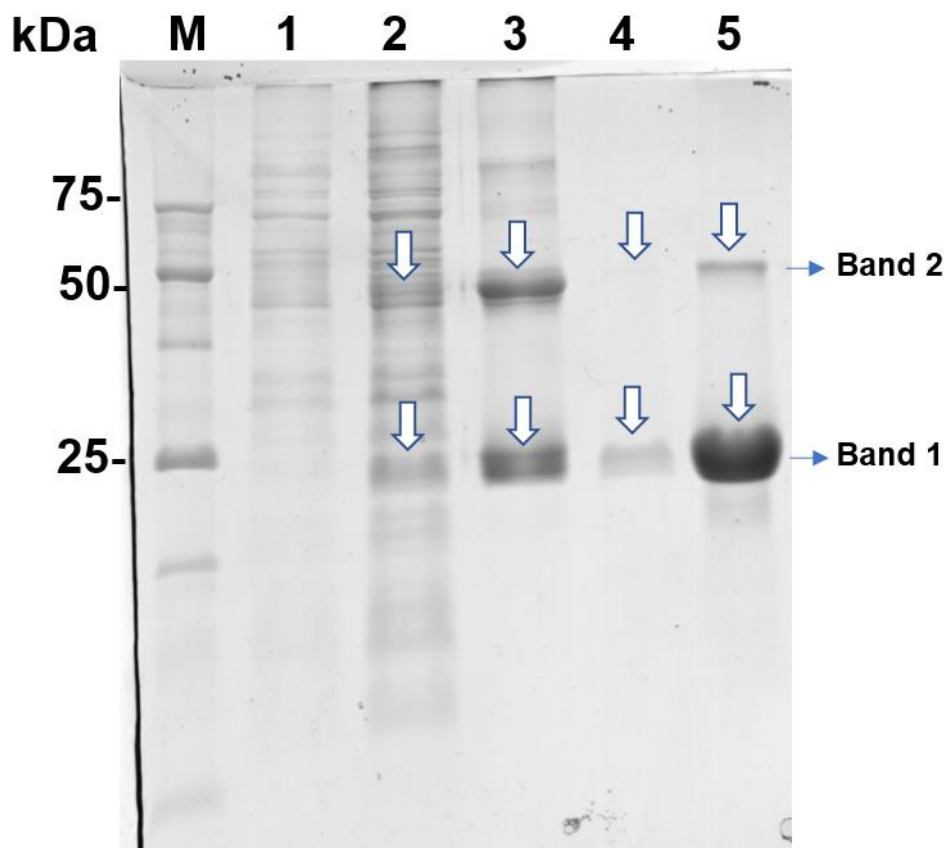
Figure 1 Multiple alignments of *N. caninum* thioredoxin-dependent peroxide reductase (NcPrx) with human and apicomplexan homologues. The Prx sequences of *N. caninum* (Nc_Prxx; XP_003885863.1), *T. gondii* (Tg_Prxx1; AF305718_1), *P. berghei* (Pb_Prxx1; XP_022713514.1), *B. besnoiti* (Bb_Prxx1; PFH38369.1) and *H. sapiens* (Hs_Prxx; NP_005800.3) were aligned using the ClustalW algorithm. Amino acids highlighted in black represent total identity and amino acids highlighted in gray represent similarity among sequences. The red box stands for the “VCP” motifs. Red bar: Ahp C-TSA domain. Blue bar: 1-cysPrx-C domain. The blue and orange arrows indicate the predicted redox-active site (C_P, peroxidatic cysteine, 51-aa) and the resolving cysteine (C_R, 171-aa), respectively.



Expression and purification of rNcPrx

The recombinant NcPrx (rNcPrx) protein was successfully cloned in pET28a and expressed in *E. coli* as a His-tagged fusion protein that was purified using Ni-affinity chromatography (Fig. 2). Compared to the non-induced sample, a prominent band of ~ 24 kDa was observed in the IPTG incubated culture extract (Fig. 2, lanes 1 and 2). rNcPrx was extracted and purified under denaturant and native conditions (Fig. 2, lanes 3 and 4), allowing the desalinization and concentration of the protein (Fig. 2, lane 5). Besides, it was detected a ~ 48 kDa band in all rNcPrx positive samples, suggesting the formation of the dimeric state of the protein (Fig. 2). Finally, the rNcPrx was identified by MS/MS (NCLIV 062630, 22.1 kDa, pI 5.96) through recognition of 38 and 31 peptide spectrum matches (PSM) for its monomeric (band 1, fig. 2) and dimeric forms (band 2, fig.2) respectively (Supplementary file 1).

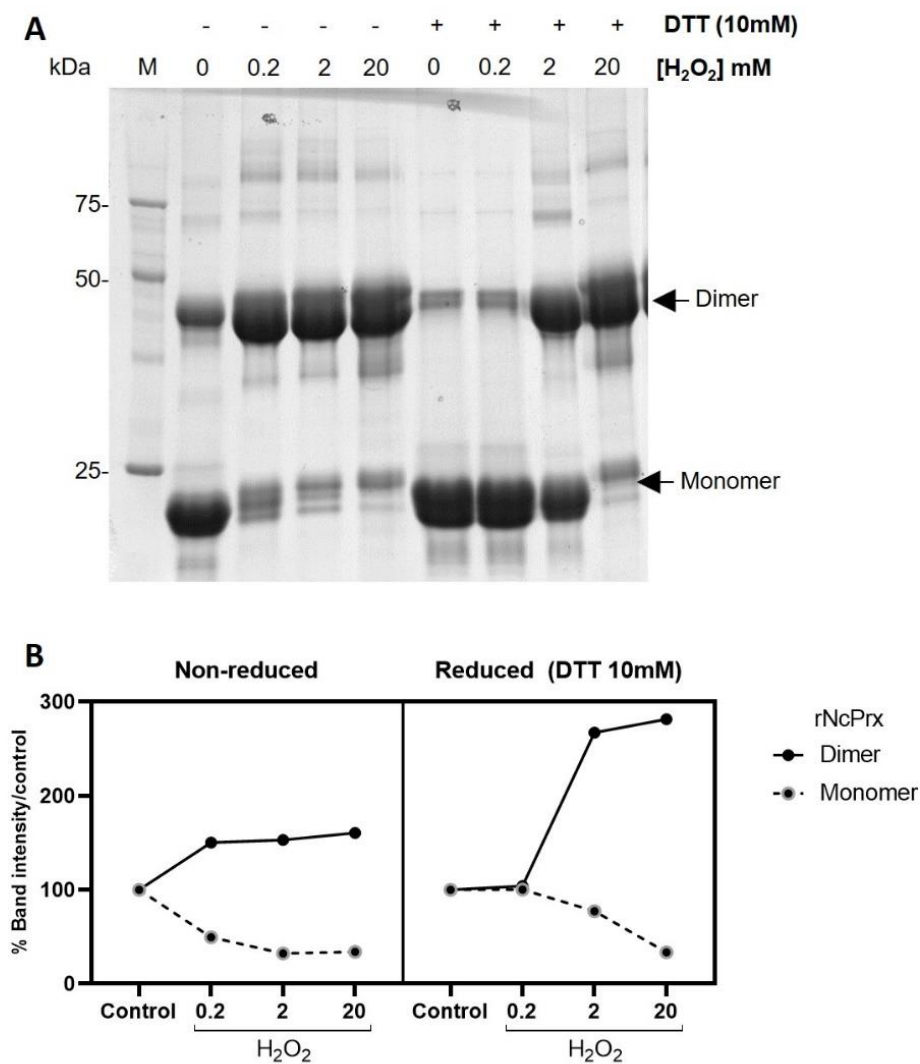
Figure 2 Expression and purification of the rNcPrx protein. The *E. coli* BL21 was electroporated with the pET28-NcPrx plasmid and the expression was induced with IPTG. The rNcPrx was purified in nickel-sepharose columns under native and denaturant conditions. M: Protein molecular weight marker. Lane 1: Non-induced culture. Lane 2: IPTG induced culture. Lane 3: rNcPrx purified under denaturant conditions. Lane 4: rNcPrx purified under native conditions. Lane 5: Desalted and concentrated rNcPrx. Arrows indicate monomeric (band 1) and dimeric (band 2) rNcPrx.



H₂O₂ effects on rNcPrx dimerization

In the absence of DTT and H₂O₂ rNcPrx showed two predominant bands, corresponding to the monomeric and dimeric forms of the protein (Fig. 3.A). The addition of H₂O₂ oxidized the rNcPrx, increasing the amount of its dimeric form (~ 48 kDa, oxidized) in contrast to the decrease of the monomeric form (~ 24 kDa, reduced) (Fig. 3.A). The DTT incorporation increased the proportion of reduced rNcPrx (monomeric form) in H₂O₂ concentrations below 2 mM (Fig. 3.A). The reducing effects of DTT was completely abolished in samples incubated with > 20 mM H₂O₂ (Fig. 3.A). In buffers without oxidant or reducing agents, the proportion of monomeric:dimeric rNcPrx was 13:8 (Fig. 3.B).

Figure 3 H₂O₂ effect on the rNcPrx dimerization. (A) rNcPrx SDS-PAGE analysis of rNcPrx in the presence and/or absence of DTT (10 mM) incubated with dilutions of H₂O₂ (0, 0.2, 2 and 20 mM). The monomer and dimer forms correspond to the reduced (~ 24 kDa) and oxidized rNcPrx (~ 48 kDa), respectively. (B) Percentage (%) of band intensity quantification of the monomer (dotted line) and dimer (black line) in relation to the control (rNcPrx in reaction buffer 50 mM Tris, 0.05% Triton and 5% glycerol).

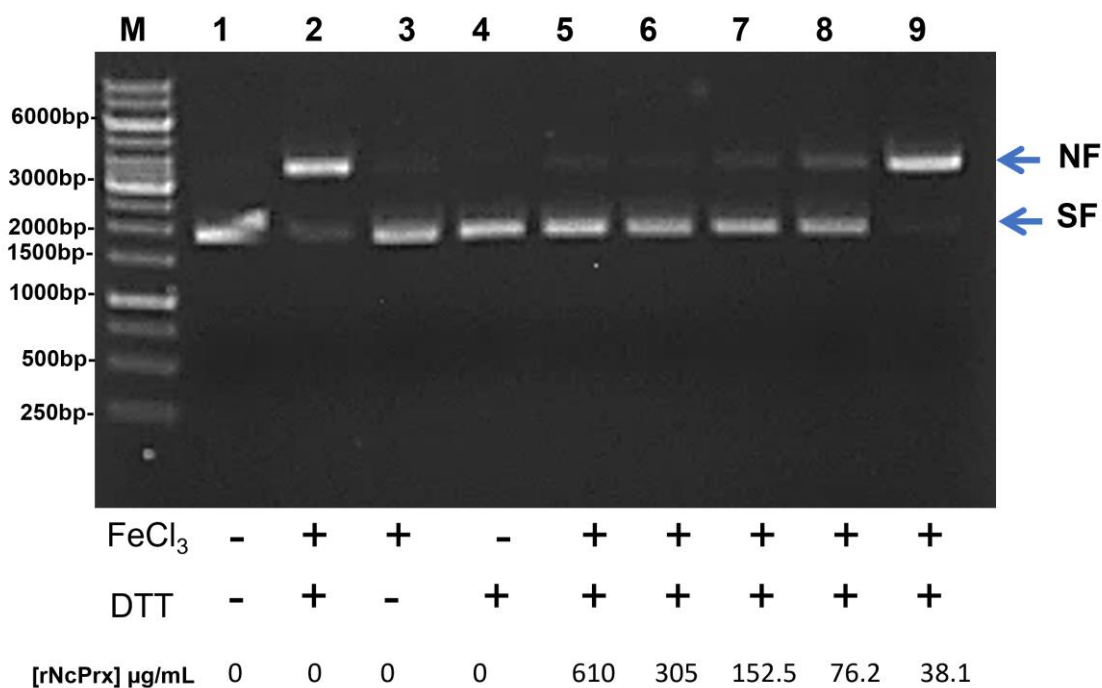


Antioxidant Activity Assay

In the mixed-function oxidation (MFO) assay, hydroxyl radicals are produced after the reaction of FeCl₃ with DTT (SAURI et al., 1995). These radicals promote plasmid DNA damage by converting its supercoiled form, present in the negative control (Fig. 4, lane 1), into the nicked form as observed for the positive control (Fig.4, lane 2). FeCl₃ or DTT applied alone did not induce the formation of nicked plasmids (Fig.4, lanes 3 and 4, respectively). The addition of rNcPrx (610 µg/ml – 76.2 µg/ml) into the MFO

reaction protected the plasmid DNA, which mostly remained in a supercoiled form (Fig. 4, lanes 5 - 8). The rNcPrx antioxidant function in protecting the DNA was mostly extinguished at 38.1 $\mu\text{g/ml}$ (Fig. 4, lane 9).

Figure 4 Antioxidant effects of rNcPrx on plasmid DNA. pGEM-t-easy plasmid DNA was incubated with the MFO mix reaction buffer and dilutions of rNcPrx for 2 h, 37°C. As controls FeCl₃ or DTT applied alone were incubated under the same conditions. After incubation, the samples were separated in an 0.8% agarose gel electrophoresis and stained with ethidium bromide. M: DNA ladder. All lanes contain pGEM-t-easy plasmid DNA incubated with: (Lane 1) control buffer (20 mM EDTA, 25 mM HEPES, pH 7); (Lane 2) MFO mix reaction buffer (40 μM FeCl₃, 10 mM DTT, 20 mM EDTA, 25 mM HEPES, pH 7); (Lane 3) FeCl₃ (40 μM FeCl₃, 20 mM EDTA, 25 mM HEPES, pH 7); (Lane 4) DTT (10 mM DTT, 20 mM EDTA, 25 mM HEPES, pH 7); (Lanes 5 to 9) MFO reagent with dilutions of rNcPrx enzyme (610 $\mu\text{g/ml}$, 305 $\mu\text{g/ml}$, 152.5 $\mu\text{g/ml}$, 76.2 $\mu\text{g/ml}$, 38.1 $\mu\text{g/ml}$, respectively). Arrows indicate the nicked (NF) and supercoiled (SF) forms of the plasmids.

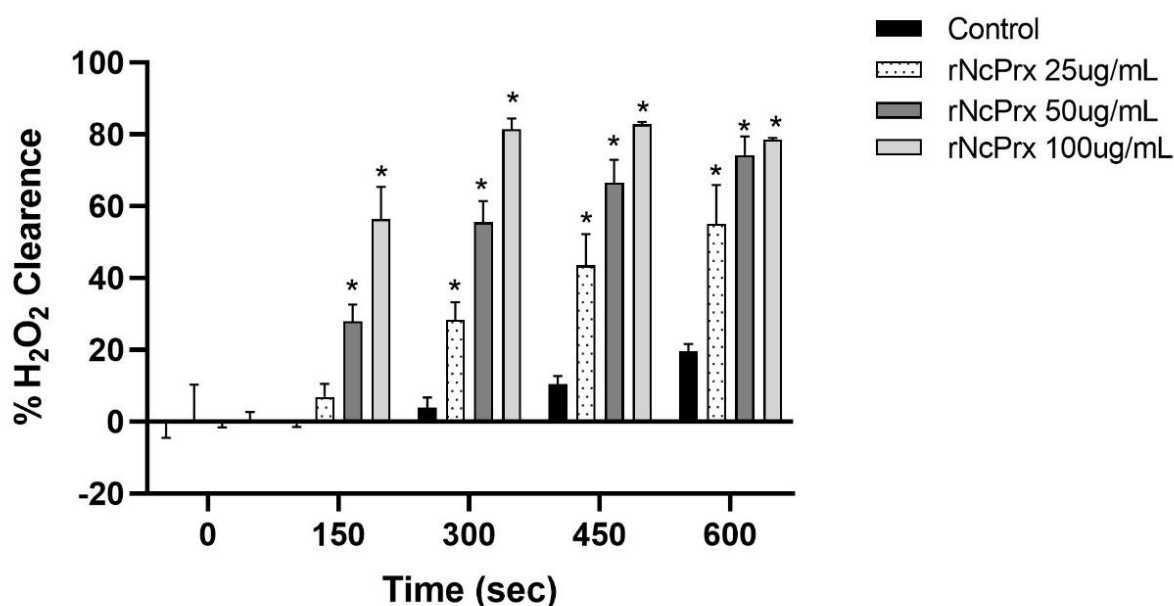


Peroxidase Assay

In vitro peroxidase activity of rNcPrx in the presence of DTT was evaluated by the ferrothiocyanate system measuring the H₂O₂ clearance over time in a range of rNcPrx concentrations. Both time and concentrations influenced the H₂O₂ clearance in the reaction (Fig. 5, time, $p < 0.0001$; enzyme concentration $p < 0.0001$; interaction time vs. enzyme concentration $p < 0.0001$). The H₂O₂ clearance at rNcPrx 50 and 100 $\mu\text{g/ml}$ was higher than the control after 150 seconds (Fig. 5, $p < 0.0001$). Otherwise, the H₂O₂

clearance at rNcPrx 25 μ g/mL becomes higher than control after 300 seconds of reaction (Fig. 5, $p < 0.0001$).

Figure 5 *In vitro* rNcPrx peroxidase activity in the presence of DTT. The H₂O₂ clearance over time (seconds) and at crescent rNcPrx concentrations (25,50,100 μ g/mL) were measured to determine rNcPrx activity. The buffer reaction was composed of 50mM HEPES, pH 7.0, 10 mM DTT, 0.2 mM H₂O₂. After incubation for 0, 150, 300, 450, 500 seconds, the reaction was stopped by trichloroacetic acid (10% w/v) addition. The remaining H₂O₂ was detected at 480nm of the ferrothiocyanate complex resulting of 10 mM Fe(NH₄)₂(SO₄)₂ and 0.1 mL of 2.5M potassium thiocyanate KSCN. The results were expressed as mean \pm standard error and the experimental groups were compared by Two-way ANOVA, Bonferroni pos-test. * Indicates $p < 0.0001$, control vs enzyme group, two independent experiments in duplicate).

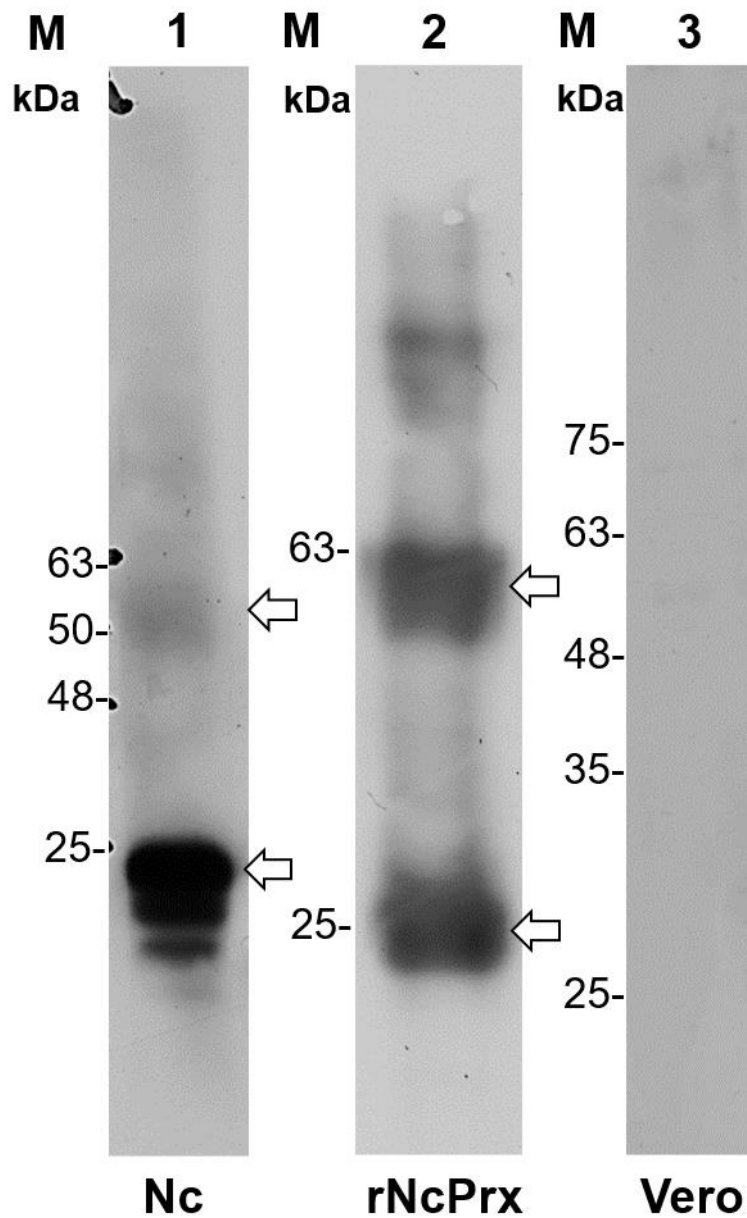


Detection of native and recombinant NcPrx by Western blot

Mice immunizations with the rNcPrx resulted in seroconversion as demonstrated by the ELISA assay (Supplementary file 2). Polyclonal rNcPrx antiserum reacted strongly with immunogen rNcPrx when compared to the negative control ($p < 0.05$) (Supplementary file 2). rNcPrx polyclonal antiserum was highly specific to detect the native monomeric (~ 24kDa Fig. 6, lane 1) and dimeric (~ 48kDa, Fig. 6, lane 1) forms of NcPrx present in the *N. caninum* extract by Western blot analysis. Similarly, rNcPrx was detected in both monomeric and dimeric forms (Fig. 6, lane 2) and there was no reactivity with the extract of Vero cells (Fig. 6, lane 3).

Figure 6 Detection of native and recombinant NcPrx by Western Blot. Purified rNcPrx or extracts of *Neospora caninum* and Vero cells were separated by SDS-PAGE and transferred to PVDF membranes. The membranes were incubated with anti-rNcPrx serum (1:5000), followed by the

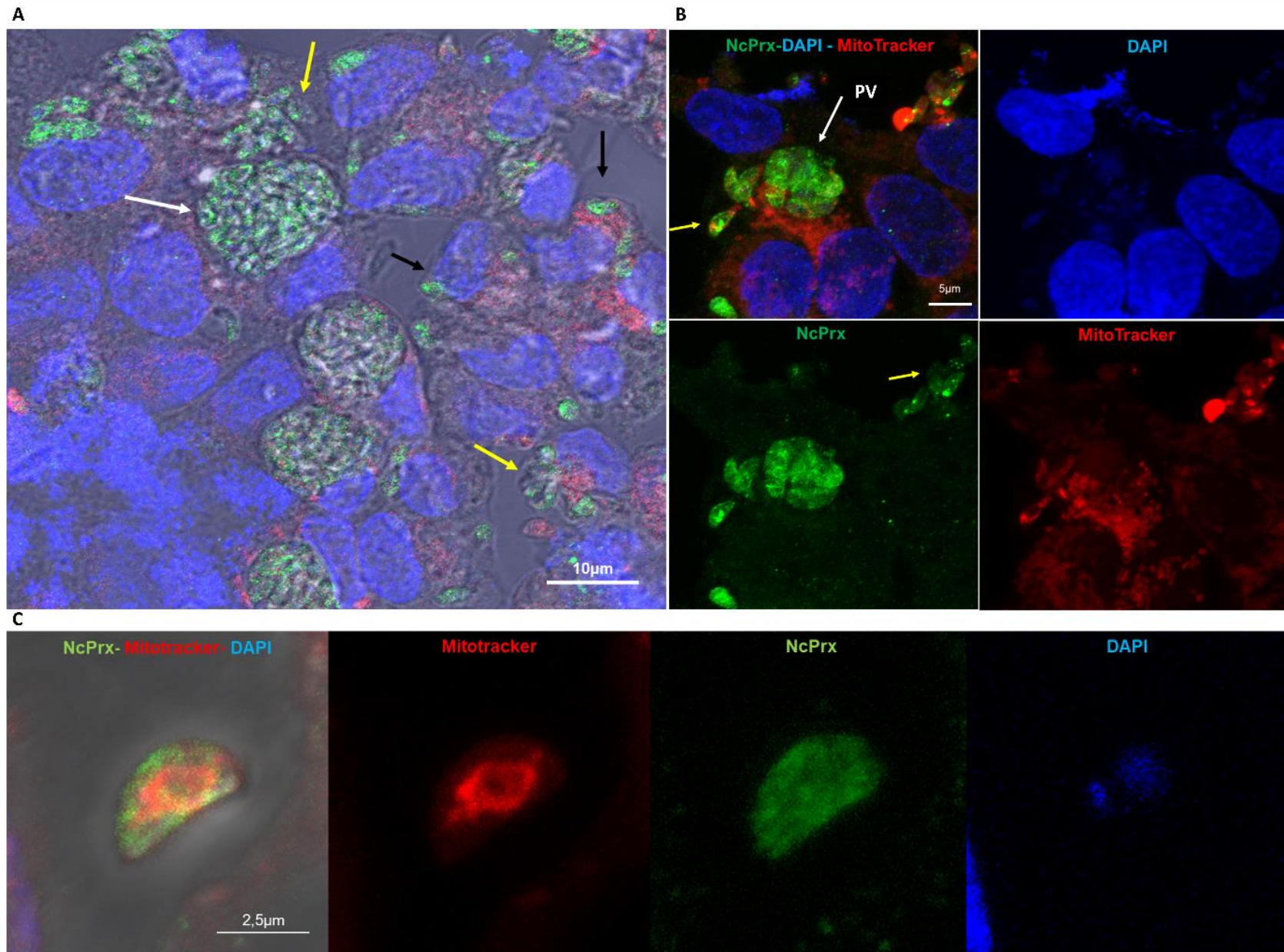
detection with anti-mouse horseradish peroxidase (HRP) conjugated antibody (1:10000). All samples were revealed using the HRP/luminol method. M: molecular weight marker (kDa). Lane 1: *N. caninum* protein extract incubated with anti-rNcPrx. Lane 2: rNcPrx incubated with anti-rNcPrx. Lane 3: Vero protein extract incubated with anti-rNcPrx. Arrows indicate the monomeric and dimeric forms of NcPrx.



Localization of NcPrx and mitochondria in N. caninum tachyzoite

The NcPrx was found delimiting the proliferating tachyzoites in parasitophorous vacuoles (PV), with a low level of fluorescence in outer PV structures (Figure 7.A, white arrow). The PV was located closer to the nucleus and surrounded by mitochondria of the host cell (Fig.7.A-C). Adhered/invaded tachyzoites (black arrows) as well as parasites in the initial phase of proliferation (yellow arrows) were also detected (Fig. 7.A). NcPrx was visualized in the cytosol of isolated (egressed) tachyzoites, and no co-localization was observed with mitochondria, which was located surrounding the nucleus (Fig. 7.B and C). Moreover, granules containing NcPrx were also visualized in the cytosol of isolated tachyzoites (Fig. 7C).

Figure 7 Detection of NcPrx in intra and extracellular *N. caninum* tachyzoites. *N. caninum* tachyzoites were incubated with Vero cell monolayers for 72 h. The cultures were treated with Mitotracker, fixed, permeabilized, and blocked. NcPrx was detected after incubations with the anti-rNcPrx serum and anti-mouse secondary antibody conjugated to Alexa Fluor® 488. Nucleus was labelled with DAPI. (A) Detection of NcPrx in parasitophorous vacuoles (VP). White and black arrows indicate PV and adhered/invaded tachyzoites, respectively. The yellow arrow indicates parasites in the initial phases of proliferation. (B) Detection of NcPrx, mitochondria, and nuclei in *N. caninum* infected cultures. (C) Detection of NcPrx, mitochondria, and nucleus in an isolated (extracellular, egressed) *N. caninum* tachyzoites. The images were acquired by multiphoton microscopy and represent maximum intensity projections of 10 individual optical planes processed by ImageJ software. The bar scales represent 10 μm (A), 5 μm (B) and 2.5 μm (C).

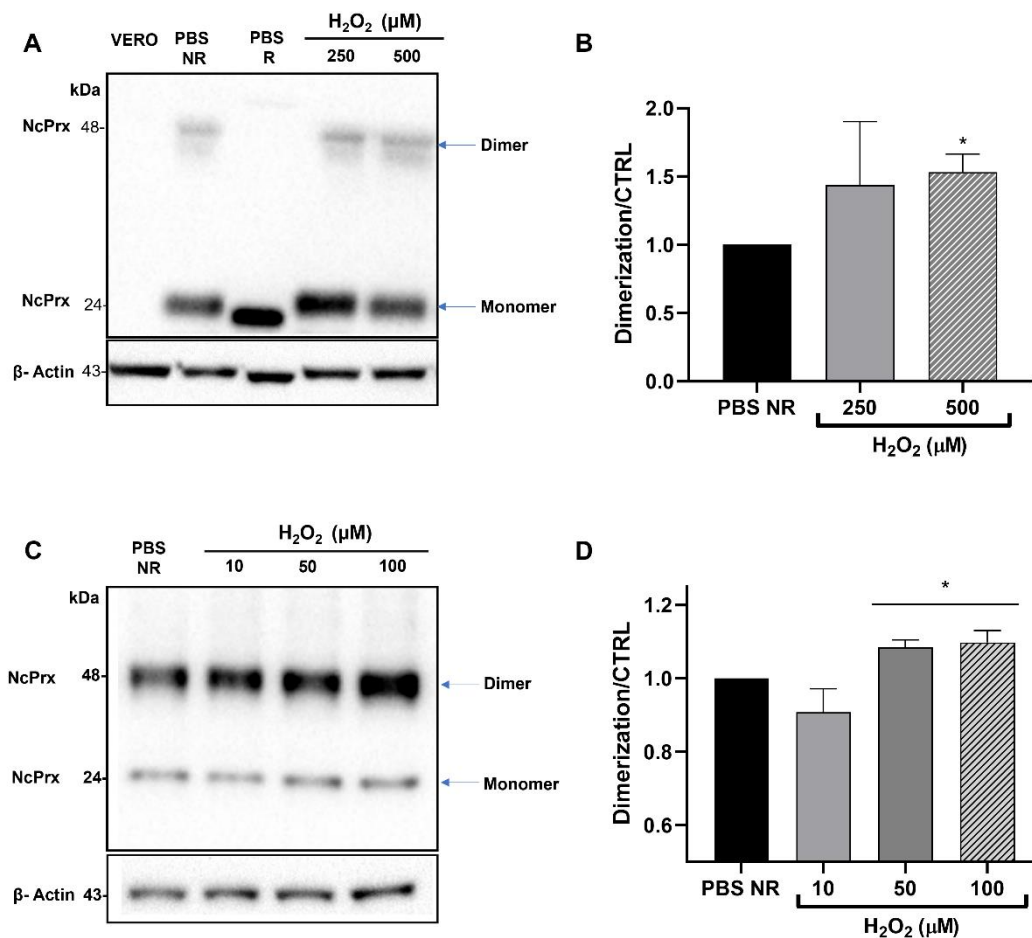


NcPrx dimerization assay

The oxidative status of NcPrx present inside the *N. caninum* tachyzoite was evaluated using the proportion between the dimer (48kDa, oxidized) and the monomer (24 kDa, reduced) forms of NcPrx, respectively. In intracellular tachyzoites, the NcPrx of non-reduced control (PBS NR) demonstrated signs of oxidation in basal conditions (Fig 8.A) with a faint dimeric NcPrx band, which was fully reduced to monomeric form by DTT (PBS R) (Fig 8.A). H₂O₂ treatment at 500 μM, for 75 minutes, increased the dimerization of NcPrx in intracellular tachyzoites (p<0.05, compared to PBS NR, Fig. 8.B) whereas 250 μM of H₂O₂ did not significantly alter the NcPrx status (Fig. 8.B).

In extracellular tachyzoites the H₂O₂ treatment at 50 and 100 μM, for 15 minutes, (Fig. 8.C-D) increased the NcPrx dimerization compared to PBS NR (p<0.05; Fig. 8.D).

Figure 8. NcPrx redox status of intracellular (A and B) and extracellular (C and D) *N. caninum* tachyzoites treated with H₂O₂. (A) Representative blot showing the NcPrx present in intracellular tachyzoites. *N. caninum* inside Vero cells were treated with H₂O₂ (250 or 500 μM) for 75 minutes and NcPrx detected by Western blot. The first column represents the Vero cell extract, non-reduced. PBS NR: Non-reduced control incubated with PBS; PBS R: Reduced control incubated with PBS and DTT (50mM). (C) Representative blot showing the NcPrx in extracellular tachyzoites. Egressed tachyzoites were treated with H₂O₂ (10, 50 or 100 μM) for 15 minutes and NcPrx was detected by Western blot. (A and C) Arrows indicate NcPrx monomeric and dimeric forms. β-actin was the housekeeping protein detected under the same conditions. The molecular weight was indicated by kDa. (B and D) Bar graphs represent the mean ± standard error of NcPrx expression in intracellular (B) or extracellular (D) tachyzoites calculated by signal intensity analysis (SI): (C and D) dimerization/control ratio (SI dimer/(SI dimer+ SI monomer)). *p<0,05 in comparison to non-reduced control (PBS NR) using the test t-student.



Discussion

The redox system has a vital role in apicomplexan parasites. As demonstrated in *Plasmodium sp.*, *Babesia sp.*, *Toxoplasma gondii*, *Cryptosporidium sp.*, the redox system assures the parasite survival dealing with oxidative challenges inside the host cell (BOSCH et al., 2015; COUTO; WOOD; BARBER, 2016; GUEVARA-FLORES et al., 2017). The most common and most studied oxidant molecules are superoxide (O²⁻) and hydrogen peroxide (H₂O₂) (LEI et al., 2015; DIEBOLD; CHANDEL, 2016). Superoxide

dismutase (SOD) catalyzes the dismutation of O_2^- into molecular oxygen and H_2O_2 (Buettner, 2012) that is scavenged by peroxiredoxins, catalases or glutathione peroxidases (RHEE et al., 2001). Despite the relevance of antioxidant enzymes as virulence factors in parasites (PIACENZA et al., 2013; DAS; ROYCHOUDHURY, 2014; ZHANG; FENG, 2018), only SOD (CHO et al., 2004b) and glutathione reductase (VENANCIO-BROCHI et al., 2021) have been characterized in *N. caninum*.

The thioredoxin-dependent peroxide reductase is part of the peroxiredoxins group, comprising enzymes that scavenge organic hydroperoxides, hydrogen peroxide, and thiol components in the cell (WOOD et al., 2003; RHEE; CHAE; KIM, 2005). Likewise, thioredoxin-dependent peroxide reductase of *N. caninum* is a peroxiredoxin family member, characterized by the presence of a conserved peroxidatic cysteine (C_P) (RHEE, 2016). Moreover, the presence or absence of the second cysteine, the resolving cysteine (C_R), is a classification criterion of peroxiredoxins, defining 3 types of Prx (WOOD et al., 2002, 2003). The 1-Cys Prx group has only cysteine peroxidase (C_P), whereas 2-Cys Prx and 2-Cys Prx atypical groups exhibit C_P and C_R . These residues of cysteine interact by an intersubunit disulphide bridge in the 2-Cys Prx group or interact with each other by an intrasubunit disulphide bridge in the atypical 2-Cys Prx group (CHAE; UHM; RHEE, 1994).

Our *in silico* analysis showed that thioredoxin-dependent peroxide reductase of *N. caninum* is a typical 2-cys Prx (AhpC/Prx1 subfamily) due to the presence of two cysteines at positions 51-aa (C_P) and the 171-aa (C_R) (NELSON et al., 2011; PERKINS et al., 2015). The C_P is in a universal conserved motif “PXXXTXXCP” (where X is any amino acid), composing the active site in all peroxiredoxins (NAKAMURA et al., 2010; PERKINS et al., 2015; RHEE, 2016) where the first Val-Cys-Pro (VCP) motif of NcPrx is found. The two VCP motifs at positions 50–52 aa and 170–172 aa in NcPrx sequence are a hallmark for the 2-Cys peroxiredoxins group (AhpC/Prx1 subfamily) (RHEE; CHAE; KIM, 2005; NELSON et al., 2011; SOITO et al., 2011). Two domains were predicted in the NcPrx sequence: an alkyl-reductase hydroperoxide (AhpC) and a thiol-specific antioxidant (TSA), indicating that NcPrx belongs to the AhpC/TSA family (NELSON et al., 2011). This family, comprising proteins with similarities to TSA and AhpC from yeast and bacteria, respectively (SEAVER; IMLAY, 2001; POOLE; NELSON, 2016), have two highly conserved and activity-essential cysteine residues,

corresponding to Cys47 and Cys170 in yeast TSA (CHAE; UHM; RHEE, 1994; RHEE; CHAE; KIM, 2005). The C-terminal “1-cys-Prx” domain, where Cys-171 is located, is involved not only with the enzymatic activity but also in the dimerization of the enzyme (WOOD et al., 2002, 2003).

rNcPrx was produced in *E. coli* as a soluble recombinant protein, allowing a robust production for further uses. The detection of the monomeric (24 kDa) and dimeric (48 kDa) forms indicates that the enzyme is expressed in an active state (NAKAMURA et al., 2010; PERKINS et al., 2015; RHEE, 2016). The conversion between monomer and dimer rNcPrx forms was verified by H₂O₂ and DTT treatment, in which rNcPrx was dimerized in an H₂O₂ concentration-dependent manner. Furthermore, DTT was able to decrease the dimer formation and promote the monomeric form of the rNcPrx, as demonstrated previously (CHAE; UHM; RHEE, 1994; KAWAZU et al., 2001) using the TSA of yeast and peroxiredoxin of *Plasmodium falciparum*.

The antioxidant potential of rNcPrx was demonstrated protecting plasmid DNA under oxidative conditions (MFO assay). Therefore, rNcPrx acts scavenging the hydroxyl radicals produced by FeCl₃ and DTT. This effect has been demonstrated by peroxiredoxins of *Babesia sp.* (TANAKA et al., 2009; MASATANI et al., 2016; HAI et al., 2017) and *Plasmodium sp.* (KAWAZU et al., 2003; HAKIMI et al., 2012, 2013). Moreover, rNcPrx showed an *in vitro* peroxidase activity similar to the observed for the typical 2-Cys Prx group (NELSON et al., 2011; SOITO et al., 2011; POOLE; NELSON, 2016). The catalytic cycle of peroxiredoxin starts with the reduction of peroxide by the monomeric Prx, yielding a water molecule and an intermediate sulfenic acid ligated to the C_P of Prx. Next, a disulphide bridge is formed by the interaction between C_P and C_R, releasing a second molecule of water, resulting in dimeric Prx. Finally, the thioredoxin or glutathione regenerates the catalytic state of peroxiredoxin by reducing the disulphide bridge (WOOD et al., 2002; ANGELUCCI et al., 2016; RHEE, 2016). As a reducing agent, DTT disrupts the intrasubunit disulphide bridge between cysteines, suggesting that rNcPrx belongs to typical 2-Cys Prx class. Moreover, we observed the formation of dimers/multimers of rNcPrx in a dose-dependent of the H₂O₂ concentration. This indicates the oligomerization of NcPrx, a behavior described for the typical 2-CysPrx group (WOOD et al., 2002; NOICHRI et al., 2015).

The antiserum anti-rNcPrx recognized a 24 and a 48 kDa band proteins in the extract of *N. caninum*, indicating the presence of the monomeric and dimeric forms of NcPrx, respectively, in the parasite. As we observed in recombinant NcPrx, NcPrx suffers oxidation (dimerization) in response to H₂O₂ treatment in intracellular and extracellular *N. caninum* tachyzoites. The NcPrx dimerization occurs at lower H₂O₂ concentration in extracellular parasites when compared with intracellular tachyzoites, reflecting the redox protection offered by the host cell and parasitophorous vacuole to these last ones. These results strongly suggest that NcPrx performs the peroxidase function in this parasite and that could act in H₂O₂ sensing. The Prx role as a redox sensor has been already demonstrated in different cell types (RHEE et al., 2012a; POYNTON; HAMPTON, 2014a), where the protein oligomeric state is associated with the function in the cell (BARRANCO-MEDINA; LÁZARO; DIETZ, 2009). According to the H₂O₂ levels, Prx can act further as a chaperone in signal transduction and in the regulation of cell the cycle, interacting with several proteins (BRANDSTAEDTER et al. 2019). Additional studies should explore the NcPrx role's in relay for H₂O₂ signal to the cell (SOBOTTA et al., 2014).

Although NcPrx is defined as a mitochondrial protein by UniProt, it lacks the N-terminal signal motif typically present in proteins targeted to mitochondria. Additionally, NcPrx did not co-localize with mitochondria that usually encircles the parasite's nucleus (SOHN et al., 2011). Instead, NcPrx was found homogeneously at the cytosol, as described for the Prx1 of *Toxoplasma gondii* (SON et al., 2001), 89% identical (Fig.1, TgPrx1 AF305718_1). The cytosol location suggests a possible role of NcPrx in scavenging H₂O₂ and other organic peroxides, representing the first defense line against ROS from the extracellular environment or cytosolic process (RHEE et al., 2012b; HEO; KIM; KANG, 2020; RHEE; WOO, 2020).

NcPrx, the first peroxidase enzyme of *N. caninum* to be described, is highly conserved among Apicomplexa homologue. NcPrx has peroxidase and antioxidant functions, and it was found at *N. caninum* cytosol, suggesting that it is enrolled in H₂O₂ clearance and sensing in intracellular and extracellular tachyzoites.

Acknowledgements

We would like to thank Maraísa Palhão Verri for the excellent technical assistance and Roberta Rosales for assistance in Multiphoton microscopy acquisitions.

Author Contributions

JCVB conceived the study, performed the experiments, analysed the results, and wrote the manuscript. LMP contribute with study design, interpretation of results and discussion. LB contribute with immunofluorescence and western blot assays. PGAF contributed with mass spectrometry assay. APY contributed with the conceptualization, funding acquisition, resources, supervision, and editing. All authors read and approved the final manuscript.

Financial Support

This research was supported by public funding from São Paulo Research Foundation (FAPESP) (Grants: 18/21020-3 to APY) and by funds from FAPESP fellowship (2019/ 05758-5 to JCVB). This study was financed in part by the Coordenação de Aperfeiçoamento de Pessoal de Nível Superior - Brasil (CAPES) - Finance Code 001.

Declarations

Conflicts of Interest: The authors declare that the research was conducted in the absence of any commercial or financial relationships that could be seen as a potential conflict of interest.

Ethical approval: All animal experimental procedures were conducted in accordance with the Animal Research Ethics Committee of the School of Pharmaceutical Sciences of Ribeirao Preto, University of Sao Paulo (CEUA-FCFRP, process 17.5.278.60.8). The authors assert that all procedures contributing to this work comply with the ethical standards of the relevant national and institutional guides on the care and use of laboratory animals.

Supplementary file

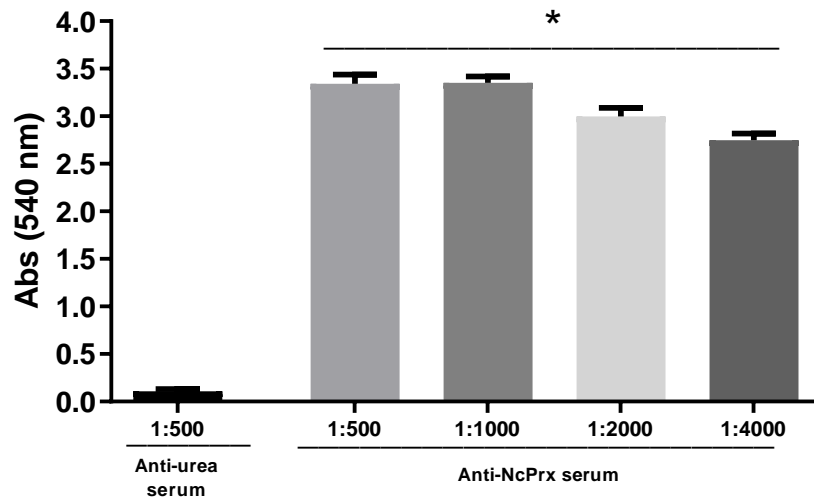
The supplementary file for this article was attached.

SUPPLEMENTARY MATERIAL

Supplementary file 1 rNcPrx analysis by MS/MS. The rNcPrx bands (Figure 2, line 5) were identified by MS/MS (MALD- TOF/TOF) using the Toxo DB (version 46) database. The table exhibits the identified bands (number), access number in ToxoDB, the description (ToxoDB), the score and coverage (percentage) based on MASCOT parameters, the number and the peptides identified by MS/MS, the start and end position of the peptides, peptide spectrum matches (PSM), the predicted molecular weight and the calculated isoelectric point (pI).

Band	Access	Description	Score	Coverage	Peptides	Position	PSM	Molecular weight (kDa)	calc. pI
1 (Monomer)	NCLIV_062630	Thioredoxin-dependent peroxide reductase	1772	29%	6 R.GLFLIDK.D K.ISLDQFK.G K.ISFPLLADVSHK.M K.MAADYGVLLPEGMALR.G K.DGVLQHSVVNNLPLGR.S K.MAADYGVLLPEGMALR.G + Oxidation (M) K.MAADYGVLLPEGMALR.G + 2 Oxidation (M) R.GLFLIDKDGVLQHSVVNNLPLGR.S	127-133 27-33 99-110 111-126 134-149 111-126 111-126 127-149	38	22174	5.96
2 (Dimer)	NCLIV_062630	Thioredoxin-dependent peroxide reductase	1188	29%	6 K.ISLDQFK.G K.ISFPLLADVSHK.M K.MAADYGVLLPEGMALR.G R.GLFLIDK.D R.GLFLIDKDGVLQHSVVNNLPLGR.S K.DGVLQHSVVNNLPLGR.S	27-33 99-110 11-126 127-133 127-149 134-149	31	22174	5.96

Supplementary file 2 Detection of rNcPrx by ELISA. The anti-rNcPrx hyperimmune serum was applied for the detection of the recombinant and native forms of NcPrx. Negative control was composed of serum collected from mice immunized with urea 8 M. (A) Plates coated with rNcPrx were incubated with dilutions of the anti-NcPrx (1:500, 1:1000, 1:2000, and 1:4000) and control serum (1:500). The results were expressed as mean \pm standard error and the experimental groups were compared by One-way analysis of variance ANOVA, Bonferroni post-test.* indicates $p < 0,05$.



CAPÍTULO II

Glutathione reductase: a cytoplasmic antioxidant enzyme and a potential target for phenothiazinium dyes in *Neospora caninum*.

Jade Cabestre Venancio-Brochi^a, Luiz Miguel Pereira^a, Felipe Antunes Calil^{b,c}, Olívia Teixeira^b, Luciana Baroni^a, Péricles Gama Abreu-Filho^a, Gilberto Úbida Leite Braga^a, Maria Cristina Nonato^b, Ana Patrícia Yatsuda^{a*}

Published in: International Journal of Biological Macromolecules Volume 187, 30 September 2021, Pages 964-975. DOI: <https://doi.org/10.1016/j.ijbiomac.2021.07.108>

^aFaculdade de Ciências Farmacêuticas de Ribeirão Preto, Universidade de São Paulo, Avenida do Café, Ribeirão Preto, Brazil.

^bLaboratório de Cristalografia de Proteínas, Faculdade de Ciências Farmacêuticas de Ribeirão Preto, Universidade de São Paulo, 14040-903, Ribeirão Preto, Brazil.

^cLudwig Institute for Cancer Research, University of California School of Medicine, 92093-0669, La Jolla, CA, USA.

* Corresponding Author at Laboratory of Molecular Parasitology. Faculdade de Ciências Farmacêuticas de Ribeirão Preto, Universidade de São Paulo, 14040-903 Ribeirão Preto, Brazil. e-mail adress: ayatsuda@fcrp.usp.br

Abstract

Neospora caninum causes heavy losses related to abortions in bovine cattle. This parasite developed a complex defense redox system, composed of enzymes as glutathione reductase (GR). Methylene blue (MB) impairs the activity of recombinant form of *Plasmodium* GR and inhibits the parasite proliferation *in vivo* and *in vitro*. Likewise, MB and its derivatives inhibits *Neospora caninum* proliferation, however, whether the MB mechanism of action is correlated to GR function remains unclear. Therefore, here, *N. caninum* GR (NcGR) was characterized and its potential inhibitors were determined. NcGR was found in the tachyzoite cytosol and has a similar structure and sequence compared to its homologs. We verified the *in vitro* activity of rNcGR (875 nM) following NADPH absorbance at 340nm (100mM KH₂PO₄, pH 7.5, 1 mM EDTA, ionic strength: 600mM, 25°C). rNcGR exhibited a Michaelian behavior ($K_{m(GSSG)}$: 0.10±0.02 mM; $k_{cat(GSSG)}$: 0.076±0.003s⁻¹; $K_{m(NADPH)}$: 0.006±0.001 mM; $k_{cat(NADPH)}$: 0.080±0.003s⁻¹). The IC₅₀ of MB, 1,9-dimethyl methylene blue, new methylene blue, and toluidine blue O on rNcGR activity were 2.1±0.2μM, 11±2μM, 0.7±0.1 μM, and 0.9±0.2μM, respectively. Our results suggest the importance of NcGR in *N. caninum* biology and antioxidant mechanisms. Moreover, data presented here strongly suggest

that NcGR is an important target of phenothiazinium dyes in *N. caninum* proliferation inhibition.

Keywords: *Neospora caninum*, glutathione reductase, phenothiazinium dyes.

Introduction

Neospora caninum is an obligate intracellular parasite representative of Apicomplexa phylum and was first described as a specie by Dubey in 1988 (DUBEY et al., 1988)The parasite has been related to neuromuscular disorders in dogs and an abortion syndrome in cattle (DUBEY, 1999; DUBEY & SCHARES, 2011).*N. caninum* infection in livestock generates significant financial losses in dairy and beef industries worldwide, estimated being around 1298.3 million dollars per year (REICHEL et al., 2013). Despite the fact that vaccines and drugs have been investigated as candidates to prevent or treat neosporosis (MARUGAN-HERNANDEZ, 2017; SÁNCHEZ-SÁNCHEZ et al., 2018), no effective and commercial therapeutic strategy has been available. Hence, studies are still required to develop drugs or vaccines to control *N. caninum* infection.

Radical oxygen species (ROS) are produced by phagocytes and other cell types in response to infections and are potentially harmful to cellular structures (PAIVA & BOZZA, 2014; WEIDINGER & KOZLOV, 2015).ROS comprise superoxide anion, hydrogen peroxide, and hydroxyl radicals, produced under aerobic metabolism, host macrophages action, heme group decomposition and drugs (SARMA et al., 2003; GUEVARA-FLORES et al., 2017). To deal with ROS, parasites dispose of a redox system with antioxidant enzymes and low molecular weight antioxidant species, such as glutathione, thioredoxin and vitamin E (SUSSMANN et al., 2017). These components maintain a reducing environment inside the cell, avoiding damages to the cellular structures and assuring the homeostasis(BEYER, 1994; PADAYATTY et al., 2003; GUEVARA-FLORES et al., 2017). The redox system is an important mechanism targeted by drugs against parasites, such as *Plasmodium* (MOHRING et al., 2014; PADÍN-IRIZARRY et al., 2016) and *Toxoplasma gondii* (AKERMAN; MÜLLER, 2005; CHARVAT; ARRIZABALAGA, 2016). Furthermore, the parasite's survival and replication inside host cells are dependent on the action of the antioxidant enzymes(BOSCH et al., 2015; KAVISHE;

KOENDERINK; ALIFRANGIS, 2017; SUSSMANN et al., 2017). Therefore, targeting the redox system represents a promising approach to control *N. caninum*.

Although poorly characterized in *N. caninum*, the glutathione system is part of the redox regulation, playing a defensive role through the action of the glutathione reductase (GR). GR is a homodimeric enzyme that catalyzes the conversion of oxidized glutathione (GSSG) into reduced glutathione (GSH), employing a nicotinamide adenine dinucleotide phosphate (NADPH) as a source of reducing equivalents (SCRUTTON; BERRY; PERHAM, 1987). This reaction maintains high levels of GSH in the cell, removing ROS and xenobiotic compounds (GRANT; DAWES, 1996). The impairment of the balance between GSH/GSSG usually induces low levels of reduced glutathione (GSH) and are related to growth delay, loss of ability to control oxidative stress, and increased DNA damage in *P. berghei* (PADÍN-IRIZARRY et al., 2016). Besides, mice immunization with *T. gondii* recombinant glutathione reductase improved the resistance against toxoplasmosis infection (HASSAN et al., 2014). Moreover, oxidative stress induced after monensin treatment increases the expression of GR in *T. gondii* (CHARVAT; ARRIZABALAGA, 2016).

GR is present throughout different organisms being relevant to evaluate differences in its susceptibility to potential antiparasitic compounds between the parasite and host enzymes. Methylene blue (MB) inhibits the recombinant form of *P. falciparum* GR (PfGR) *in vitro* at a low micromolar concentration, whereas no interference is observed on recombinant form of human GR (FÄRBER et al., 1998; BUCHHOLZ et al., 2008). MB is a tricyclic phenothiazinium dye (WAINWRIGHT; AMARAL, 2005) and was the first synthetic compound employed in malaria treatment in 1891 by Gutmann and Ehrlich (SCHIRMER et al., 2011; KRAFTS; HEMPELMANN; SKÓRSKA-STANIA, 2012; LU et al., 2018) until the development of chloroquine, in the middle of the 20th century. The revival of MB for malaria treatment is being boosted by the occurrence of resistance to chloroquine, pyrimethamine, and artemisinin analogs by human cases of *Plasmodium sp.* (VENNERSTROM et al., 1995; FALL et al., 2015; MWANGI et al., 2016; XIE; RALPH; TILLEY, 2020). Besides GR inhibition, MB interferes with the heme metabolism in the digestive vacuole of *P. falciparum in vitro* (ATAMNA et al., 1996) and with the oxidative balance of the parasite showed through hGrx1-roGFP-based biosensor analyses (KASOZI et al., 2013). The antimalarial properties of the MB have

been also related to the improvement of the parasite sensitivity to chloroquine in resistant lineages, due reduction of glutathione content in the cell (GINSBURG et al., 1998; MANDI et al., 2005). New methylene blue (NMB), 1,9-dimethyl methylene blue (DMMB) and toluidine blue O (TBO) are phenothiazinium dyes, MB derivatives, and also exhibit antimalarial activity against different strains of *Plasmodium sp.* (VENNERSTROM et al., 1995). The accessibility, safety, and low cost of phenothiazinium dyes drew the attention for their use as antiparasitic compounds against *N. caninum*. The anti-*N. caninum* properties of MB and derivatives have been reported both *in vitro* and *in vivo* models (PEREIRA et al., 2017, 2018, 2020). However, the mechanisms of action of phenothiazinium dyes in *N. caninum* are still missing, despite the advances in their understanding in *Plasmodium sp.* (SCHIRMER et al., 2003; BUCHHOLZ et al., 2008).

In the present work, we report the molecular and functional characterization of NcGR for the first time. Since antioxidant enzymes are interesting target structures, our work may allow the development of new and more effective phenothiazinium dye-based candidates for the *N. caninum* control. The *N. caninum* GR was cloned and the recombinant form expressed and purified after expression in *E. coli*. The *N. caninum* rNcGR antiserum was applied for detection of NcGR in *N. caninum* by western blot and immunofluorescence, confirming the cytoplasmic localization of the enzyme. As also observed for *Plasmodium sp.*, the *N. caninum* rGR was inhibited by MB and derivatives (at low micromolar concentrations) in kinetic assays under previously determined parameters.

Methods

Animals

Male BALB/c mice (6–8 weeks of age) were acquired from the vivarium of the campus of University of São Paulo at Ribeirão Preto, São Paulo, Brazil and housed in the animal facility of the School of Pharmaceutical Sciences of Ribeirão Preto, University of São Paulo. Water and feed were provided *ad libitum* and the animals were maintained in a temperature ($21 \pm 2^\circ \text{C}$) and light (12 h) controlled room.

Sequence analysis of NcGR

The complete protein sequence of the glutathione reductase NcGR (NcLIV063590 of *N. caninum*, strain liverpool) was obtained from the ToxoDB database version 46.0 and submitted to a BLASTp 2.0. The presence of the signal peptide and domains were predicted by SignalP 5.0 (ALMAGRO ARMENTEROS et al., 2019) and Pfam 3 (FINN et al., 2016), respectively. Subsequently, the amino acid sequence of NcGR was aligned with the *Hammondia hammondi*, *P. falciparum*, and *T. gondii* homologs using the hierarchical clustering method (clustal W) performed by the MegAlign software (Lasergene, DNASTar). The identity and similarity were calculated by Genedoc software, and the alignment image was generated by Multalin software (Multiple sequence alignment by Florence Corpet).

NcGR modeling

Homology modeling strategy was used to predict the tertiary structure of NcGR. The Modeller software (version 9.23) (ŠALI; BLUNDELL, 1993) was used to generate optimized models based on an advanced tutorial that uses multiple templates for the structural prediction. The X-ray structures of *Streptococcus mutans* (PDB: 5V36); *Plasmodium falciparum* (PDB:1ONF); *Saccharomyces cerevisiae* (PDB: 2HQM) and *Yersinia pestis* (PDB:5VDN) were used to build the NcGR homology model. The 3D models were ranked based on the DOPE score and e-value parameters followed by the validation using Molprobit (WILLIAMS et al., 2018). The following Molprobit parameters supported the structure selection: clashscore, Molprobit score and Ramachandran plot. The refinement was performed using GalaxyRefine (HEO; PARK; SEOK, 2013) and validated again using MolProbit and SAVES 6.0. The NcGR homology model was aligned with the templates by MultAlin and the figure was generated by ENDScript 3.0 (ROBERT; GOUET, 2014). Finally, the homodimer of the NcGR homology model was obtained in the GalaxyHomomer server (BAEK et al., 2017). The 3D NcGR homology model was visualized, aligned with templates structures and the root-mean-square deviation (RMSD) of atomic positions were calculated in QtGesamt (CCP4). NcGR-FAD interactions were plotted using the LIGPLOT program of LIGPLUS software using default parameters. Images were generated by PyMol software and LigPlot.

In vitro culture of *N. caninum*

The *N. caninum* Nc-1 strain (DUBEY et al., 1988) was used. *N. caninum* tachyzoites were obtained from monolayers of Vero cells, maintained in RPMI-1640 medium supplemented with 5 % fetal bovine serum (FBS, Gibco, Invitrogen, Carlsbad, USA) at 37°C and 5% CO₂. The tachyzoites were cultured in RPMI-1640 medium, under the same conditions. The parasites were purified by lysis of infected Vero cells using a needle (0,45×13mm) followed by syringe filtration (5µm). The suspension containing *N. caninum* was centrifuged (3 minutes, 5000 g, 4°C) and the pellet resuspended in phosphate-buffered saline (PBS).

***Neospora caninum* tachyzoite protein extract and control**

The purified *N. caninum* parasites were counted in a hemocytometer and the average recovery on 25 cm² culture flask was 1×10⁷ tachyzoites. The *N. caninum* tachyzoite and Vero protein extracts were obtained as described by Pereira et al. (2011). The tachyzoites (2 × 10⁸ per 0.5 ml) or the Vero cells (5 × 10⁶ per 0.5 ml) were sonicated (three cycles of 30 seconds at 70 % amplitude) in 8 M urea.

RNA extraction

Total RNA was extracted from purified *N. caninum* tachyzoites using the Trizol™ reagent (Gibco), following the manufacturer's instructions, and diluted in nuclease-free water. The isolated DNA and RNA were quantified by spectrophotometer (Genequant, GE Healthcare, USA). RNA samples with an appropriate degree of purity (260/280 nm ratio between 1.6 and 2.0) were selected for cDNA synthesis.

Synthesis of cDNA, amplification and NcGR ligation in pET28

The cDNA was synthesized using the GoScript™ Reverse Transcription System (Promega, Madison, WI, USA), following the manufacturer's instructions. The NcGR (NcLIV 063590) coding sequence was amplified (Expand™ High Fidelity PCR System, Roche) using the primers forward GRForNde (5'TTTCATATGACGCGACGACACTTTGATCTG 3'; position 13-33bp) and reverse GRRevHind (5' TTTAAGCTTCCAGGGAGGGAGAGTGACGAC 3'; position 24-45bp), flanked by the NdeI and HindIII restriction sites. After amplification, the NcGR

fragment (NcGR sequence, except for the 3 first amino acids) was purified and inserted into the cloning vector pGEM-Teasy (Promega). The reaction was transformed into *Escherichia coli* electrocompetent bacteria (Top 10, Invitrogen, Waltham, Massachusetts, USA) (Genepulser Xcell Electroporation System, Bio-Rad, Hercules, CA, USA) and selected with 50 $\mu\text{g}/\text{mL}$ Ampicillin. Subsequently, the plasmid containing the fragment (pGEM-NcGR) was treated with restriction NdeI and HindIII enzymes (10u) and ligated into the previously prepared pET28 plasmid, using T4 DNA ligase (1u, Thermo Fisher Scientific, Waltham, Massachusetts, EUA). The pET28/GR plasmid was transformed by electroporation into *E. coli* BL21 (DE3) and selected with kanamycin (50 $\mu\text{g}/\text{ml}$).

Expression and purification of the recombinant NcGR

The transformed BL21 colonies were inoculated into 5 mL of LB (LuriaBertani) broth with kanamycin (50 $\mu\text{g}/\text{ml}$) and incubated for 18 h, 37°C, 112g. The suspensions were inoculated (1:100) in 500 mL of LB supplemented with kanamycin (50 $\mu\text{g}/\text{ml}$) and incubated at 37°C, 112g until an optical density of 0.6 was reached at 600 nm. Then, the cultures were chilled in ice for 30 minutes and 0.5 mM of isopropyl β -D-1-thiogalactopyranoside (IPTG, Sigma-Aldrich, Darmstadt, Germany) was added. The induction was performed at 18°C for 16 hours, 112 g, followed by centrifugation at 15000 g for 10 minutes, 25°C. The supernatant was discarded and the bacterial pellet sonicated (15 cycles of 30 seconds at 70 % amplitude) with either a denaturing buffer (8 M urea, 20 mM sodium phosphate, 500 mM NaCl, pH 8.0, ionic strength 620mM) or a native buffer (50mM NaH_2PO_4 , 50 mM Tris, 300mM NaCl, 0.3 mM β -mercaptoethanol, 5 % v/v glycerol, pH 8.0, ionic strength: 25mM) containing 20 μM FAD (Sigma-Aldrich, Darmstadt, Germany) in ice for immunization or enzyme assays, respectively. For protein purification in both conditions, lysates were centrifuged (10,000 g, 15 minutes, 4°C) and the supernatants were filtered in a 0.45 μm syringe filter (Millipore, Bedford, MA). Subsequently, the filtered lysates were loaded into 200 μL of nickel-sepharose resin (HisPur™ Ni-NTA Resin, Thermo Fisher Scientific), packed in PD-10 columns (GE Healthcare) and purified by gradient step at 25°C. The resin ligated to rNcGR for immunization (generation of anti-rNcGR) was washed with 25mL of denaturing washing buffer (8 M urea, 20 mM sodium phosphate, 500 mM NaCl, pH 6.3). The rNcGR was efficiently eluted from the nickel-sepharose resin using 5mL of denaturing elution buffer (8 M urea, 20 mM sodium phosphate, 500 mM NaCl, pH 4.5,

25°C, μ : 620mM,). For enzymatic procedures, the rNcGR was purified under native conditions at 25°C. The resin was washed with 50mL of native washing buffer (native lysis buffer supplemented with 50 mM imidazole). Then, elution of rNcGR was performed with 10mL of native buffer supplemented with 250 mM imidazole. rNcGR was kept at 4 °C (pH 7.5) up 2 weeks without losses in enzyme activity. All positive eluted samples for Bradford reaction were analyzed by SDS-PAGE, followed by Coomassie Brilliant Blue G250 staining. The rNcGR concentration was determined using Bradford assay and for enzymatic analyses the extinction coefficient of $10,3M^{-1}cm^{-1}$ was determined and calculated as described by Padua et al.(2014).

Size exclusion chromatography (SEC) and Dynamic light scattering (DLS)

In order to determine the oligomeric status of rNcGR, SEC was performed on a Superdex 200 10/300 GL (GE Healthcare) column in an Akta Purifier system (GE Healthcare Life Science®, Chicago, USA). The column was equilibrated and run with 50mM NaH₂PO₄, 300mM NaCl, 50mM Tris, pH 7.5, at flow rate of 0,3 mL/min, at 4°C. The calibration curve was performed with the gel filtration calibration kit (GE Healthcare) containing Ferritin (440 kDa), Aldolase (158 kDa), Conalbumin (75 kDa) and Ribonuclease A (13.7 kDa) and protein elution was monitored by the absorbance at 280 nm. The molecular weight determination by gel filtration was carried out by comparing the Kav of rNcGR, an elution volume parameter, with the values obtained for several known calibration standards. Kav was calculated by the follow equation:

$$K_{av} = \frac{(V_e - V_o)}{(V_c - V_o)} \quad (1)$$

Where V_o is column void volume, V_e is the elution volume, and V_c is the geometric column volume. Afterwards, rNcGR sample (7mg/mL) was centrifuged for 10 min at 15800g and the Dynamic light scattering (DLS) was performed in a Zetasizer Nano ZS (Malvern Instruments, Malvern, UK) at 25 °C, with a volume of 50 L in a quartz cuvette ZEN2112. Data analysis was performed using the Zetasizer software.

rNcGR identification by mass spectrometry MS/MS

The SDS-PAGE bands corresponding to recombinant protein NcGR were excised and submitted to trypsin digestion, according to Pollo-Oliveira et al

(OLIVEIRA, 2013). Briefly, the samples were diluted in 1:1 proportion in an alpha-cyano-4-hydroxycinnamic acid matrix (10 mg/mL in 50% acetonitrile and 0.1% TFA) and spotted in MALDI plates. Polyethylene glycol (PEG) diluted in matrix solution (1:1) was used as a calibrator. The identification was performed in MALDI-TOF-TOF-MS (Axima Performance, Kratos-Shimadzu, UK- Centro de Química de Proteínas-FMRP-USP). The data were searched against the protein data bank of *N. caninum* ToxoDB (version 46), using the Mascot software (<http://www.matrixscience.com>) (version 2.6.1, Matrix Science, London, UK). The search was performed with the following parameters: carbamidomethylation as a fixed modification of cysteine and oxidation of methionine as a variable modification. Peptide and ion tolerance were established at 50 ppm and 0.6 Da, respectively, allowing the loss of two cleavages. Protein and peptide identifications with a probability higher than 95% were accepted for analysis.

Differential scanning fluorimetry

Differential scanning fluorimetry was performed in a thermocycler Mx3005P (Agilent Technologies, Santa Clara, USA), using SYPRO® orange (Invitrogen, Carlsbad, USA) (492/610 nm) as a fluorescent probe in a 96-well PCR plate (Bio-Rad, Hercules, USA). The thermal stability of rNcGR was evaluated in water and in native buffer the 20 μ L reaction mixture contained 75 μ g/mL of protein and 5 \times SYPRO® orange. The samples were heated from 25 to 95 °C at 1 °C/min and fluorescence measurements were taken every minute. Thermal melting curves were processed as described by Niesen et al.(2007) and the melting temperature (T_m) was calculated using GraphPad Prism software (San Diego, USA). The melting temperature (°C) is in which 50% of the protein is folded and 50% of the protein is melted. The T_m values are displayed in the melt curve plots.

Anti-rNcGR serum production

Polyclonal antibodies against the recombinant protein rNcGR were generated using male mice (BALB/c, 6 to 8 weeks of age). The animals (five per group) were immunized by subcutaneous injection with 0.5 μ g/ μ L of rNcGR protein (experimental groups) or 50 μ L of 8 M urea (negative control) in 50 μ L of aluminum hydroxide (1:1, Alhydrogel 2%, Brenntag, Biosector A/S, Denmark). The immunization was performed

at weeks 0, 3, 5 and, 7. In the 9th week after the first immunization, the animals were anesthetized intraperitoneally with ketamine (80 mg/kg) and xylazine (8 mg/kg) (KAWAI et al., 2011). The animals were euthanized by exsanguination (cardiac puncture) and the hyperimmune serum collected.

Enzyme-Linked Immunosorbent Assay (ELISA)

The rNcGR (5 $\mu\text{g/mL}$, 0.5 $\mu\text{g/well}$) was immobilized in coating buffer (60 mM Na_2CO_3) for 18 h in a 96-well plate (ELISA-Plate, Microlon, flatbottom, medium binding inhibitor, Greiner Bio-One, Austria). Subsequently, the samples were blocked for one hour with 0.5% gelatin (Sigma-Aldrich, St. Louis, USA) diluted in PBS-T (0.05% Tween-20 in PBS). After blocking, the anti-rNcGR (dilutions: 1:500; 1:1000; 1:2000; 1:4000) or negative control serum (dilution 1:500) diluted in PBT-T with 0.05% gelatin were added and incubated for one hour at 37°C. As secondary antibody, peroxidase-conjugated rabbit anti-mouse antibodies (dilution 1:5000, IgG – whole molecule – Peroxidase, Sigma-Aldrich- USA) were incubated at 37°C for one hour. Washes (3 \times) were performed with PBS-T between every incubation step. The TMB chromogen solution (Invitrogen, USA) was added and the plate was incubated for 15 minutes at room temperature, in the dark. The reaction was stopped by the addition of 100 μL of 2M HCl. The absorbance was measured at 450 nm in an ELISA reader (Synergy H1, Biotek, USA). The results were analyzed by software GraphPad Prism 8.0 (Graph Pad, USA). The results were expressed as mean \pm standard error and the experimental groups were compared by one-way analysis of variance ANOVA followed by Bonferroni post-test.

Western blot

The samples (Vero control protein extract, *N. caninum* tachyzoite protein extract, and rNcGR) were diluted in 4 \times SDS-PAGE sample buffer (0.5 M Tris HCl pH 6.8, 10% glycerol, 2% SDS, 0.01% bromophenol blue) and applied on a 12.5% acrylamide gel. After electrophoresis, proteins were transferred to a PVDF membrane (ImmobilonTM-P, Millipore, USA). The membranes were blocked with 0.8% PBS-GT (0.8% swine gelatin, in PBS-T) for 1 h followed by incubation (16 h) with anti-rNcGR polyclonal antibodies (1:1.000) at room temperature. Anti-mouse IgG conjugated to peroxidase (Sigma, USA), diluted 1:5000 or 1:10000, was used as a secondary antibody.

Finally, membranes were incubated with a luminol solution (SuperSignal West Pico Chemiluminescent Substrate, Thermo Fisher Scientific, USA) for 5 min followed by radiographic films exposition. The images were documented in a densitometric scanner (Image Scanner, GE Healthcare, UK) using LabScan v5.0 software.

Localization of NcGR in *N. caninum* tachyzoites by confocal microscopy

Purified *N. caninum* tachyzoites were immobilized on poly-lysine-coated glass coverslips and fixed with 3.6% formaldehyde (Sigma-Aldrich, USA) in PBS for 15 minutes at 25°C. The slides were rinsed with PBS and permeabilized with 0.2% Triton X-100 for 40 min at 25°C. After permeabilization, the tachyzoites were blocked with PBS containing 3% bovine serum albumin (BSA) and 20 mM glycine for 18 h at 10°C. Next, the tachyzoites were incubated with anti-rNcGR (1:50) or negative control (1:50) polyclonal serum diluted in PBS containing 0.3% BSA and 2 mM glycine for 45 min. The anti-mouse secondary antibody AlexaFluor® 488 (Molecular Probes®, Eugene, Oregon, USA) was diluted 1:500 in PBS (0.3% BSA and 2 mM glycine) and the nucleus labeled with 0.5 µM propidium iodide (PI, Santa Cruz Biotechnology®, Dallas, Texas, USA). In parallel, a group of tachyzoites was incubated with Mitotracker (400 nM, Red CMXRos, Life Technologies, Carlsbad, California, USA) for 20 minutes, 37°C before the fixation and permeabilization steps. Next, the parasites were immunostained for NcGR detection as described above, and the nuclei were detected by DAPI (300 nM, 4',6-diamidino-2-phenylindole, Life technologies). The experiments were carried out using a confocal microscope (LeicaSP8 Laser Scanning Confocal Microscope, Leica Microsystems, Germany) connected to a digital camera of the Multi-User Laboratory of High-Resolution Images and Cellular Studies (LHRICS), School of Pharmaceutical Sciences of Ribeirão Preto, University of São Paulo/USP. The image capturing was performed on software LAS AF (version 3.2.0.9652) using the 63× objective with a 4× optical zoom in oil immersion. The Alexa Fluor 488, DAPI and PI/Mitotracker were detected with excitation/emission wavelengths of 490/525 nm, 358/461 nm, and 579/599 nm, respectively. The captured images were processed in ImageJ 1.46r (National Institute of Health, USA).

NcGR enzyme kinetics determination

To avoid any interference of imidazole in the activity assays, recombinant protein NcGR was desalted in a Sephadex G-25 PD-10 column (GE Healthcare, UK) using the desalting buffer (100 mM KH₂PO₄, 50mM Tris, 5% glycerol, pH 7.5, ionic strength: 625mM) and afterwards rNcGR was purified in Superdex 200 10/300 GL (GE Healthcare). The rNcGR demonstrated a high thermal stability at physiologic temperatures (37°C), allowing a reproducible use of the enzyme in kinetic assays. The enzymatic activity of rNcGR was determined according to Xue et al. (XUE et al., 2017), with modifications. Considering that one NADPH is consumed for each molecule of reduced GSSG (GSSG→GSH), it is conceivable that the reduction of GSSG is evaluated indirectly by the measurement of the consumption of NADPH, which decreases the absorbance at 340 nm (A₃₄₀) over time (FÄRBER et al., 1998). In a UV transparent 96 well plate (Corning, NY, USA), 200 μL of reaction buffer (100 mM KH₂PO₄, pH 7.5, 1 mM EDTA, ionic strength: 600mM) with NADPH and GSSG were added to 5 μL of rNcGR enzyme (875nM) and the NADPH consumption was monitored in the SpectraMax Plus 384 (Molecular Devices, San Jose, California) plate reader at room temperature for 30 seconds. The substrates concentrations were ranged separately 0.004 - 0.25 mM of NADPH at 1mM GSSG and of 0.008 – 2 mM of GSSG at 0.25mM NADPH to apparent kinect parameters determination. Consumption of NADPH was determined using the following the equation:

$$\frac{\left(\left(\frac{\Delta Absorb_{340}}{time}\right) - \left(\frac{\Delta Blankabs_{340}}{time}\right)\right)}{(\varepsilon * [rNcGR])} \quad (2)$$

The blank represents the spontaneous oxidation of NADPH in the presence of GSSG in the same concentrations of experimental samples without enzyme. *Varepsilon* represents molar extinction of NADPH: 6,22 mM⁻¹ cm⁻¹. To determine the apparent K_m (Michaelis-Menten constant) and k_{cat} (turnover number) values, the assay was performed in a range of GSSG and NADPH concentrations. The apparent K_m and k_{cat} were calculated by non-linear regression (software Graphpad Prism 8.0) using the equation: Y = V_{max}*X/(K_m + X), where X is substrate concentration and Y is enzyme velocity. One single experiment was performed in triplicate. The results were expressed as mean ± standard error.

Activity of rNcGR incubated with phenothiazinium dyes

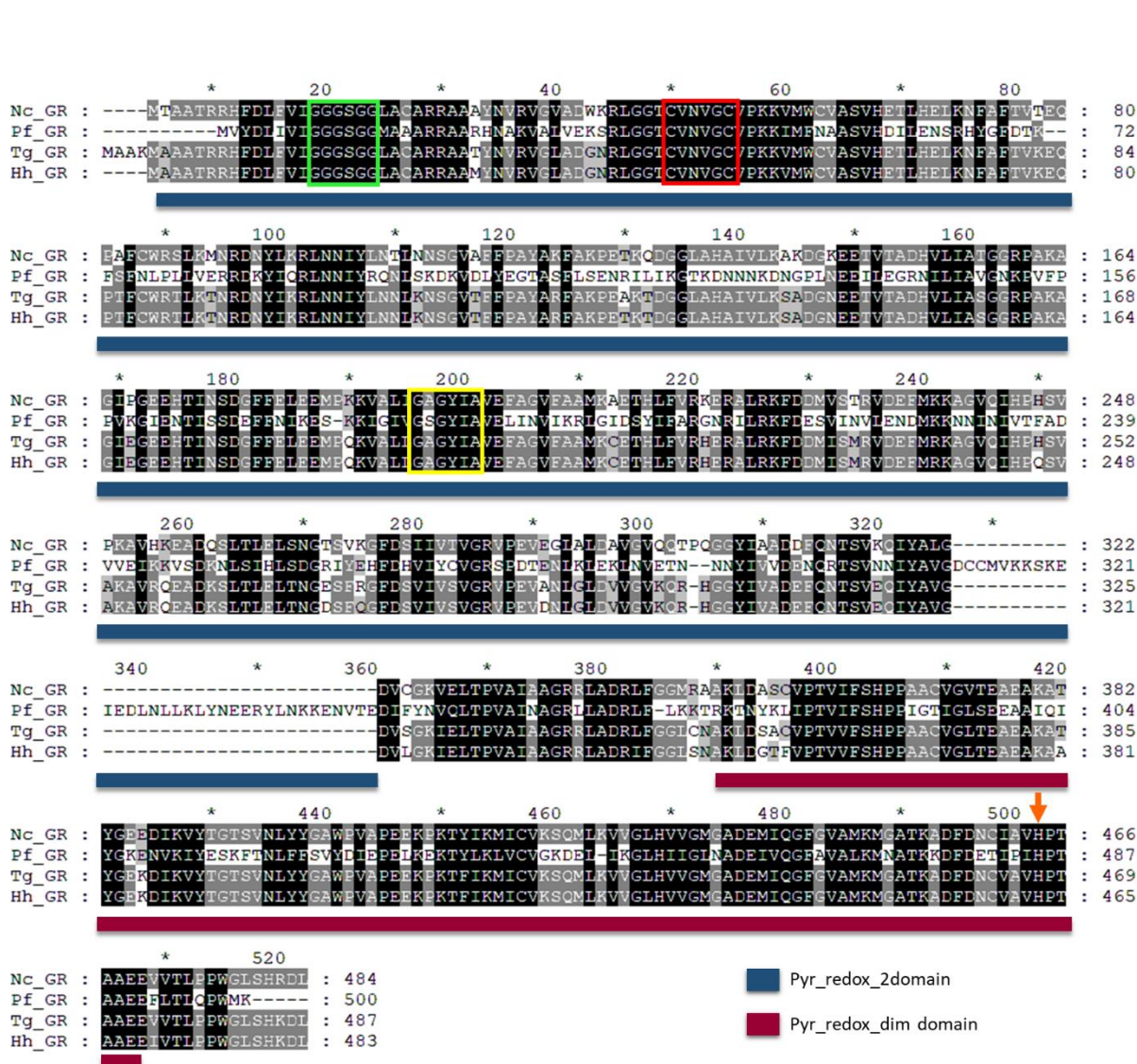
At the apparent K_m determined values for NADPH and GSSG, the enzymatic activity of rNcGR was evaluated in the presence of following phenothiazinium dyes: methylene blue (MB), new methylene blue (NMB), 1,9 dimethyl methylene blue (DMMB) and toluidine blue O (TBO) at concentrations between $300\mu\text{M}$ - $0,15\mu\text{M}$. The initial rate of the reaction in the absence of the inhibitor was set as 100% active and the inhibition percentage was plotted against the logarithmic concentration of phenothiazinium dyes. The data was fitted using sigmoidal non-linear regression by software Graphpad Prism 8.0. The IC_{50} was defined as the concentration that inhibits 50% of enzymatic activity. One single experiment was performed in triplicate. The results were expressed as mean \pm standard error

Results

In silico analysis of *N. caninum* glutathione reductase

NcGR revealed to share higher level of sequence identity/similarity (I/S) with *T. gondii* M49 (I/S: 86/92%) and *Hammondia hammondi* (I/S: 86/93%) GR proteins compared to the *P. falciparum* (I/S:38/55%) homolog. The two main domains predicted for NcGR belong to the superfamilies of pyridines nucleotide-disulfide oxidoreductase (Pyr) and NAD (P) H-nitrite reductase (Nirb) (Fig.1, red and blue bars). According to PFAM, there are two active sites in NcGR at positions 51-aa(-CVNVGC-, Fig.1, red box) and 464aa(Fig.1, orange arrow). Two Rossmann fold motifs (Fig.1, green and yellow box), were identified in the Pyr-redox domain. These motifs are conserved sequences composed of a series of beta strand (β) and alpha helical (α) as secondary structures (KLEIGER; EISENBERG, 2002). The first motif is a consensus sequence between the aa-14 and aa-18 (G-X-G-X-X-G, where X can be any amino acid) that binds to a flavin adenine dinucleotide FAD (Fig.1, green box). The second motif, between the aa-192 and the aa-197 (G-X-G-X-X-A) is predicted to have affinity to nicotinamide adenine dinucleotide phosphate (NADPH, Fig.1, yellow box). Finally, the predicted isoelectric point of NcGR is 8.11, the molecular weight is 52 kDa (ToxoDB) and no peptide signal was detected.

Figure 1 Multiple alignments of *Neospora caninum* glutathione reductase (NcGR) with homologs from Apicomplexan organisms. GR sequences from *N. caninum* (NcGR; CBZ55933.1), *P. falciparum* (PfGR; CAA63747.1), *T. gondii* M49 (TgGR; XP018634939.1) and *H. hammondi* (HhGR; XP008883741.1) were aligned using the Clustal W algorithm. The black and grey residues represent identity and similarity among sequences, respectively. The main GR domains and motifs are indicated by bars and boxes respectively. Blue bar: Pyr redox 2 (Pyridine nucleotide-disulphide oxidoreductase domain; PF07992). Red bar: Pyr redox dim (Pyridine nucleotide-disulphide oxidoreductase, dimerization domain; PF02852). Green Box: Rossmann fold motif FAD ligand. Red box: thioldisulfide redoxactive core. Yellow box: Rossmann fold motif NADP ligand. Orange arrow: histidine active site.



NcGR homology modeling

Four GR annotated tertiary sequences were selected as template for NcGR homology modeling. The PDB ID primary sequences from *Streptococcus mutans* (SmGR, 5V36), *Plasmodium falciparum* (PfGR, 1ONF), *Saccharomyces cerevisiae* (ScGR, 2HQM), and *Yersinia pestis* (YpGR, 5VDN) demonstrated 50%, 45.77%,

46.74% and 51.23% of identity compared to NcGR, respectively. The NcGR homology model was aligned with the PDB template sequences (Fig. S1. and Fig.S2.) exhibiting RMSD values of the C alpha atomic coordinates of 0.739, 0.920, 0.765 and 0.803 for SmGR, PfGR, ScGR and YpGR, respectively, indicating conserved features (Rossmann folds motif, thiol-disulfide redox-active center and active histidine). Besides, the secondary structure of NcGR exhibited 12 α -helices and 21 β -strands (Fig.S1.). The NcGR homology model was generated in the monomeric form of the protein (Fig. 2.A) with the FAD cofactor (Fig.2A-B) based on the templates. The clashscore was 5.98 (90th percentile) and molprobity score was 1.49 (95th percentile), which validated the refinement process. The Ramachandran plot analysis for the refined model revealed that 97.1% of the residues were localized in favored regions. Moreover, 99.6% of the residues were detected in allowed regions (Fig. 2.B) and only 2 outliers residues were found: 367-Pro and 465-Pro. The NcGR homology model and templates structures (1ONF, 2HQM, 5V36, 5VDN) quality were verified in ERRAT, VERIFY 3D, PROVE, PROCHECK and WHATCHECK through the SAVES 6.0 server. NcGR homology model presented quality factor 95.11 in ERRAT, and passed in VERIFY analysis. It showed few errors in PROVE, WHATCHECK and PROCHECK that were the same errors found in the templates structures. Therefore, NcGR model reflects the templates quality. Given that GR are enzymatically active as a homodimer, the homodimeric NcGR homology model was predicted (Fig 3.A and Fig.S3.). The dimeric NcGR was generated in GalaxyHomomer (BAEK et al., 2017), a web server for protein homo-oligomer structure prediction from a monomer sequence or structure by both template-based modeling and ab initio docking. This server has been employed by several authors in homo-oligomer structure prediction (SAJIB et al., 2018; DOROSTI et al., 2019; GUERRIERO et al., 2019; RAHBAR et al., 2020). NcGR dimeric structure (Fig. 3.A) was validated through Molprobity parameters, the clashscore was 9.8 (76th percentile) and molprobity score was 1.59 (93th percentile). The Ramachandran plot analysis for the NcGR dimeric mode (SAJIB et al., 2018; DOROSTI et al., 2019; GUERRIERO et al., 2019; RAHBAR et al., 2020) revealed that 97.51% of the residues were localized in favored regions and 99.8% of the residues were detected in allowed regions. Two outliers residues were found: 367-Pro in chain A and B. The conserved features (Rossmann motifs and active histidine at aa-464) and thiol-disulfide redox-active center (-CVNVGC-) of NcGR were observed on internal cavities of the homology model (Fig. S3.). Moreover, Pyr_redox_2 and the Pyr_redox_dim domains were demonstrated in

monomer and dimer NcGR forms (Fig.2.A and Fig.S3.B, respectively). Finally, NcGR interacts with FAD ligand (Fig. 3.A) through hydrogen bonds with Asp-323, Ala-37, Cys46, Gly-19, Lys-54, Thr-45 (Fig 3.B-C) and hydrophobic interactions (Fig 3.C).

Figure 2. Cartoon representation for NcGR homology model and its respective Ramachandran plot. (A) Monomeric NcGR generated by Modeller and GalaxyRefiner showing the Py redox 2 (dark blue, Pyridine nucleotide-disulphide oxidoreductase domain; PF07992) and Pyr redox dim (magenta, Pyridine nucleotide-disulphide oxidoreductase, dimerization domain; PF02852) domains. FAD: Flavin Adenine Dinucleotide; Met-1 and Leu-484 represent the first and last amino acid in the NcGR sequence, respectively. (B) Ramachandran plot of NcGR homology model generated by MolProbity.

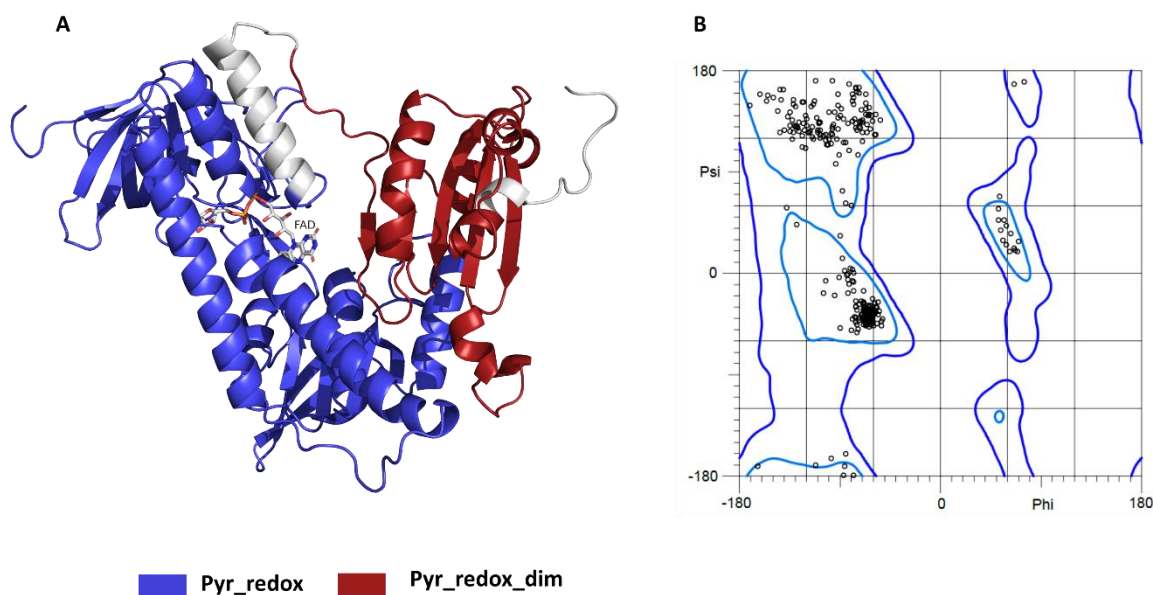
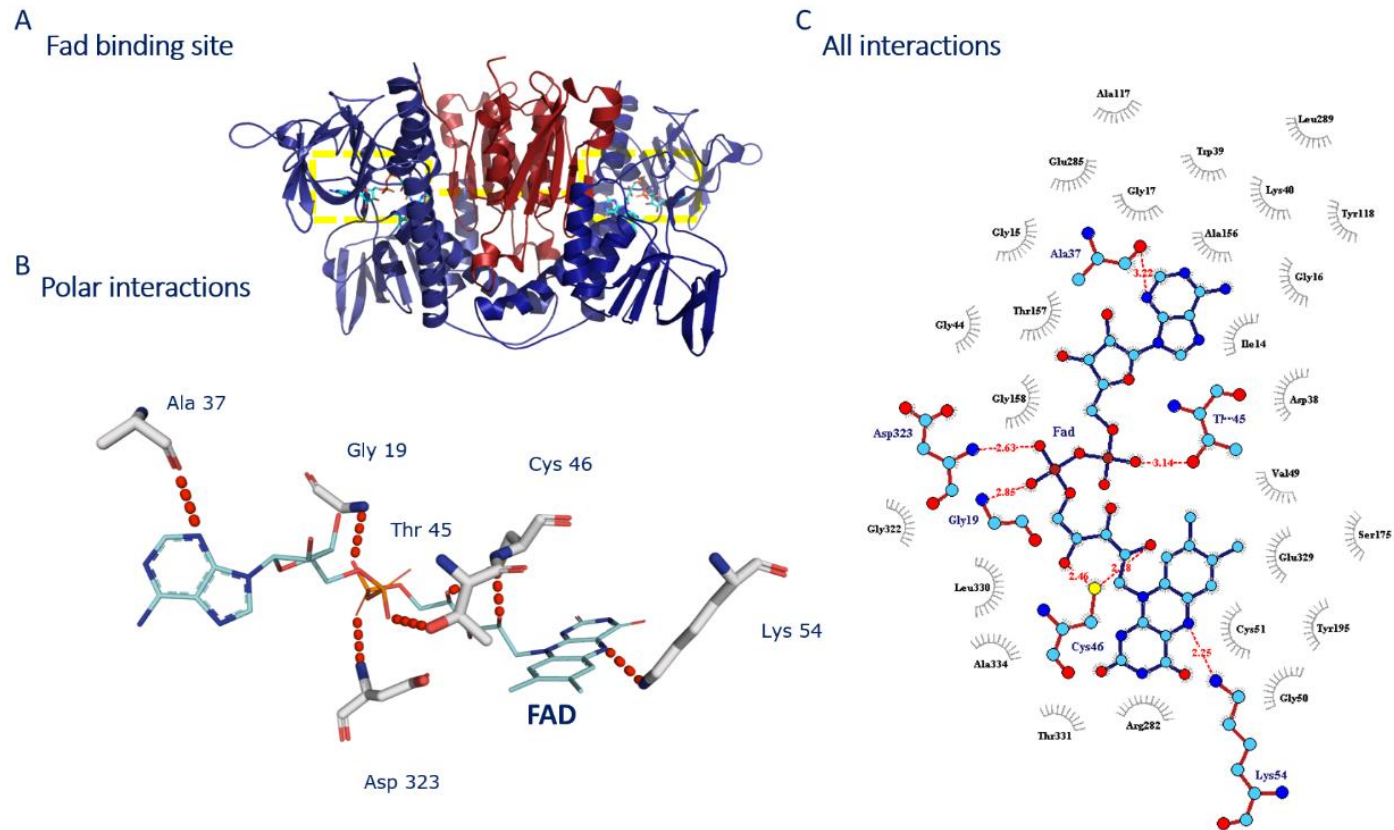


Figure 3. FAD binding site in NcGR homology model. (A) Dimeric NcGR showing FAD binding site delimited by yellow dotted line. (B) FAD polar interactions (red dotted line) with NcGR residues: Ala-37, Asp 323, Cys-46, Gly-19, Lys-54, Thr-45. C. All FAD interactions (Polar and hydrophobic) with NcGR residues. Protein-ligand interactions were plotted using the LIGPLOT program of LIGPLUS software using default parameters. Images were generated by PyMol software and LigPlot.



Cloning, expression, and purification of rNcGR

The full loading of rNcGR prepared under the optimized conditions was 6 mg/L (protein mass (mg)/BL21 culture volume(L)). NcGR was expressed with 52 kDa and solubilized in saline buffer (Fig. 4. lane 2). There was no expression in non-induced control (Fig. 4. lane 1). The NcGR was purified in a nickel-sepharose resin with high purity, under both denaturing and native conditions (Fig. 4. lanes 3 and 4, respectively). Both main purified bands of NcGR (band 1 and 2, white and black arrows, respectively, Fig. 4) were detected and identified as *N. caninum* glutathione reductases (NCLIV 063590), confirming the formation of homodimer (Table.S1.). A similar pattern of peptides identified was observed for the monomer and homodimer forms of rNcGR. Three peptides were identified for the monomer (score 233, PSM 8) and homodimer (score 251, PSM 4), covering 11% of the protein (Table.S1.). rNcGR was eluted at an elution volume of 11,85mL in SuperdexTM S-200 column that corresponds to a molecular weight of 104 kDa when compared to the molecular weight standards (Fig. 5). In addition, DLS analysis showed that the hydrodynamic diameter of rNcGR was 9.7 nm, compatible with the diameter of the dimeric NcGR homology model measured in PyMol software (Fig. S4.) Therefore, under native conditions rNcGR is found in dimeric form. Finally, the melting temperature (T_m) in water and in native buffer for rNcGR was 62.5°C and 64.6°C, respectively (Fig. S5.).

Figure 4. Reducing SDS-PAGE analysis for expression and purification of *N. caninum* recombinant glutathione reductase (rNcGR). Expression of NcGR cloned in pET28 plasmid was induced with IPTG (0.8 mM) and purified in Nickel-Sepharose resin under native or denatured conditions. Lane 1: Non-induced culture; Lane 2: IPTG induced culture; Lane 3: rNcGR (0,6ug/ul) purified under denaturing conditions (8 M urea); Lane 4: rNcGR (0,6μg/μl) purified under native conditions (250 mM imidazole). M: Molecular weight markers in kDa. Gels (12,5%) were stained with Coomassie Brilliant Blue. White and black arrows indicate the monomer and homodimer forms of rNcGR, respectively.

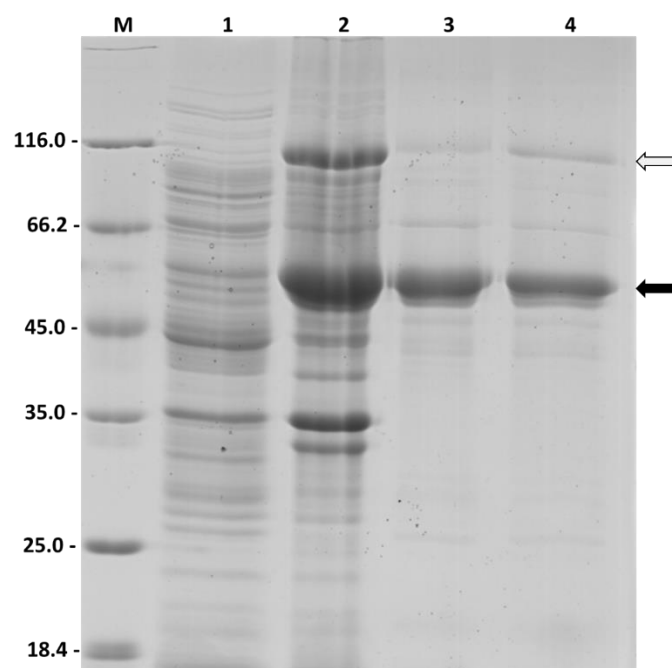
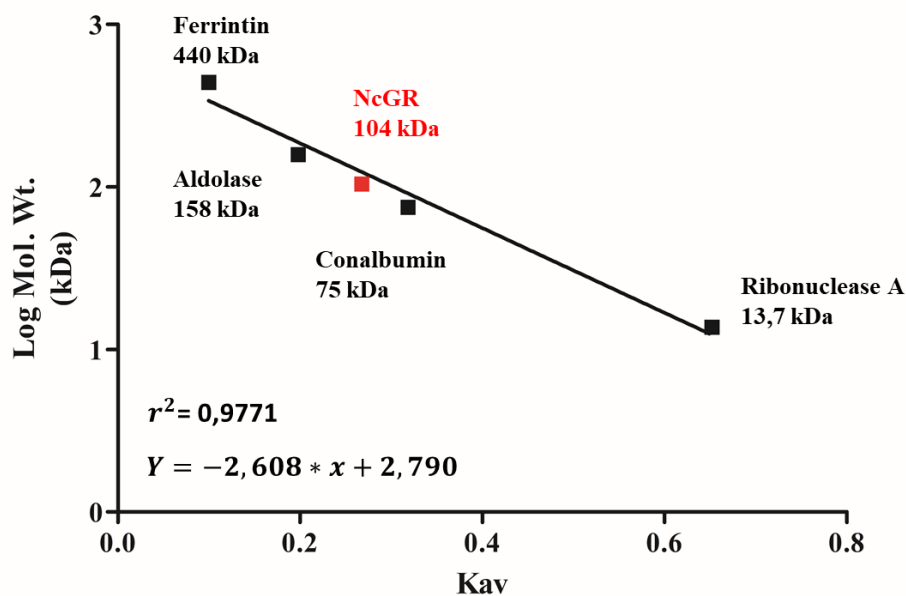


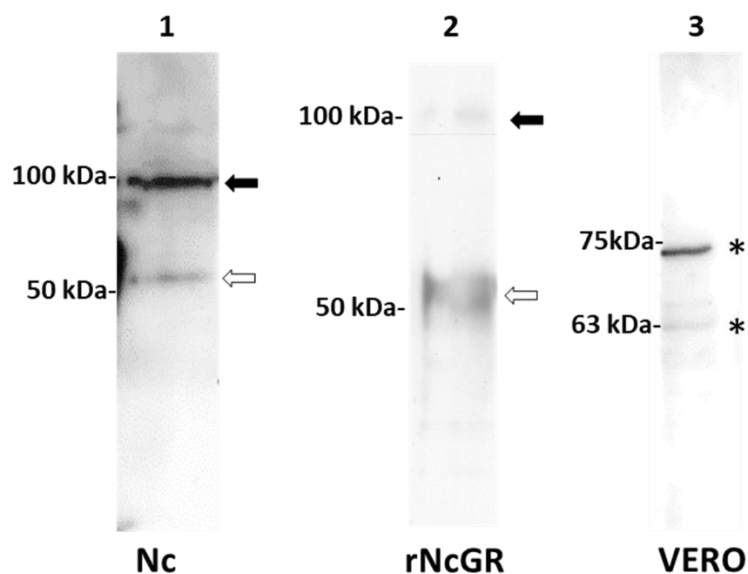
Figure 5. Size exclusion chromatography (SEC) analysis of rNcGR in Superdex™ S200. SEC analysis was performed to access the oligomeric status of rNcGR under native conditions. Calibration curve is represented by standards: Ferritin (440 kDa), Aldolase (158 kDa), Conalbumin (75 kDa) and Ribonuclease A (13.7 kDa). The molecular weight determination by gel filtration was carried out by comparing the K_{av} of rNcGR, an elution volume parameter, with the values obtained for the known calibration standards.



Detection of native and recombinant NcGR proteins by ELISA and Western blot

The anti-NcGR serum was validated by ELISA (Fig. S6.). The monomer and homodimer forms of NcGR, with 52 kDa and 100 kDa ((Fig. 6, white and black arrows, respectively), respectively), were detected both in recombinant and *N. caninum* extracts (Fig. 6, lanes 1 and 2) by anti-NcGR serum in Western Blot. These bands demonstrated a similar molecular weight compared to the predicted ones (52 kDa and 104 kDa). In Vero cell extracts, two bands of 63 kDa and 72 kDa were detected by the anti-rNcGR. However, these bands did not correspond to the molecular weight of the predicted mammalian GR (45 kDa) (Fig. 6, lane 3,*).

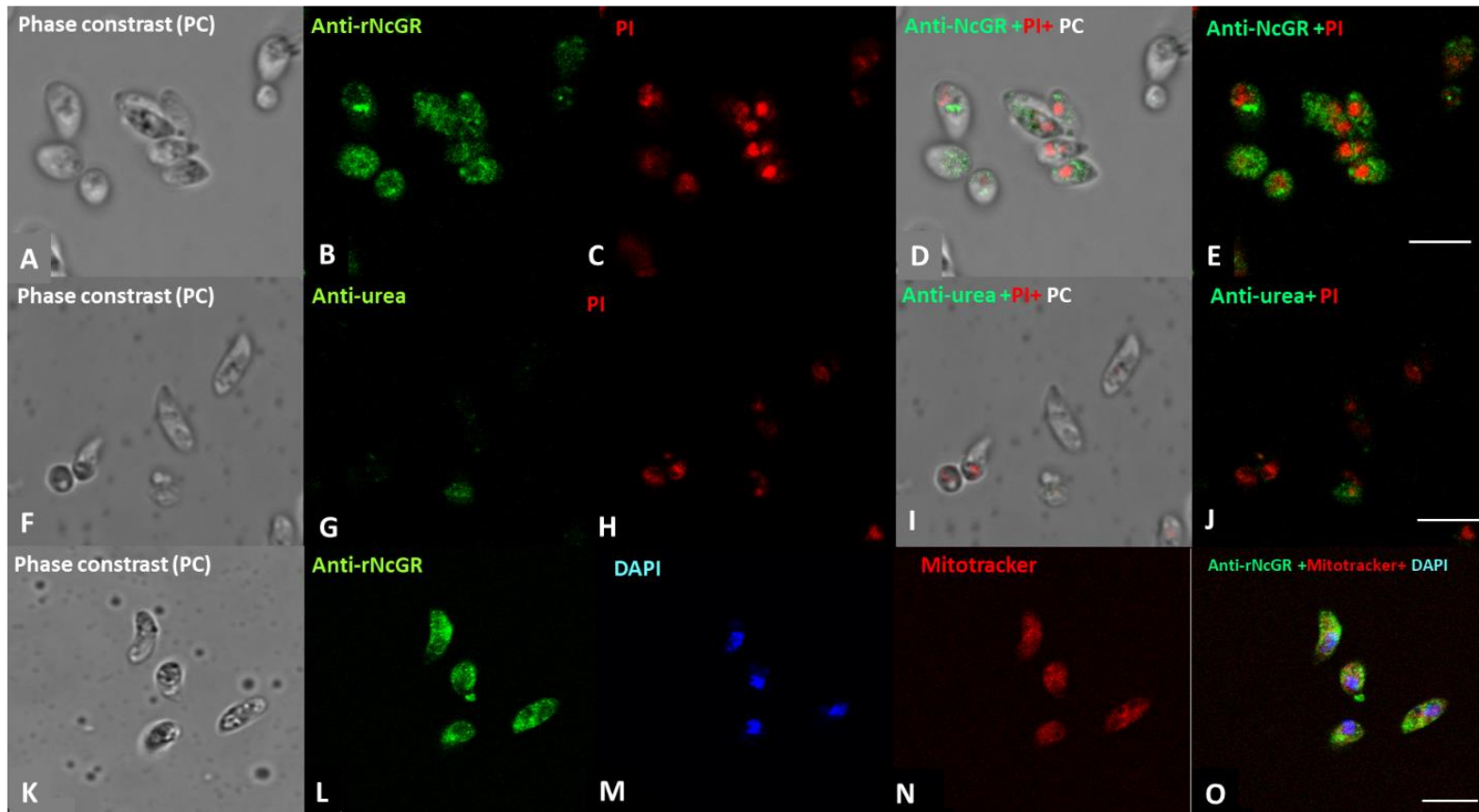
Figure 6. Detection of NcGR by Western blot. *N. caninum* (Nc), Vero cells extracts, or recombinant protein NcGR were separated by SDS-PAGE (12,5%). The proteins were transferred to PVDF membranes and incubated with the anti-rNcGR polyclonal antibody at 1:1000 dilution, followed by HRP anti-mouse antibody at 1:5000 (for recombinant NcGR) or 1:10.000 (for native Nc and Vero extract) dilutions. The detection was revealed using a luminol solution. Lane 1: *N. caninum* extract. Lane 2: purified recombinant NcGR. Lane 3: Vero cell extract. White arrows: NcGR monomeric NcGR; Black arrows: dimeric NcGR; *: 63 kDa and 72 kDa bands.



Localization of NcGR proteins on *N. caninum* tachyzoite by confocal microscopy

NcGR was found homogeneously distributed in the cytoplasm of the tachyzoites (Fig.7.A-E, L). No fluorescence was observed in tachyzoites incubated with negative control (urea anti-serum) (Fig.7, F-J.). Moreover, the anti-rNcGR serum did not colocalize with mitochondrial or nuclear structures when comparing to mitotracker, DAPI or PI staining (Fig.7).

Figure 7. Immunolocalization of NcGR in the tachyzoites of *Neospora caninum*. Tachyzoites were purified, immobilized, and labeled with anti-rNcGR serum (1: 50) or with antiurea serum (1:50, as negative control). The immunostaining was visualized with Alexa Fluor 488 and the nucleus stained with propidium iodide (PI) or DAPI. The mitochondria were localized with mitotracker. A, F, K: Phase contrast (PC). B and L: Anti-rNcGR. G: anti-urea. C and H: PI. M: DAPI. D and I: Anti-rNcGR/anti-urea, PC, and PI merge. N: Mitotracker. E and J: Anti rNcGR/anti-urea and PI merge. O: Anti-rNcGR, mitotracker, DAPI. Scale Bar = 5 μ m.



rNcGR enzymatic assay and inhibitory effects of phenothiazinium dyes on rNcGR activity

The rNcGR enzyme catalysis the reduction of the GSSG to GSH by NADPH consumption. The reaction rate as a function of the concentration of NADPH and GSSG revealed a Michaelian behavior (Fig.8) and the apparent kinetic parameters in relation to GSSG and NADPH was determined (Table 1.). The phenothiazinium dyes methylene blue (MB), 1,9-dimethyl methylene blue (DMMB), new methylene blue (NMB) and toluidine blue O (TBO) inhibited the rNcGR activity at micromolar concentrations (Fig.9 and Table 1.).

Figure 8. rNcGR enzymatic activity plots and apparent kinetic parameters. The reaction rate curve (k_{obs} (s^{-1})) as a function of NcGR substrates concentration: NADPH (A) and GSSG (B). The k_{obs} values represent the consumption of substrate over time, corrected by protein molarity. The apparent Michaelis-Menten constant (K_m) and k_{cat} of rNcGR were calculated in relation to GSSG and NADPH substrates. The assays were represented by a single experiment in triplicate.

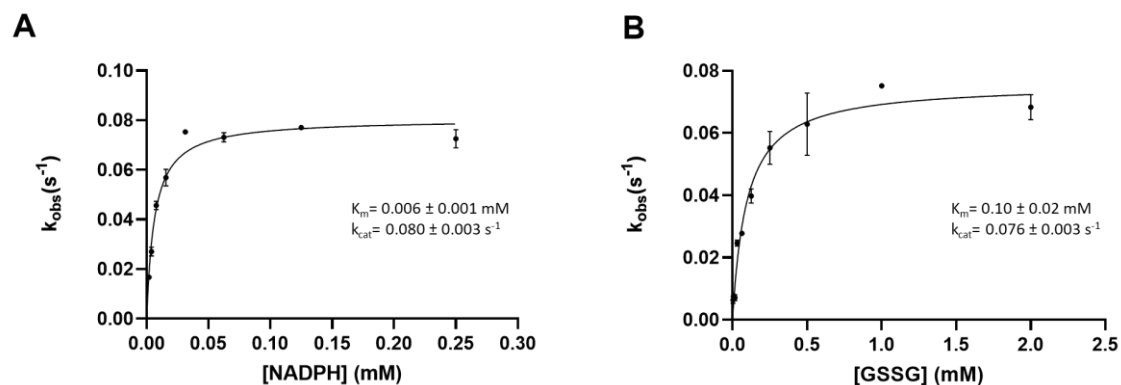
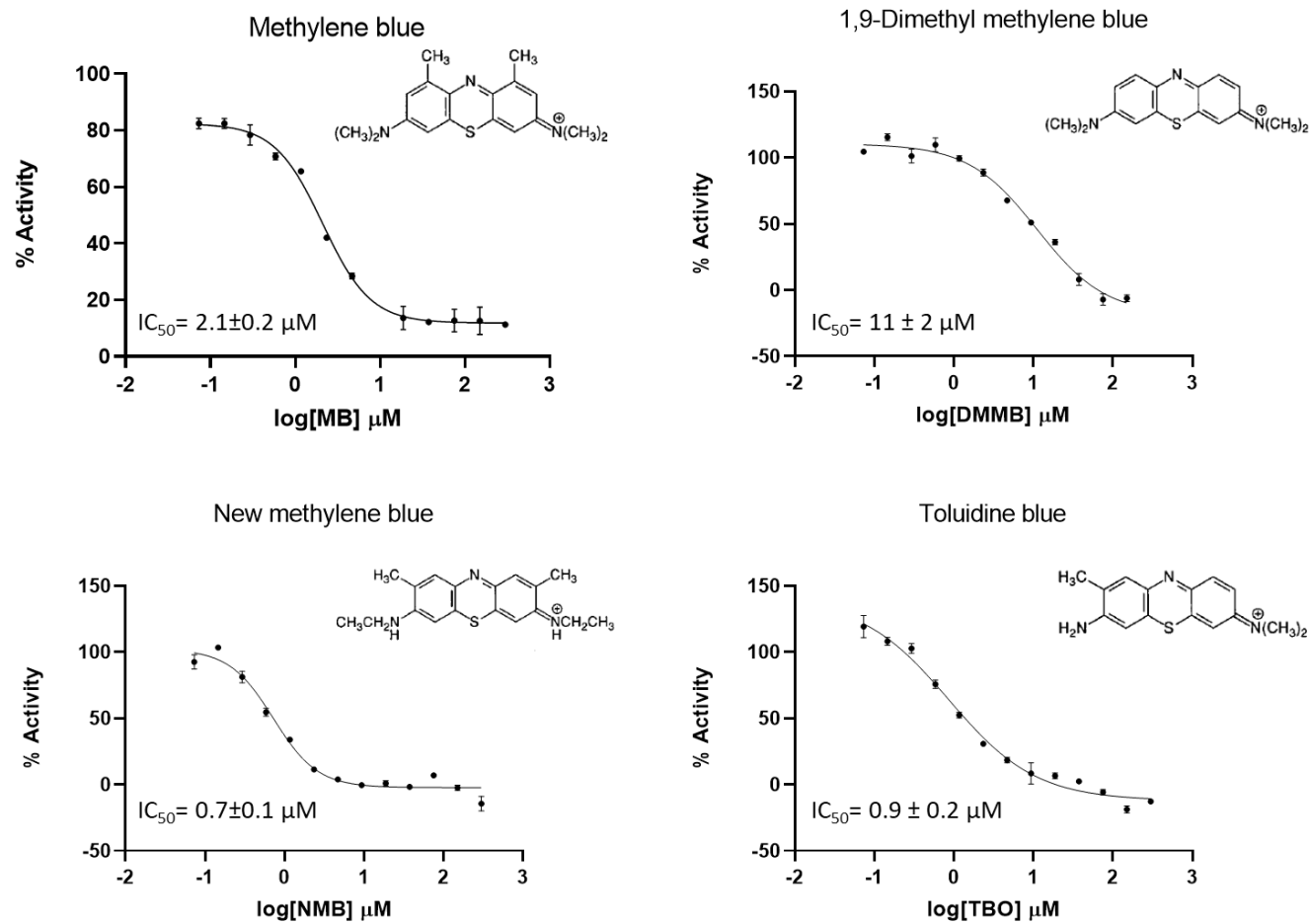


Table 1. Apparent kinetic parameters of rNcGR and inhibitory concentration (IC_{50}) of phenothiazinium dyes. K_m : Michaelis-Menten constant; k_{cat} : turnover number; MB: methylene blue; DMMB: 1,9 dimethyl methylene blue; NMB: new methylene blue; TBO: Toluidine blue O. Data are present as mean \pm standard error.

NADPH		GSSG		IC_{50} (μM)			
K_m (mM)	k_{cat} (s^{-1})	K_m (mM)	k_{cat} (s^{-1})	MB	DMM B	NMB	TBO
0.006 ± 0.001	0.080 ± 0.003	0.10 ± 0.02	0.076 ± 0.003	2.1 ± 0.2	11 ± 2	0.7 ± 0.1	0.9 ± 0.2

Figure 9. Inhibition profile (IC_{50}) of the phenothiazinium dyes (μM) against rNcGR. The rNcGR activity was measured in the presence of the phenothiazinium dyes under different concentrations. The percentage of inhibition was calculated compared to the solvent control. The IC_{50} were determined by plotting the percentage of activity versus log of the inhibitor concentration. The data fitting used was a sigmoid curve obtained in the Origin Lab Software. (A) methylene blue (MB). (B) 1,9-dimethyl methylene blue (DMMB). (C) new methylene blue (NMB). (D) toluidine blue O (TBO). The graphs were represented by a single experiment in triplicate.



Discussion

Under normal physiological conditions, cells regulate the balance between the pro and antioxidant mechanisms, controlling the oxidative stress. However, the disturbance of the oxidative balance leads to the overproduction of free radicals, resulting in DNA, proteins, and lipids damage, and consequently might induce cell injury and death (PIZZINO et al., 2017). On the other side, the oxidative stress elements such as ROS and reactive nitrogen species (RNS) play a key mechanism in the host defense against pathogens (NOVAES; TEIXEIRA; DE MIRANDA, 2019). As an evolutionary adaptation, the pathogens have a complex system of enzymes to control the overproduction of ROS as well as the utilization of the host cell antioxidant resources (FERRARI et al., 2011). The disruption of the antioxidant mechanisms related to pathogen survival is an important target for the control of infectious diseases. For example, Artemisinin, Methylene blue, and Chloroquine improve the ROS content in erythrocytes, blocking the *Plasmodium* proliferation (PAL; BANDYOPADHYAY, 2012). We have shown a potential use of pro-oxidant drugs against *N. caninum* (PEREIRA et al., 2018, 2020) and here we report NcGR as an anti-oxidative mechanism in parasite survival and a potential target for drugs against neosporosis.

In silico analysis demonstrated that NcGR belongs to the pyridines nucleotide disulfide oxidoreductase superfamily of homodimeric flavoenzymes, including oxidoreductases, NADH oxidases, and peroxidases. This superfamily is characterized by two major domains: the Pyr redox 2 domain and Pyr Redox dimerization domain, playing roles in the oxidation-reduction reaction and the protein dimerization, respectively (BELTRAME-BOTELHO et al., 2016). NcGR shared high sequence identity with apicomplexan representatives, including the presence of conserved sequences of Rossmann fold motifs and thiol-disulfide redoxactive center in all homologs. However, the GR sequence of *P. falciparum* has an insertion (317-aa to 350-aa), with unknown function and no interference in enzyme function (SARMA et al., 2003), which decreases the identity in comparison to NcGR. NcGR sequence exhibits the thiol-disulfide redox-active center (CVNVGC-) at 51-aa, where the proximal and distal cysteines form a disulfide bond and are involved in the nucleophilic interchanges and charges transfers (SCHULZ et al., 1978; DEPONTE, 2013; COUTO; WOOD; BARBER, 2016). The second feature in NcGR is found at 464-aa that is an

active histidine (His) important for substrate binding and catalysis (SCHULZ et al., 1978; DEPONTE, 2013; COUTO; WOOD; BARBER, 2016). These conserved features have already been described in *Saccharomyces cerevisiae*, *Escherichia coli*, human and *Plasmodium falciparum* glutathione reductases (ARSCOTT; THORPE; WILLIAMS, 1981; RIETVELD et al., 1994; BÖHME et al., 2000; BERKHOLZ et al., 2008). The NcGR homology model exhibited spatial proximity among the Rossmann fold motifs, thiol-disulphide redoxactive center and the active histidine of the second chain of homodimer composing the sites where NADPH, FAD and GSSG bind, such as demonstrated in human and *P. falciparum* glutathione reductase (SARMA et al., 2003; BUCHHOLZ et al., 2008). The proximity among those sites is relevant for the two-phase catalytic cycle. First, in the reductive phase, NADPH binds to GR and reduces FAD transiently. Next, the FAD reduces the disulphide bond in the redox-active center, resulting in a charge-transfer complex with the proximal Cys. The distal Cys is protonated by histidine of the other subunit. The first phase is finished by the NADP⁺ dissociation from GR. During the oxidative phase, the GSSG binds to GR in conserved residues in both subunits whereas the distal-Cys reduces the disulphide bond in GSSG, resulting in the release of the first GSH. Finally, the thiolate leaving group of the second GSH molecule is protonated by active histidine and the molecule is released (BERKHOLZ et al., 2008; DEPONTE, 2013).

The residues found to interact with FAD cofactor in NcGR model are conserved in GR of other species as *Homo sapiens*, *Escherichia coli*, *Bartonella henselae str. Houston*, *Enterococcus faecalis*, *Plasmodium falciparum*, *Saccharomyces cerevisiae*, *Streptococcus mutans*, *Streptococcus pneumoniae*, *Vibrio parahaemolyticus*, *Yersinia pestis* (fig. S7 and table S2). Most residues are strictly conserved and whether not conserved, substitutions usually have similar physical and chemical properties (table S2). The NcGR FAD binding site showed two fingerprints reported: G-G-G-S-G-G that stabilizes the pyrophosphate moiety of FAD by dipole interactions (SCHULZ et al., 1978) and T-X-X-X-X-hy-h-h-G-D where h is small and non-polar, y is aromatic (RESCIGNO; PERHAM, 1994). In PfGR the conserved Asp-311 is essential to FAD binding in *Plasmodium falciparum* (SARMA et al., 2003). On the other hand, the role of those interactions in NcGR function will require further studies involving specific residues mutations.

The dimeric form of NcGR was expected once glutathione reductase is an obligatory homodimeric enzyme, being the GSSG binding site composed of both subunits in human and *Plasmodium* GR (NORDHOFF et al., 1993; SARMA et al., 2003). The recombinant NcGR protein was expressed with a molecular weight equivalent to the predicted monomer (52 kDa) and homodimer (104 kDa), confirmed by mass spectrometry (NcLIV 063590); and both NcGR forms were presumably detected in the *N. caninum* extract. Moreover, in native conditions rNcGR exists in dimeric form.

The colocalization with mitotracker and PI/DAPI indicated that NcGR is a cytoplasmic enzyme, homogeneously distributed in the cytosol of *N. caninum* tachyzoites. Likewise, the *Plasmodium* GR (the most studied GR of the Apicomplexa phylum) is also detected in the cytosolic compartment (KEHR et al., 2010). However, in *Plasmodium*, the same GR can be also found in apicoplast, demonstrating a dual-target inside the parasite. Kehr et al. (2010) suggested that the apicoplast isoform of GR is generated by alternative-translation initiation (ATI) due to the presence of star-codon upstream of the canonical start that is absent in the *N. caninum* GR RNAm.

The classical GR assay confirmed the rNcGR enzymatic activity, also described for recombinant GR of *Schistosoma mansoni* (KUNTZ et al., 2007), *Homo sapiens* (BRANDSTAEDTER et al., 2018) and *Plasmodium* sp. (FÄRBER et al., 1998). rNcGR reduced GSSG with NADPH consumption and the K_m for GSSG values of rNcGR (100 μM) was higher compared to the rGR of *P. falciparum* (K_m : 83 μM), *Homo sapiens* (K_m : 65 μM) (NORDHOFF et al., 1993; FÄRBER et al., 1998) and *E. coli* (K_m : 66 μM) (LÓPEZ-BAREA; PINTO, 1984), and lower than rGR of *Streptococcus pneumoniae* (K_m : 231.2 μM) (SIKANYIKA et al., 2019). Furthermore, rNcGR K_m for GSSG was higher comparing to the recombinant Thioredoxin Glutathione Reductase (TGR), a homodimeric selenocysteine that exhibits thioredoxin reductase, glutaredoxin and glutathione reductase activity, of *Fasciola gigantica* (K_m : 61.15 μM), *Fasciola hepatica* (K_m : 30 μM), *Schistosoma mansoni* (K_m : 71.5 μM), *S. japonicum* (K_m : 49.55 μM) (KUNTZ et al., 2007; SONG et al., 2012; GUPTA et al., 2016; GUEVARA-FLORES et al., 2017). On the other hand, the K_m for NADPH (K_m : 6 μM) of rNcGR was similar to rGR of *P. falciparum* (K_m : 8.3 μM), *Homo sapiens* (K_m : 6.6 μM) and lower than rGR of *E. coli* (K_m : 16.6 μM) *Streptococcus pneumoniae* (K_m : 23.2 μM) (LÓPEZ-BAREA;

PINTO, 1984; NORDHOFF et al., 1993; FÄRBER et al., 1998; SIKANYIKA et al., 2019). Despite the differences between K_m of rNcGR and the other species, the comparison is limited once the experimental conditions are diverse among the studies and we reported apparent K_m values, that could be influenced by substrate concentration.

Moreover, NcGR was inhibited by phenothiazinium dyes: methylene blue, new methylene blue, 1,9-dimethyl methylene blue and toluidine blue O. The inhibitory effect of methylene blue on GR (non-competitive inhibition) was previously demonstrated in *P. falciparum*, being GR the first molecular target described in this parasite (non-competitive inhibition) (FÄRBER et al., 1998). In *P. falciparum*, the GR enzymatic activity is essential to deal with the oxidative stress caused by the haemoglobin degradation inside the erythrocytes, requiring a robust antioxidant enzymatic response (JORTZIK; BECKER, 2012; MOHRING et al., 2014). The MB IC_{50} against NcGR (2.1 μ M) was similar to GR of *P. falciparum* (5.4 μ M) (BUCHHOLZ et al., 2008). On the other hand, the IC_{50} value of MB is 11 nM and 88 nM in ring stages and schizonts proliferation inhibition of the *Plasmodium*, respectively (ATAMNA et al., 1996; AKOACHERE et al., 2005), while in *N. caninum* tachyzoites MB IC_{50} is 371 nM (PEREIRA et al., 2017, 2018). These data imply that MB may have multiple targets in the parasites beyond GR inhibition. For example, the hemozoin polymerization inhibition by MB in *Plasmodium* infected erythrocytes is an absent phenomenon during the *N. caninum* life cycle (WAINWRIGHT; AMARAL, 2005; MÜLLER et al., 2019). Indirect evidence suggests that the MB inhibits GR through the binding in the intersubunit cavity of the enzyme, on the dimeric interface (SARMA et al., 2003). Furthermore, MB interferes secondarily in GR enzymatic activity by affecting the GSSG/GSH balance in the cell. Reductases convert MB to the reduced form, leucomethylene blue, resulting in an exacerbated consumption of NADPH and oxygen (O_2) with the production of water (H_2O) (BUCHHOLZ et al., 2008). This process probably decreases the NADPH necessary for the GR catalytic activity and consequently decreases the GSH concentration, increasing the toxic effects of GSSG in the cell (CARLBERG; MANNERVIK, 1985; MÜLLER et al., 2001; SCHIRMER et al., 2003). Phenothiazinium dyes exhibit bactericidal and antimalarial effects (WAINWRIGHT, 2000).

Our study showed for the first time the inhibitory activity of compounds derived from MB on glutathione reductase. All the phenothiazinium dyes assayed on the present work inhibit the *N. caninum* proliferation *in vitro* (PEREIRA et al., 2020) and data in the present study showed that the mechanism of action might involve the NcGR inhibition. The recombinant NcGR is more susceptible to NMB and TBO in comparison to MB. Besides, DMMB demonstrated the lower inhibitory effect in comparison to the other phenothiazinium dyes, contrasting with the higher anti-*N. caninum* activity in proliferation assays (PEREIRA et al., 2020). The differences in the inhibitory efficiency among the phenothiazinium dyes against NcGR are due to the different chemical groups bond to the phenothiazine core. Those differences in the structure of phenothiazinium dye as well as its physicochemical properties influencing the dye uptake, distribution within the cell and interaction with the enzyme GR (VENNERSTROM et al., 1995; WAINWRIGHT; AMARAL, 2005). Furthermore, the effects of phenothiazinium dyes in NcGR enzymatic activity and *N. caninum* proliferation are different (PEREIRA et al., 2020), suggesting a multitargeted mechanism of action. Thus, novel approaches are necessary to elucidate the complete inhibitory mechanism of phenothiazinium dyes in *N. caninum*.

Conclusions

The redox system is essential for the parasite survival inside the host cell. Hence, the first characterization of glutathione reductase in *N. caninum* enlarges the knowledge for the apicomplexan redox system and the interactions between the parasite and host cell. As successfully performed in other models, the NcGR was cloned, and its recombinant form expressed and purified. Using anti-rNcGR serum, the monomeric and dimeric forms of NcGR, as well as its cytoplasmic localization, were confirmed by Western blot and immunofluorescence, respectively. The purified rNcGR was found in dimeric form (104 kDa) and demonstrated adequate stability and activity, which allowed the use in kinetic assays. rNcGR showed Michaelian behavior and it was successfully inhibited by phenothiazinium dyes, revealing a possible mechanism of action of these molecules against *N. caninum*. On the other hand, the better understanding of NcGR structure-function relationship and inhibitory mechanism of phenothiazinium dyes will require mutational studies in the future. Finally, the homology NcGR model can be investigated through molecular docking approaches to

provide new potential inhibitors. Therefore, the findings presented here will contribute to research advances in treatment of neosporosis and other diseases caused by apicomplexan parasites, allowing the screening of novel anti-*N. caninum* candidates.

Ethics approval and consent to participate

All procedures using animals were approved by the local Ethical Committee for Animal Research (CEUA) of the School of Pharmaceutical Sciences of Ribeirão Preto, University of São Paulo (CEUA-FCFRP, process 17.5.278.60.8).

Availability of data and materials

Data supporting the conclusions of this study are included within the article and its Supplementary material. Raw data are available from the corresponding author upon request.

Competing interests

The authors declare that they have no competing interests.

Funding

This research was supported by public funding from São Paulo Research Foundation (FAPESP) (Grants: 18/21020-3 to APY) and by funds from FAPESP fellowship (2019/ 05758-5 to JCVB). This study was financed in part by the Coordination for the Improvement of Higher Education Personnel (CAPES, Brazil) - Finance Code 001.

Author's contributions

JCVB conceived the study, performed the experiments, analyzed and validated the results and wrote the manuscript. **LMP** contributed with study design, interpretation of results, discussion and reviewing the manuscript. **FAC** and **MCN** contributed with all the steps of enzymatic assays and interpretation of results, discussion and reviewing the manuscript. **OT** and **MCN** contributed with differential scanning fluorimetry, size exclusion chromatography (SEC) and dynamic light scattering (DLS) experiments, protein homology modeling analysis, discussion and reviewing the manuscript. **LB**

contributed with protein homology modeling, confocal assays, discussion and reviewing the manuscript. **PGAF** contributed with mass spectrometry assay and reviewing the manuscript. **GULB** contributed providing the phenothiazinium dyes and reviewing the manuscript. **APY** contributed with the conceptualization, funding acquisition, resources, supervision, editing and reviewing the manuscript. All authors read and approved the final manuscript.

Acknowledgements

We would like to thank Maraísa Palhão Verri for the excellent technical assistance and Eduardo Tozatto for assistance in confocal microscopy acquisitions.

Appendix A. Supplementary data

Supplementary data to this article can be found online at <https://doi.org/10.1016/j.ijbiomac.2021.07.108>.

Appendix A. Supplementary data

Fig.S1. *NcGR* secondary structure. The *NcGR* sequence (XP003885959.1) was aligned with the templates from *Plasmodium falciparum* (PfGR, PDB:1ONF); *Yersinia pestis* (YpGR, PDB:5VDN); *Streptococcus mutans* (SmGR, PDB: 5V36) and *Saccharomyces cerevisiae* (ScGR, PDB: 2HQM) using the ENDScript 3.0. The main regions Rossmann fold motif FAD ligand (green box), thiol-disulfide redox-active core (red box), Rossmann fold motif NADP ligand (yellow box), and the histidine active site (yellow arrow) were also highlighted.

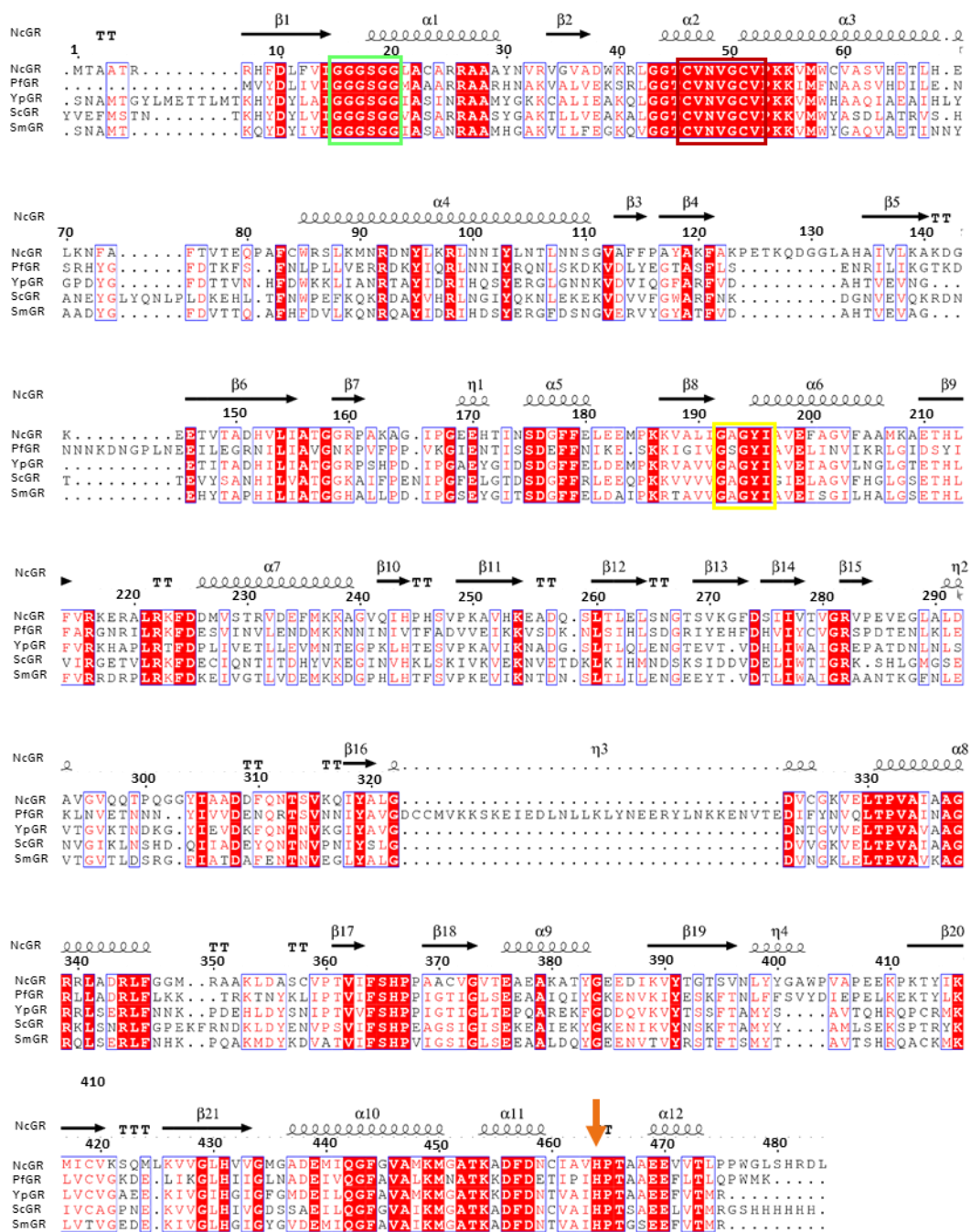


Fig.S2. Tertiary structure superposition of NcGR homology model and templates. NcGR homology model is represented by green cartoon structure aligned with (A) *Plasmodium falciparum* (blue color, PfGR, PDB:1ONF) (B) *Saccharomyces cerevisiae* (pink color, ScGR, PDB: 2HQM); (C) *Streptococcus mutans* (white color, SmGR, PDB: 5V36) and (D) *Yersinia pestis* (salmon color, YpGR, PDB:5VDN) structures. The alignments were performed in PyMol Software.

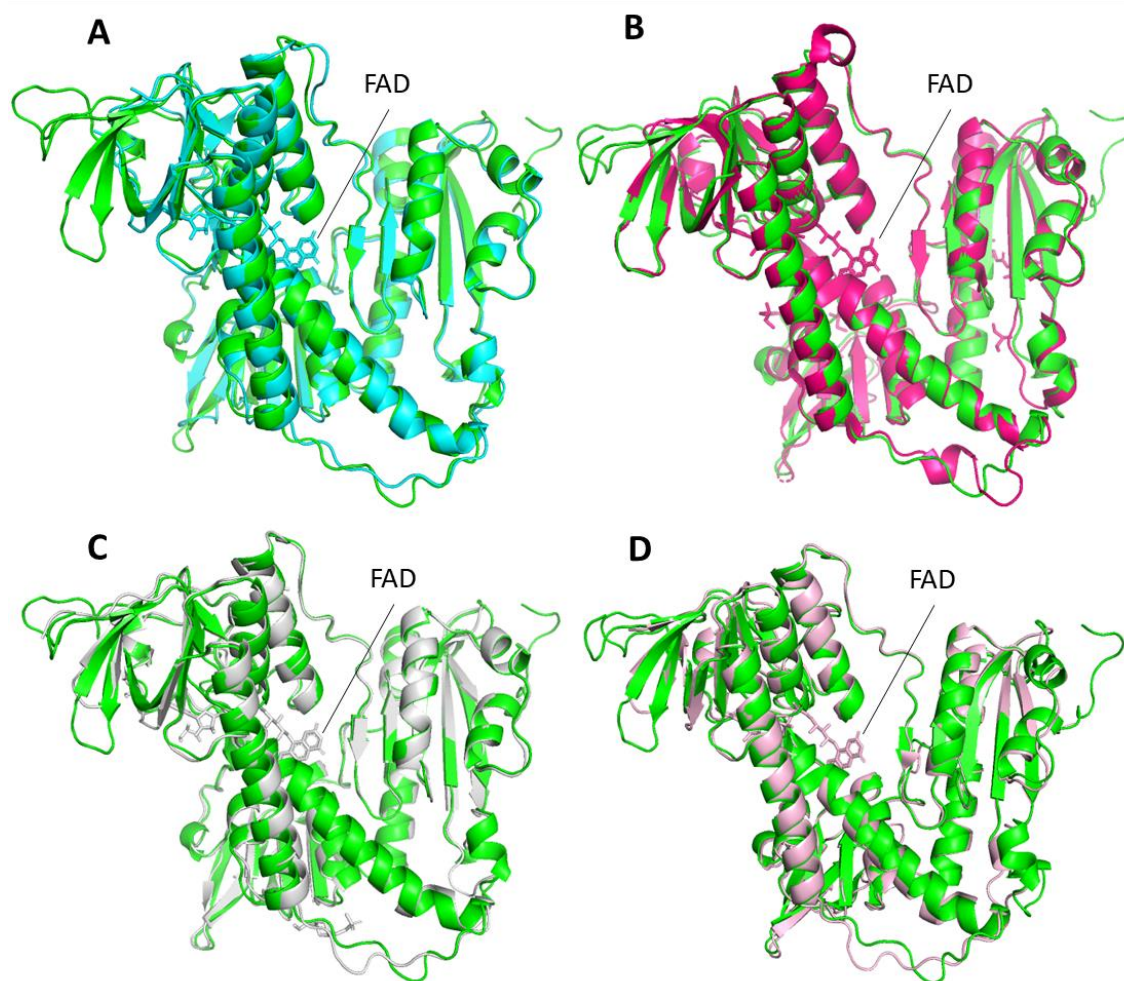


Fig.S3. Homodimeric NcGR homology model. (A) Homodimeric NcGR model showing the active site (pink), the Nterminal Rossman fold (purple), the active histidine (yellow), and the Cterminal Rossmann fold (orange). Chain A and B are represented in green and blue, respectively. The first and last amino acid of each model structure are indicated. (B) Homodimeric NcGR model showing the Pyr_redox 2 (dark blue, Pyridine nucleotide-disulphide oxidoreductase domain; PF07992) and Pyr redox dim (magenta, Pyridine nucleotide-disulphide oxidoreductase, dimerization domain; PF02852) domains. Homodimeric NcGR model was obtained in Galaxyhomer and images were generated in PyMol software.

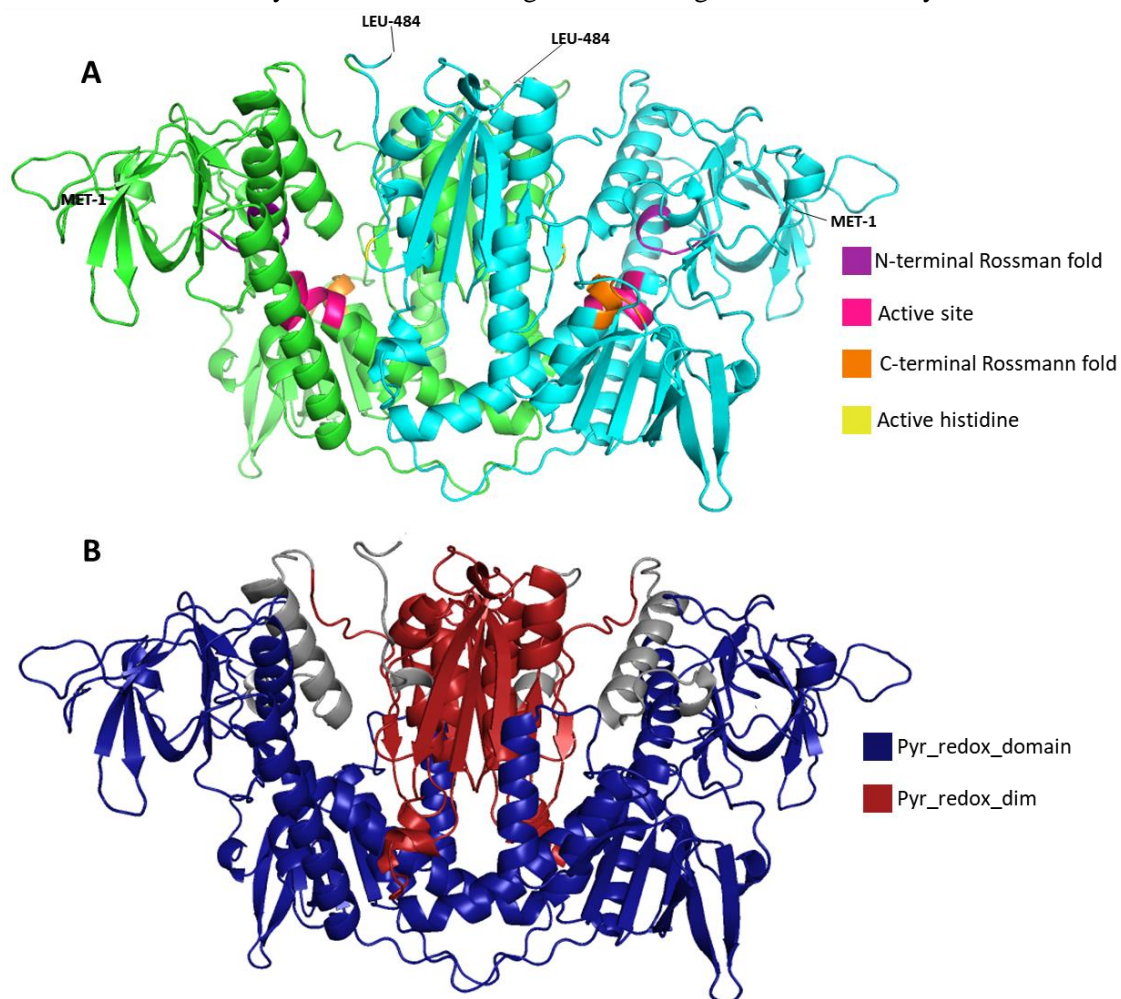
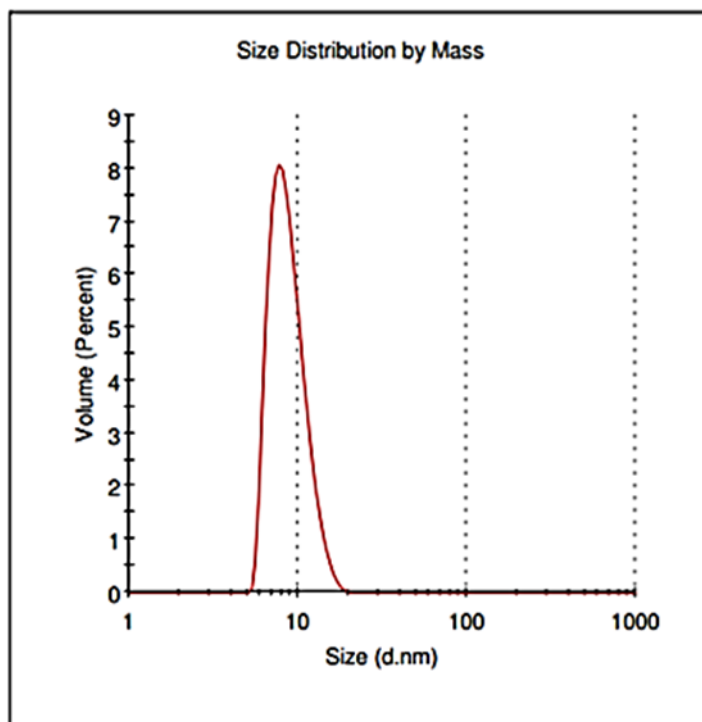


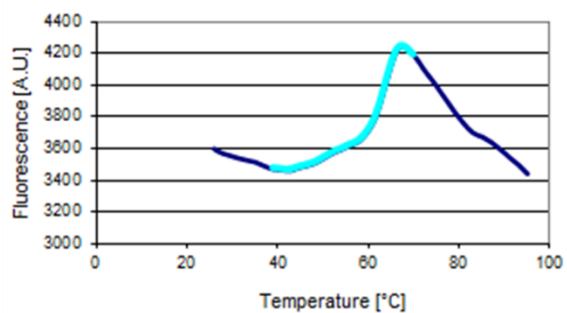
Fig. S4. Mass distribution of light scattered by protein (rNcGR) solution as a function of particle diameter. rNcGR in buffer containing 100 mM of KH₂PO₄, 50mM Tris, 5% Glycerol, pH 7,5.



Diameter (nm)	%Pd	%Mass
9.77±2.72	25.7	100.0

Fig.S5. Thermal denaturation profile for rNcGR in water (A) and in native buffer (B). The highlighted color (cyan) indicates the range used to calculate the melting temperature - T_m . T_m for rNcGR was 62.5°C in water and 64.6°C in buffer containing 100 mM of KH_2PO_4 , 50mM Tris, 5% Glycerol, pH 7,5. The samples were monitored using the fluorescence signal of the SYPRO® orange (492/610 nm).

A



B

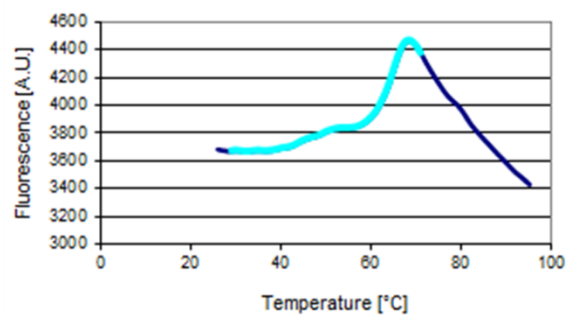


Fig.S6. Detection of rNcGR by ELISA. The rNcGR was immobilized on 96 well plates and incubated with dilutions (1:500, 1:1000, 1:2000, 1:4000) of anti-rNcGR. As a control, the antiurea serum diluted to 1:500 was applied under the same conditions. After washing, the samples were incubated with the peroxidase-conjugated rabbit anti-mouse and revealed with TMB. The plates were read at 540 nm and the results expressed as mean \pm standard deviation. The experimental groups were compared by One-way analysis of variance ANOVA, using the Bonferroni post-test. * Indicates $p < 0.05$. The rNcGR induced a robust immune response in mice. All dilutions of the anti-NcGR serum detected the recombinant protein NcGR above 2.5 of absorbance at 540 nm. Comparatively, the negative control (anti-urea serum) diluted at 1:500 reached 0.187 under the same conditions.

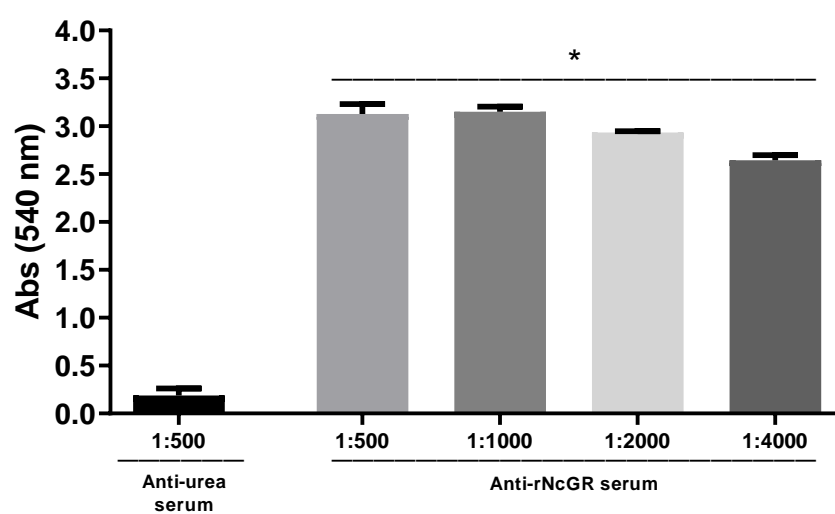


Fig.S7 Multiple alignments of *N. caninum* glutathione reductase (NcGR) sequence with other GR's species. Multiple alignments of *N. caninum* glutathione reductase (NcGR) sequence with *Escherichia coli* (EcGR, ID:1GER), *Yersinia pestis* (YpGR, ID:5VDN), *Vibrio parahaemolyticus* (VpGR, ID:5U10), *Streptococcus mutans* (SmGR, ID:5V36), *Enterococcus faecalis* (EfGR, ID:6B40), *Streptococcus pneumoniae* (SpGR, ID:6DU7), *Homo sapiens* (HsGR, ID:3DK9), *Saccharomyces cerevisiae* (ScGR, ID:2HQM), *Plasmodium falciparum* (PfGR, ID:1ONF), *Bartonella henselae str. Houston* (BhGR, ID:300H) Glutathione reductases. Yellow boxes indicated FAD binding sites. Blue*: residues that interact with FAD through hydrophobic interactions, Pink*: residues that interact with FAD through hydrogen bonds.

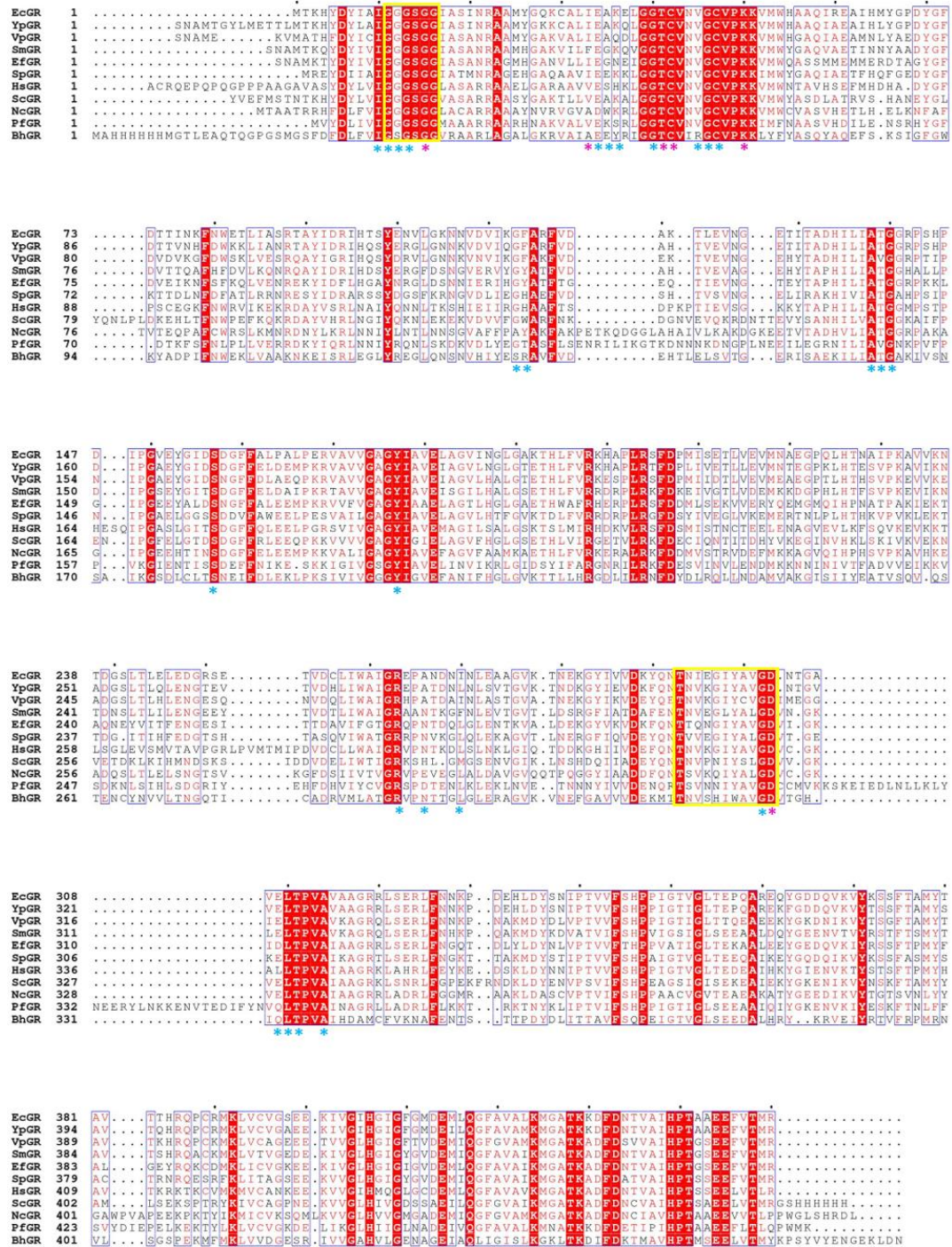


Table.S1. Identification of the rNcGR by MS/MS. The bands correspondent to the rNcGR monomer and homodimer (figure 7) were excised and identified by MS/MS (MALDI-TOF/TOF). The excised band, access number in ToxoDB, the description (according to ToxoDB), the MASCOT score, the coverage concerning the whole sequence, the position and identification of the peptides, the peptide spectrum matches (PSM), the predicted molecular weight and isoelectric point (pI) were displayed in the table.

Band	Access	Description	Score	Coverage	Peptides	Position	PSM	Molecular weight (kDa)	calc. pI
1 (Monomer)	NCLIV_063590	Glutathione reductase, related	233	11%	3	164-186	8	52711	8,21
					K.AGIPGEEHTINSDGFFELEEMPK.K K.AGIPGEEHTINSDGFFELEEMPK.K Oxidation (M) K.VELTPVAIAAGR.R K.VVGLHVVGMGADEMIQFGVAMK.M 2 Oxidation (M) K.VVGLHVVGMGADEMIQFGVAMK.M 3 Oxidation (M)	164-186 328-339 427-449 427-449			
2 (Dimer)	NCLIV_063590	Glutathione reductase, related	251	11%	3	164-186	4	52711	8,21
					K.AGIPGEEHTINSDGFFELEEMPK.K K.VELTPVAIAAGR.R K.VVGLHVVGMGADEMIQFGVAMK.M	328-339 427-449			

Table S2. NcGR predicted residues that bind FAD through hydrophobic interaction and hydrogen bonds compared with other GR's species. NcGR predicted residues that bind FAD through hydrophobic interaction and hydrogen bonds compared with with *Homo sapiens* (HsGR; ID:3DK9), *Escherichia coli* (EcGR; ID:1GER), *Bartonella henselae str. Houston* (BhGR; ID:3O0H), *Enterococcus faecalis* (EfGR; ID:6B4O), *Plasmodium falciparum* (PfGR; ID:1ONF), *Saccharomyces cerevisiae* (ScGR; ID:2HQM), *Streptococcus mutans* (ScGR; ID:5V36), *Streptococcus pneumoniae*(SpGR; ID:6DU7), *Vibrio parahaemolyticus* (VpGR; ID:5U10), *Yersinia pestis* (YpGR; ID:5VDN). C: strictly conserved residues (Light blue); X: non-conserved residues (dark blue); Substitutions are specifically indicated (pink).

Hydrophobic interactions			
Ile14	C	Ala156	C
Gly15	C	Thr157	V-PfGR/VpGR
Gly16	S-BhGR	Gly158	C
Gly17	C	Ser175	C
Asp38	E-All	Tyr195	C
Trp39	x	Arg282	C
Lys40	x	Glu285	x
Gly44	C	Leu289	x
Val49	R-BhGR	Gly322	C
Gly50	C	Glu329	x
Cys51	C	Leu330	C
Ala117	x	Thr331	C
Tyr118	x	Ala334	C
Hydrogen bonds			
Gly19	C	Cys46	C
Ala37	x	Lys54	C
Thr45	C	Asp323	C

CAPÍTULO III

Title: Extracellular H₂O₂, peroxiredoxin and glutathione reductase alters *Neospora caninum* invasion and proliferation in Vero cells.

Jade Cabestre Venancio Brochi¹; Luiz Miguel Pereira¹ and Ana Patrícia Yatsuda^{1*}

¹ Faculdade de Ciências Farmacêuticas de Ribeirão Preto, Universidade de São Paulo, Av do Café, sn/n, 14040-903, Ribeirão Preto, SP, Brazil.

* **Author for correspondence:** Ana Patrícia Yatsuda, ORCID: 0000-0001-7957-2279, e-mail:

ayatsuda@cfrrp.usp.br.

Submitted to: *Experimental Parasitology*.

ABSTRACT

Neospora caninum is a protozoan member of the Apicomplexa phylum and closely connected with abortion in cattle. The development of the parasite in host cells is characterized by the active secretion of proteins, allied to the tight control of the redox status. In this sense, the elucidation of the mechanisms related to the role of the redox agents and enzymes during the invasion and proliferation of *N. caninum* may contribute to the development of novel forms of neosporosis control. In this study, we verified the effects of the recombinant forms of *N. caninum* glutathione reductase (rNcGR) and peroxiredoxin (rNcPrx) as well as H₂O₂ in the tachyzoite invasion and proliferation. rNcPrx interfered in the *N. caninum* invasion in a redox state manner. Oxidized rNcPrx inhibited the *N. caninum* invasion and proliferation with no toxic effects observed in Vero cells. In contrast, lower concentrations of H₂O₂ (10 µM) stimulated the *N. caninum* invasion, which was reverted in higher doses (> 100 µM). H₂O₂ inhibited the parasite proliferation in lower concentrations compared to the cytotoxicity in host cells, resulting in a positive selectivity index (1.8). Our results indicate the connection between the *N. caninum* development and the redox state, contributing to the elucidation of mechanisms related to parasite propagation and control.

Key words: Peroxiredoxin, glutathione reductase, *Neospora caninum*, redox control, proliferation, invasion.

Highlights

- rNcGR, reduced rNcPrx and low H₂O₂ concentrations improved the *N. caninum* invasion.
- High H₂O₂ concentrations and non-reduced NcPrx inhibited the *N. caninum* invasion.
- Reduced rNcPrx and rNcGR increased Vero cell viability and inhibited the tachyzoite proliferation.
- The H₂O₂ IC₅₀ of tachyzoite proliferation was 320 μM and of Vero cells was 586 μM.
- *N. caninum* and infected cells showed more sensitivity to the H₂O₂ effects compared to non-infected Vero cells.

Introduction

Neosporosis is a relevant cause of abortion in cattle and neurodegeneration in dogs (DUBEY; BUXTON; WOUDA, 2006; DUBEY; SCHARES, 2011). This disease draws attention by the significant worldwide financial impact, around 1,3 billion dollars in milk and meat industries (REICHEL et al., 2013). Up to date, the control and prevention of neosporosis have not been effective through drugs or vaccines (HORCAJO et al., 2016). *Neospora caninum*, neosporosis etiological agent, is an Apicomplexa protozoan that has the tachyzoite form capable of actively invading and proliferating in host cells. The parasite has a resistance form, bradyzoite, fundamental for evasion and resistance from the immune system mechanisms (DUBEY; BUXTON; WOUDA, 2006; FERREIG; NISHIKAWA, 2020). The knowledge about *N. caninum* biology has been increasing since its discovery in 1988 by Dubey, evidencing a plethora of similarities and differences in comparison to *Toxoplasma gondii* (DUBEY et al., 1988).

To survive inside the host cells, Apicomplexa parasites must deal not only with radical oxygen species (ROS) produced by their own metabolism, but also by host mitochondrial aerobic respiration and further by host defense mechanisms or drugs (MÜLLER et al., 2003; MÜLLER, 2004). To avoid the death induced by oxidative stress, parasites exhibit plenty of antioxidants and redox enzymes, such as superoxide dismutase, peroxiredoxin, glutathione

reductase and catalase that assure the appropriated ROS scavenge. In addition, as described in *Plasmodium*, parasites can be benefited by the host redox apparatus to resist oxidative stress (KONCAREVIC et al., 2009; BRIZUELA et al., 2014). Superoxide dismutase catalyzes the decomposition of superoxide anion into hydrogen peroxide (H₂O₂) and molecular oxygen (WANG et al., 2018). High levels of H₂O₂ can damage the cellular structures inducing apoptosis (CALABRESE et al., 2019). Therefore, H₂O₂ is scavenged by peroxiredoxins or catalase, protecting the cells from its harmful effects. Glutathione reductase catalyzes the conversion of oxidized glutathione in reduced glutathione, an essential antioxidant agent that regulates the cellular redox homeostasis.

Peroxiredoxin (unpublished data), superoxide dismutase (CHO et al., 2004a) and glutathione reductase (VENANCIO-BROCHI et al., 2021) have been described in *N. caninum*, supporting the presence of a conserved redox mechanism in this parasite. Thioredoxin-dependent peroxide reductase (NcPrx) was experimentally described as a 2-Cys-Prx antioxidant and peroxidase cytoplasmic enzyme (unpublished data). Besides, glutathione reductase of *N. caninum* is also a cytosolic enzyme and the recombinant form of NcGR successfully recycles reduced glutathione in the presence of NADPH (VENANCIO-BROCHI et al., 2021).

ROS produced by macrophages restrain *T. gondii* proliferation in the early stages of infection, however this parasite can evade the ROS challenge through cellular respiratory burst suppression (SHRESTHA et al., 2006). Similarly, *N. caninum* early infection also increases oxidative stress (TONIN et al., 2014b; GLOMBOWSKY et al., 2017b) and it has been demonstrated that ROS induce inflammasome activation and control the parasite proliferation (MOTA et al., 2020).

Although the redox regulation is crucial to the host defense against *Neospora caninum* (MOTA et al., 2020), its impact in the *N. caninum* *in vivo* and *in vitro* invasion and proliferation remains unclear. Therefore, in this study, we investigated the proliferation and invasion facing different levels of H₂O₂ and/or recombinant redox enzymes (rNcPrx and rNcGR). Our results contribute to the understanding of the redox dynamics in *N. caninum*, elucidating some features of the antioxidant enzymes activities. It is the first time that the Apicomplexa invasion and proliferation in the host cell is evaluated in the presence of recombinant antioxidant enzymes.

Material and Methods

Neospora caninum cultivation and tachyzoite protein extract

N. caninum Nc-1 (DUBEY et al., 1988) tachyzoites were cultivated in Vero cell monolayers in RPMI-1640 at 37°C, 5% CO₂. The Vero cells were propagated in RPMI-1640 supplemented with 5% fetal bovine serum (FBS) under the same conditions. The parasites were purified after lysis of Vero cells using a needle (0.45x13mm) followed by syringe filtration at 5 mm (syringe filter). Next, the suspension was centrifuged at 5,000 g for 3 minutes at 4°C and the pellet was suspended in PBS. *N. caninum* tachyzoites were counted in a hemocytometer and adjusted to 2×10⁸ tachyzoites/ml. The *N. caninum* tachyzoite (2×10⁸ per 0.5 ml) and Vero protein (5×10⁶ per 0.5 ml) extracts were obtained by lysis in Triton-X-100™ 1%.

Cloning, expression and purification of rNcPrx and rNcGR

Cloning, expression, and purification of rNcPrx and rNcGR were performed according to previously published studies with modifications (VENANCIO-BROCHI et al., 2021). Briefly, the colonies of transformed *E. coli* BL21 (DE3) containing pET28-NcPrx or pET28-NcGR were inoculated into 5 ml of LB medium (Luria-Bertani) with kanamycin (50 µg/ml) for 18 hours, 37°C, 150 rpm. The suspensions were inoculated (1:100) in 500 ml of LB with kanamycin (50 µg/ml) and incubated at 37°C, 150 rpm until the optical density of 0.6 was reached at 600 nm. Next, the cultures were cooled down by ice incubation for 30 minutes and the expression of recombinant thioredoxin-dependent peroxide reductase (rNcPrx) and recombinant glutathione reductase (rNcGR) was induced by isopropyl β-D-1-thiogalactopyranoside (IPTG, 0.25 mM and 0.5 mM, respectively) at 18° C for 16h, 150 rpm. After centrifugation (15,000 g, 15 minutes), the supernatant was discarded and the bacterial pellet sonicated (15 cycles of 30 seconds at 70% amplitude; QSonica, Q500-110, CT, USA). Sonication was performed with different lysis buffer for immunization (denaturant lysis buffer: 8 M urea, 20 mM sodium phosphate 500 mM NaCl, pH 8.0) or enzymatic assays (native lysis buffer: 50 mM Tris HCl, 0.3 mM β-mercaptoethanol, 5% v/v glycerol, 0.2% TritonX-100). After sonication, samples were centrifuged (10000 g, 15 minutes, 4°C) and the supernatant was filtered in a 0.45 µm syringe filter (Millipore, MA, USA). The protein purification was carried out on a nickel column (packed GE PD-10 columns, NiSepharose, GE, USA). rNcPrx and

rNcGR purification under native conditions was performed with elution buffer (50 mM Tris HCl, 0.3 mM β -mercaptoethanol, 5% glycerol, 0.05% TritonX-100) containing 250 mM imidazole followed by desalting in Sephadex G-25 PD-10 column (GE Healthcare, UK) in reaction buffer (50 mM Tris, 0.05% Triton and 5% glycerol). The purified protein was concentrated in Pierce™ Centrifuge Column (Thermo Fisher, MA, USA). Finally, the integrity and the purity of the recombinant proteins were confirmed by SDS-PAGE, followed by Coomassie Brilliant Blue staining. Bradford assay was applied for protein concentration determination (BRADFORD, 1976).

Invasion assays

The enzyme rNcPrx was reduced in DTT 10 mM for 30 minutes. The DTT excess was removed using a Sephadex-G25 in a PD-10 column (Cytiva life sciences). *N. caninum* Lac-Z (PEREIRA; YATSUDA, 2014) was purified in a 5 μ M filter. The tachyzoites (1×10^6) were incubated with serial dilutions of rNcPrx (previously reduced or non-reduced; 200-12.5 μ g/mL), rNcGR (100-12.5 μ g/mL) and H₂O₂ (1000-100 e 10 μ M), or PBS (control), for 90 minutes at 37 °C. The tachyzoites were inoculated in triplicate (for each treatment) in 24 well-plate with Vero cells and incubated for 2 hours at 37°C for invasion, The wells were washed with PBS and the cells were incubated with 350 μ L of the lysis buffer (100 mM 2-[4-(2-hydroxyethyl)-1-piperazinyl] acid, pH 8,0; 1 mM CaCl₂; 1% Triton X-100, 0.5% SDS; 5 mM DTT (dithiothreitol)) and frozen overnight. The plate was thawed for 90 minutes at 50°C. The reaction of CPRG was performed in 96 well-plate with 100 μ L of CPRG buffer (5 mM Chlorophenol Red- β -D-galactopyranoside (Sigma, San Luis, Missouri, EUA), 5 mM 2-mercaptoethanol in PBS) and 150 μ l of the cells/Nc lysed in duplicate for 4 h, at 37° C. The absorbance was measured at 570 nm in an ELISA reader (Epoch, Biotek).

***N. caninum* proliferation assays**

For the *N. caninum* proliferation, the rNcPrx reduction was performed as described in the invasion assay. The *N. caninum* Lac-Z (PEREIRA; YATSUDA, 2014) tachyzoites were distributed (1×10^4 /well) in Vero cell cultures (in 96 well plates) and incubated for 2 hours, 37°C, 5% CO₂ to allow the parasite invasion. After the invasion, different treatments were performed. Serial dilutions of H₂O₂ (6.6-0.006 mM); reduced or non-reduced rNcPrx (2.7-0.004 μ M); rNcGR (0.24-0.004 μ M) were applied in *N. caninum* cultures and incubated for 72 hours, 37°C, 5% CO₂. Subsequently, the wells were washed twice with the PBS and the cells were

lysed with 125 μ L of lysis buffer (100 mM 2-[4-(2-hydroxyethyl)-1-piperazinyl] acid, pH 8,0; 1 mM CaCl_2 ; 1% Triton X-100, 0.5% SDS; 5 mM DTT (dithiothreitol)). The plate was frozen for 24 hours at -20°C followed by incubation at 50°C for 1 hour. Finally, 125 μ L/well of CPRG buffer (5 mM chlorophenol red β -D-galactonoside, CPRG, in lysis buffer) was added and the absorbance was measured at 570 nm in an ELISA reader (Epoch™ Microplate Spectrophotometer). In parallel, the cytotoxicity was performed in non-infected cells treated under the same conditions. After the treatment, cells were incubated with MTT solution (500 μ g/ml in RPMI) for 4 hours and the formazan diluted in DMSO. The absorbance was measured in an ELISA reader at 570 nm. Data were expressed in % of proliferation inhibition and % of cytotoxicity concerning the respective non-treated control group.

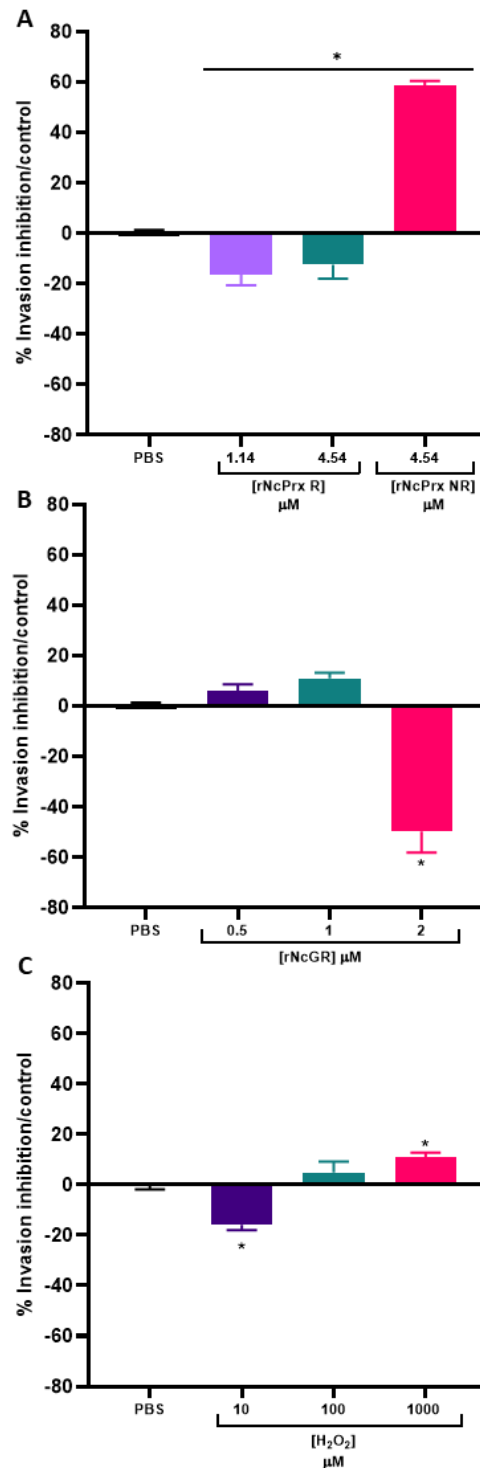
Statistical analysis

Results were analyzed using the software GraphPad Prism 8.0 (Graph Pad, USA). The invasion data were expressed as mean \pm standard error and the experimental groups were compared by One-way ANOVA. Subsequently, the data were submitted to the Bonferroni post-test and statistical significance was considered when the level of statistical error was less than 5% (or $p \leq 0.05$). The IC_{50} and the combination index (CI) were obtained fitting the curve of \log [concentration] vs normalized response, and the selective index ($\text{CC}_{50}/\text{IC}_{50}$) was determined.

Results

The incubation of the rNcPrx enzyme with tachyzoites induced different patterns in the cellular invasion, depending on its oxidation state. Non-reduced rNcPrx inhibited the tachyzoite invasion 59 ± 2 % in comparison to the control (rNcPrx NR, $p < 0.05$, Fig. 1.A). However, when the enzyme was reduced before the experiment, an increase in parasite invasion of 12.4 ± 5.5 % at $4.54 \mu\text{M}$ and of 16.3 ± 4.4 % at $1.14 \mu\text{M}$ was observed (rNcPrx R, $p < 0.05$, Fig. 1.A). Likewise, the rNcGR increased 49.7 ± 8.4 % parasite invasion at $2 \mu\text{M}$ ($p < 0.05$, Fig. 1.B). Moreover, the H_2O_2 demonstrated a dual action in the invasion according to the concentration. At low concentration ($10 \mu\text{M}$) H_2O_2 raised 15.9 ± 2.2 % the tachyzoite invasion and at high concentration ($1000 \mu\text{M}$) inhibited 11 ± 2 % the parasite invasion (Fig. 1.C).

Figure 1. Invasion of *N. caninum* tachyzoites in Vero cells after incubation with rNcPrx (A), rNcGR (B), H₂O₂ (C). Purified tachyzoites were incubated with different concentrations of rNcPrx (4.54-1.14 μ M), rNcGR (2-0.25 μ M) and H₂O₂ (1000, 100 and 10 μ M) for 90 minutes. After the incubation, the parasites were allowed to invade Vero cells for 2 hours. The cultures were lysed, incubated with CPRG and the absorbance was measured in an ELISA reader. The absorbance values were applied for the calculation of the percentage of inhibition using the non-treated controls as reference. **PBS:** Control; **R:** reduced enzyme. **NR:** non-reduced enzyme. * $p < 0,05$, One-way ANOVA, with Bonferroni posttest, confidence interval: 95%. Results represent three independent experiments in triplicate.



The proliferation of *N. caninum* was evaluated in the presence of the recombinant enzymes rNcGR and rNcPrx. The rNcPrx was evaluated in two conditions: reduced state and in absence of the reducing agent. The *N. caninum* proliferation was inhibited by non-reduced rNcPrx from $78 \pm 1 \%$ to $89.1 \pm 0.4 \%$ ($2.27 \mu\text{M}$ - $0.0044 \mu\text{M}$; $\log[\text{rNcPrx}]$:0.36 to -1.15) (Fig. 2.A, black line). In Vero cells, non-reduced rNcPrx reached $29 \pm 10 \%$ of cytotoxicity at the highest concentration ($2.27 \mu\text{M}$) (Fig. 2.A, red line).

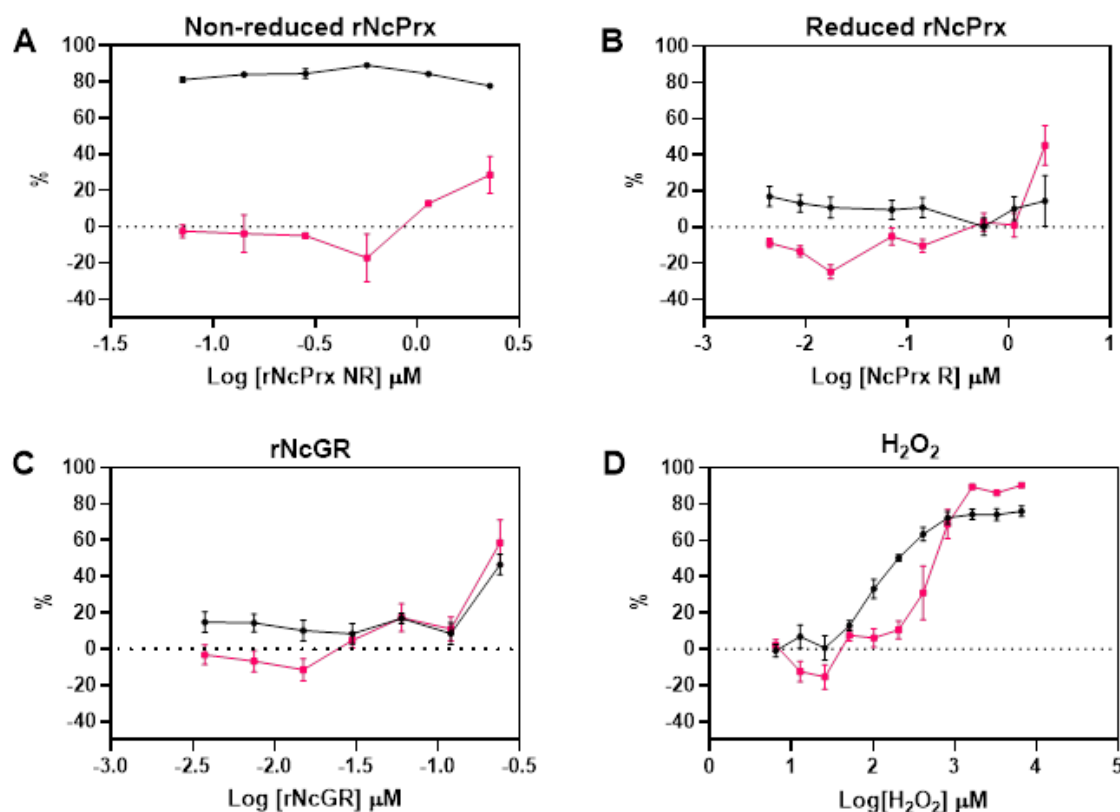
Reduced rNcPrx showed differential effects on *N. caninum* proliferation and Vero cell cytotoxicity. At higher concentrations ($2.27 \mu\text{M}$ - $0.07 \mu\text{M}$; $\log[\text{rNcPrx}]$:0.36 to -2.35), reduced rNcPrx inhibited *N. caninum* proliferation from $0.22 \pm 4.78\%$ to $16.9 \pm 5.6\%$ (Fig 2.B, black line). On the other hand, reduced rNcPrx at low concentrations (0.0044 - $0.14 \mu\text{M}$; $\log[\text{rNcPrx}]$: -2.35 to -0.85) increased Vero cell viability between $5.23 \pm 4.73 \%$ and $24.841 \pm 3.769 \%$ (Fig. 2.B, red line).

rNcGR ($0.004\mu\text{M}$ - $0.24\mu\text{M}$; $\log[\text{rNcGR}]$: -2.43 to -0.62) inhibited *N. caninum* proliferation from $8.616 \pm 6.115\%$ to $46.528 \pm 5.633\%$ (Fig. 2.C, black line). The protein was cytotoxic to Vero cells at concentrations above $0.03 \mu\text{M}$, which reversed at lower concentrations ($0.004 \mu\text{M}$ to $0.015 \mu\text{M}$; $\log[\text{rNcGR}]$: -2.43 to -1.83) and increased Vero cell viability by $11.48 \pm 5.99\%$ at $0.015 \mu\text{M}$ (Fig. 2.C, red line).

The incubation with H_2O_2 showed an inhibitory effect in *N. caninum* proliferation following a dose-response pattern (Fig 2.D, black line). On the other hand, H_2O_2 ($25.63 \mu\text{M}$; $\log[\text{H}_2\text{O}_2] \mu\text{M}$: 1.41) increased $15 \pm 7\%$ the Vero cell viability. However, the increase of H_2O_2 concentration (51.25 - $6560 \mu\text{M}$; $\log[\text{H}_2\text{O}_2] \mu\text{M}$:1.71 – 3.82) led to cytotoxic effects in Vero cells (Fig 2.D, red line). The H_2O_2 IC_{50} and CC_{50} for *N. caninum* proliferation and Vero cells cytotoxicity were $320 \mu\text{M}$ and $586 \mu\text{M}$, respectively, and the selective index (SI) was 1.8. The IC_{50} values and the SI indicated that Vero cells were more resistant to H_2O_2 than the intracellular *N. caninum*.

Figure 2. Effect of rNcPrx, rNcGR and H₂O₂ in *N. caninum* proliferation and Vero cell cytotoxicity. Vero cell monolayers were infected with *N. caninum* and incubated with rNcPrx (reduced or not) and rNcGR for 72 h. After incubation, the cultures were lysed and the *N. caninum* proliferation evaluated by CPRG. In parallel, non-infected Vero cells were treated under the same conditions and the cytotoxicity was determined by MTT. The percentage of inhibition was calculated in relation to the non-treated controls. Graphs represent the following treatments: (A) Non reduced rNcPrx. (B) Reduced rNcPrx in DTT (10mM). (C) rNcGR (D) H₂O₂. Red line: % cytotoxicity in Vero cell; black line: % of proliferation inhibition of *N. caninum*. Results represent three independent experiments in triplicate.

→ % Proliferation inhibition → %Cytotoxicity



Discussion

Here, we evaluated the effects of the redox balance alteration on the *N. caninum* invasion and proliferation. H₂O₂ and recombinant forms of antioxidant enzymes (rNcPrx and rNcGR) treatments indicated the sensitivity of *N. caninum* to factors linked to the extracellular environment.

NcPrx is predicted to be an unstable enzyme in solution (Instability index II: 42,73-Protparam, <https://web.expasy.org/protparam/>), tending to form dimers (oxidized). Therefore, we evaluated the action of rNcPrx reduced using DTT or non-reduced. The antioxidant actions of the recombinant enzymes rNcPrx (reduced) (Unpublished results) and rNcGR (VENANCIO-

BROCHI et al., 2021) are to scavenge H₂O₂ and to convert oxidized glutathione in reduced glutathione, respectively. On the other hand, whereas the thioredoxin can be secreted by cells and be found in extracellular medium (Tanudji et al., 2003), we suggest that non-reduced rNcPrx could deplete extracellular thioredoxin and indirectly contribute to the decrease of oxidant scavenge in this environment.

We have shown different tachyzoite response patterns to H₂O₂, depending on the parasite environment. *N. caninum* proliferate within the host cell in the parasitophorous vacuole until the cell lysis. After that, the egressed parasite faces the challenge of adapting to new extracellular conditions. In *T. gondii*, the metabolism of the egressed tachyzoite is directed through the glycolytic pathway to minimize the oxidative stress (SOLDATI; DUBREMETZ; LEBRUN, 2001; BIDDAU et al., 2018). When the parasite finds a new host cell, the parasite initiates an active invasion process, a finely regulated and orchestrated process. Several parasite proteins act during the cell invasion, where their folding and activity are regulated by the oxidative state (SOLDATI; DUBREMETZ; LEBRUN, 2001; BIDDAU et al., 2018). Therefore, modifications in the redox state of the parasite will alter the invasion success. The increase of *N. caninum* invasion after treatment with reduced rNcPrx, rNcGR and low levels of H₂O₂ is consistent with literature: low level of free radicals is more conducive for parasite invasion, as reported for *Entamoeba histolytica* (SEN et al., 2007) and *Toxoplasma gondii* (CAMPS; BOOTHROYD, 2001). On the other hand, the oxidative environment is a disadvantage for the *N. caninum* invasion, as observed in high H₂O₂ levels and non-reduced rNcPrx treatment.

In *N. caninum*, the low concentrations of H₂O₂ increased the invasion rate, suggesting the role of this oxidative molecule in cellular signaling (FOREMAN et al., 2003; GEISZT; LETO, 2004; DIEBOLD; CHANDEL, 2016). It has been reported a dual effect of H₂O₂ and other peroxides (VEAL; DAY; MORGAN, 2007), usually associated with the concentration, resulting, for example, distinct transcriptional responses in *Schizosaccharomyces pombe* (QUINN et al., 2002) and in different patterns of p53-regulated gene expression in cancer cell lines (SABLINA et al., 2005).

Higher levels of H₂O₂ induce pro-oxidant proteins involved in apoptosis in cancer and endothelial cells (CAI, 2005; SABLINA et al., 2005), which may be associated with the decrease of *N. caninum* invasion observed. On the other side, low H₂O₂ levels induce the expression of antioxidant proteins in cancer cells (SABLINA et al., 2005), and this phenomenon

could be involved in the *N. caninum* invasion success after low H₂O₂ levels (10μM) treatment. Further studies exploring apoptosis markers and antioxidant proteins expression in *N. caninum* measurements will help elucidating those hypotheses.

As described for *Plasmodium sp.*, *N. caninum* development benefits from the host cell's antioxidant defenses to maintain its own redox balance (KONCAREVIC et al., 2009; MÜLLER, 2015). The difference between the IC₅₀ values from Vero cytotoxicity and *N. caninum* proliferation suggests that the host cells present more defenses against oxidative challenges than the parasite in the host cell. Therefore, external oxidative stimulus, represented by low H₂O₂ levels, could inhibit the parasite proliferation without damaging the cell, representing an interesting approach to control neosporosis proliferation. Moreover, the Vero cell showed moderate viability at low H₂O₂ levels (subtoxic concentrations) as demonstrated in other mammalian cells, such as TOTL-86 cells, BHK-21 cells and hybridoma cells in culture (BURDON; ALLIANGANA; GILL, 1995; OSTROVIDOV et al., 1998; OHGURO et al., 1999). Subtoxic concentrations of H₂O₂ has also been associated with a role in signaling during the proliferation of cells (SUZUKI; FORMAN; SEVANI, 1997). In contrast, for *Trypanosoma cruzi*, the oxidative stimulus (Paraquat and H₂O₂) favors the parasite proliferation of the epimastigote form (NOGUEIRA et al., 2015).

Further studies will investigate the H₂O₂ amount that defunds to the parasitophorous vacuole, and the mechanisms related to *N. caninum* proliferation. Curiously, the H₂O₂ IC₅₀ for Dd2 and 3D7 isolates of *Plasmodium falciparum* is 46 mM and 78 mM, respectively (WEZENA et al., 2017). These concentrations are higher compared to the value determined for *N. caninum* (320.5 μM). Therefore, the intracellular tachyzoite form of *Neospora caninum* (in Vero cell) is more susceptible to H₂O₂ than *P. falciparum* trophozoite in the erythrocyte. This difference is probably associated with the higher antioxidant defense in erythrocytes when compared with Vero cells (SIEMS; SOMMERBURG; GRUNE, 2000). Moreover, our results are congruent with inhibition of *T. gondii* proliferation in macrophage cells at high levels of H₂O₂ (200uM and 600uM) (XUE et al., 2017).

Conclusions

Our data demonstrated that the reducing treatments (rNcGR and reduced rNcPrx) or low concentrations of H₂O₂ improved the invasion success by the parasite. On the other hand, the oxidizing treatments (high H₂O₂ concentrations) and the presence of non-reduced rNcPrx

showed an inhibitory effect in the parasite invasion. In proliferation assays, we observed that the reducing treatments (reduced rNcPrx and low concentrations of rNcGR) or low concentrations of H₂O₂ act in favor of the Vero cell viability as well as inhibiting the tachyzoite proliferation. Furthermore, the parasite showed more sensitivity to the H₂O₂ effects compared to non-infected Vero cells. Our results indicated, for the first time, several *N. caninum* features under extracellular H₂O₂ challenge. These data will contribute to the elucidation of the oxidative balance role during the invasion and proliferation, which comprises key pathways for the development of novel anti-*N. caninum* molecular strategies.

Acknowledgements

We would like to thank Maraísa Palhão Verri for the excellent technical assistance.

Author Contributions

JCVB: Conceptualization; Data curation; Formal analysis; Investigation; Methodology; Project administration; Software; Validation; Visualization; Writing original draft. **LMP:** Formal analysis; Methodology; Supervision; Resources; Writing - review & editing. **APY:** Funding acquisition; Formal analysis; Methodology; Project administration; Resources; Supervision; Writing - review & editing.

Financial Support

This research was supported by public funding from São Paulo Research Foundation (FAPESP) (Grants: 18/21020-3 to APY) and by funds from FAPESP fellowship (2019/ 05758-5 to JCVB). This study was financed in part by the Coordenação de Aperfeiçoamento de Pessoal de Nível Superior - Brasil (CAPES) - Finance Code 001.

Declarations

Conflicts of Interest: The authors declare that the research was conducted in the absence of any commercial or financial relationships that could be seen as a potential conflict of interest.

3. DISCUSSÃO FINAL

3. DISCUSSÃO FINAL

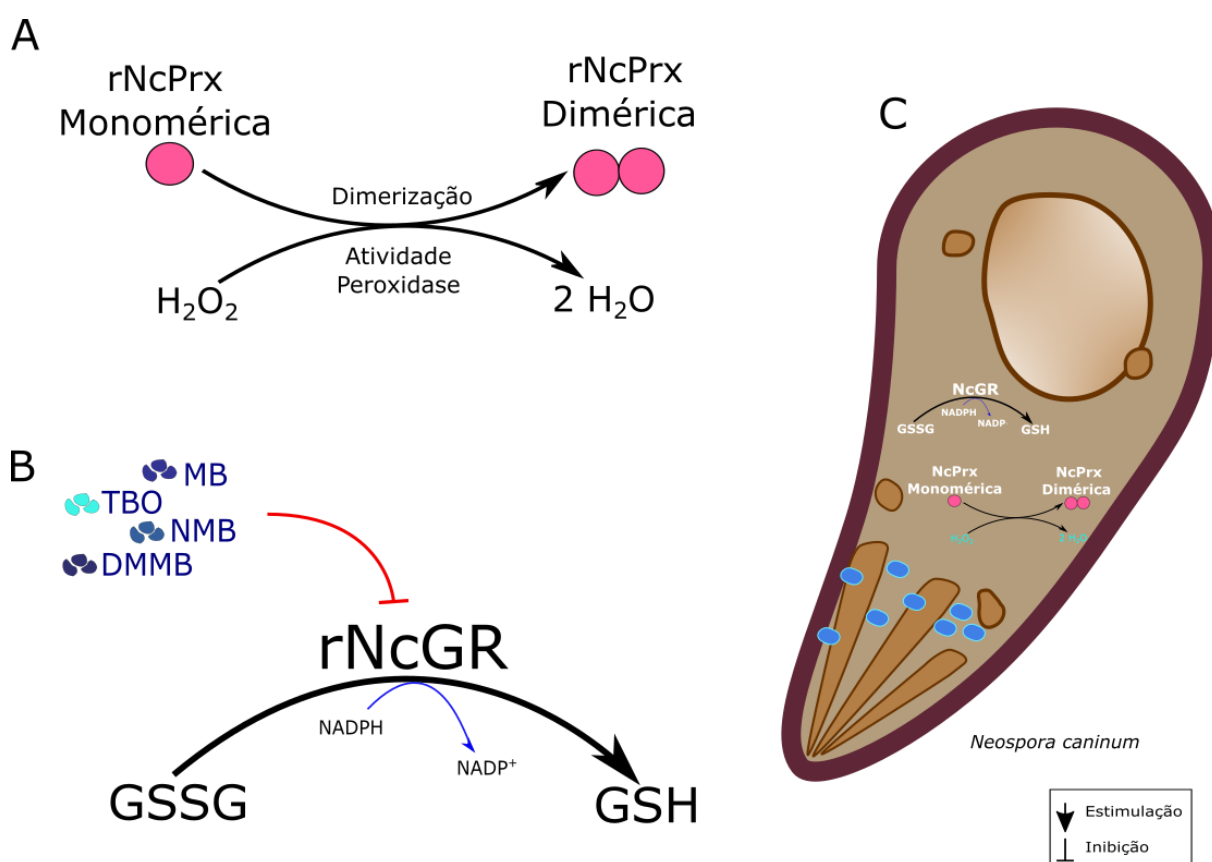
N. caninum é um parasita descrito há 33 anos (Dubey et al., 1988) e é relativamente novo dentre os Apicomplexas, de forma que sua biologia se encontra em fase de ampla investigação e novas descobertas. Ao revisar a literatura disponível para *N. caninum*, percebe-se uma tendência em estudar proteínas envolvidas na invasão e proliferação como alvos de medicamentos e vacinas (HEMPHILL; AGUADO-MARTÍNEZ; MÜLLER, 2016), porém pouca atenção é dada para alvos do sistema redox deste parasita. Por outro lado, estudos mostram que a progressão da neosporose ocorre em meio ao acentuado aumento da produção de EROs e ERNs e da elevação de níveis de biomarcadores de estresse oxidativo e inflamação nos tecidos do hospedeiro, (FIDAN et al., 2010; TONIN et al., 2015; GLOMBOWSKY et al., 2017a; BAHRAMI et al., 2019) podendo resultar em sinais clínicos ou até mesmo estimular a conversão da forma taquizoíta em bradizoíta (VONLAUFEN et al., 2002). Ademais, já foi demonstrado que a replicação de *N. caninum* pode ser inibida através de mecanismos ativados por EROs (MOTA et al., 2020; PEREIRA et al., 2020). No organismo hospedeiro o estudo do estresse oxidativo é embasado em um corpo de evidências de longa data e grande parte de seus componentes são profundamente conhecidos (NORDBERG; ARNÉR, 2001; SORDILLO; AITKEN, 2009), por outro lado, quando olhamos para *N. caninum*, apenas poucas características de seu sistema redox são conhecidas tanto das proteínas envolvidas como do comportamento frente ao estresse oxidativo (CHO et al., 2004a; MOTA et al., 2020; PEREIRA et al., 2020; SONG et al., 2020, 2021). Assim, para contribuir com o entendimento do controle redox em *N. caninum* e buscar novos alvos de tratamento e vacinas, buscamos descrever duas enzimas conservadas do sistema redox e avaliar o comportamento do parasita frente ao estresse oxidativo. As enzimas escolhidas para estudo foram as que apresentaram uma expressão abundante na análise proteômica do parasita feita pelo nosso grupo de pesquisa (OLIVEIRA, 2013).

Como parte importante do sistema redox, peroxirredoxinas são peroxidases e, portanto, atuam na linha de frente da defesa redox eliminando peróxidos produzidos em diversos processos e em especial pela degradação do radical superóxido pela enzima superóxido dismutase (RHEE, 2016). Em nosso trabalho (Capítulo 1), a peroxirredoxina de *N. caninum* apresentou alta homologia com relação Prx de outros Apicomplexas, sendo que sua forma recombinante apresentou atividade peroxidase e antioxidante sugerindo que a enzima exerça essas funções no parasita. Nos ensaios utilizando taquizoítas em cultura de células Vero

verificamos a presença de NcPrx no citosol do parasita e que a enzima se torna oxidada após o tratamento com H_2O_2 , sugerindo sua ação peroxidase no parasita (Figura 5. A,C).

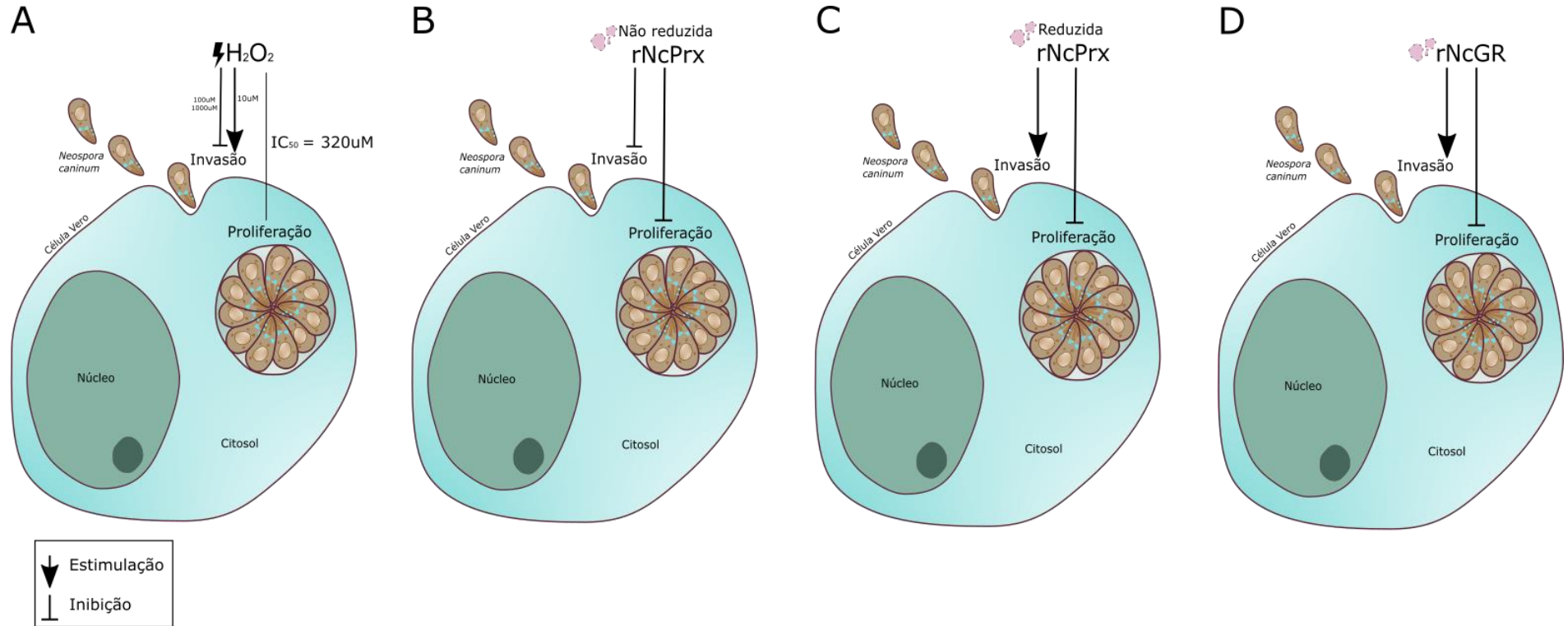
Da mesma forma, a enzima NcGR foi descrita (Capítulo 2) apresentando alta homologia em relação aos Apicomplexas e a enzima, assim como NcPrx, também foi detectada no citosol do parasita. Além disso, NcGR foi inibida por corantes fenotiazínicos sugerindo que a inibição da proliferação de *N. caninum* em células Vero tratadas com os corantes observada em Pereira et al., (2018, 2020) pode ter como um dos mecanismos de ação a inibição da enzima GR, uma vez que esta recicla os níveis de glutatona reduzida na célula, um importante tampão redox (Figura 5. B,C).

Figura 5. NcPrx e NcGR são enzimas do controle redox de *N. caninum*. (A) rNcPrx apresentou atividade peroxidase e antioxidante, sofrendo dimerização ao reduzir o H_2O_2 . (B) rNcGR catalisa a conversão de GSSG em GSH, com consumo de NADPH, e é inibida pelos corantes fenotiazínicos MB, TBO, NMB e DMMB. (C) *N. caninum* expressa as enzimas NcGR e NcPrx no citosol. NcPrx pode atuar como um biossensor redox no citosol de taquizoítas de *N. caninum*. GSSG: glutatona oxidada; GSH: glutatona reduzida; MB: azul de metileno; TBO: azul de toluidina; NMB: novo azul de metileno; DMMB: 1,9-dimetil-azul de metileno.



Dessa forma, tanto uma peroxidase, NcPrx, como um importante componente do sistema glutationa, NcGR, foram descritos no parasita através dos resultados aqui apresentados. Por outro lado, ainda resta investigar se essas enzimas exercem funções essenciais para o controle redox e virulência do parasita ou se suas funções podem ser completamente ou parcialmente compensadas pela ação de outras enzimas do sistema redox. Dessa forma, NcGR e NcPrx são potenciais candidatos para estudos envolvendo nocaute em *N. caninum*. Apesar dessas perguntas não terem sido respondidas no presente estudo, exploramos e padronizamos técnicas importantes para avaliar novas drogas/fármacos/compostos em *N. caninum*. Primeiramente, através da determinação dos parâmetros cinéticos de NcGR poderemos avaliar o efeito de outras drogas e/ou compostos nessa enzima bem como futuramente utilizar sua estrutura tridimensional no processo de *drug design* para elencar novos candidatos. Segundo, Prx é um importante biomarcador redox em células de mamíferos, bactérias e leveduras (POYNTON; HAMPTON, 2014b). Nesse sentido, NcPrx demonstrou-se sensível ao peróxido de hidrogênio em *N. caninum* podendo ser uma ferramenta interessante para avaliar flutuações redox no parasita frente ao tratamento com drogas, requerendo futuros estudos para investigar seu papel como biomarcador. Além disso, é válido investigar NcPrx como uma vacina em modelos animais, já que estudos mostram que Prx em *T. gondii* é capaz de gerar atividade imunológica protetora (MARSHALL et al., 2011; FERREIG; NISHIKAWA, 2016; FERREIG et al., 2017). Por fim, os dados apresentados no Capítulo 3 nos ajudaram a compreender de que forma podemos manipular o ambiente redox do parasita e da célula infectada para inibir a invasão e proliferação de *N. caninum* (Figura 6), contribuindo para o desenvolvimento de novas estratégias no tratamento da neosporose.

Figura 6. Efeitos do H_2O_2 , rNcPrx (não reduzida e reduzida) e rNcGR na invasão e proliferação de *N. caninum* em células Vero. **(A)** O tratamento de taquizoítas com H_2O_2 nas concentrações de 100 e 1000 μM inibiu e na concentração de 10 μM estimulou a invasão de *N. caninum*. O IC_{50} de H_2O_2 da inibição da proliferação de *N. caninum* em células Vero foi de 320 μM . **(B)** rNcPrx não reduzida inibiu a invasão e a proliferação de *N. caninum*. **(C)** rNcPrx reduzida estimulou a invasão e inibiu a proliferação de *N. caninum*. **(D)** rNcGR estimulou a invasão e inibiu a proliferação de *N. caninum*.



4. CONCLUSÕES

As enzimas recombinantes NcPrx e NcGR obtidas a partir da clonagem e expressão heteróloga apresentaram a identidade confirmada por espectrometria de massas.

A enzima rNcGR apresentou perfil cinético michaeliano ($K_m(\text{GSSG}): 0.10 \pm 0.02 \text{ mM}$; $k_{\text{cat}}(\text{GSSG}): 0.076 \pm 0.003 \text{ s}^{-1}$; $K_m(\text{NADPH}): 0.006 \pm 0.001 \text{ mM}$; $k_{\text{cat}}(\text{NADPH}): 0.080 \pm 0.003 \text{ s}^{-1}$).

A atividade de rNcGR foi inibida pelos corantes fenotiazínicos ($\text{IC}_{50(\text{MB})}: 2.1 \pm 0.2 \mu\text{M}$, $\text{IC}_{50(\text{DMMB})}: 11 \pm 2 \mu\text{M}$, $\text{IC}_{50(\text{NMB})}: 0.7 \pm 0.1 \mu\text{M}$, e $\text{IC}_{50(\text{TBO})}: 0.9 \pm 0.2 \mu\text{M}$) sugerindo um possível mecanismo de ação dessas moléculas em *N. caninum*.

N. caninum expressa as enzimas NcGR e NcPrx no citosol, sugerindo que exerçam suas funções antioxidantes nesse compartimento do parasita.

rNcPrx desempenha função antioxidante e peroxidase *in vitro* e sofre dimerização proporcional à concentração de H_2O_2 .

Em taquizoítas intracelulares e egressos, a enzima NcPrx responde ao H_2O_2 sofrendo dimerização, sugerindo que esteja envolvida no *clearance* de H_2O_2 no citosol e que seja um sensor redox em *N. caninum*.

Altas concentrações das enzimas recombinantes NcPrx (reduzida) e NcGR ou baixos níveis de H_2O_2 favorecem a invasão de *N. caninum* na célula Vero, ao passo que o ambiente oxidativo (altas concentrações de H_2O_2 ou NcPrx não reduzida) inibem.

A proliferação de *N. caninum* é inibida tanto pela presença das enzimas antioxidantes rNcGR e rNcPrx como do H_2O_2 .

H_2O_2 inibiu a proliferação do parasita em uma menor concentração ($\text{IC}_{50}: 320 \mu\text{M}$) quando comparado com a citotoxicidade em células Vero ($\text{CC}_{50}: 586 \mu\text{M}$), resultando em um índice de seletividade positivo (1.8).

5. REFERÊNCIAS BIBLIOGRÁFICAS

- AKERMAN, S. E.; MÜLLER, S. 2-Cys peroxiredoxin PfTrx-Px1 is involved in the antioxidant defence of *Plasmodium falciparum*. **Molecular and Biochemical Parasitology**, v. 130, n. 2, p. 75–81, 31 ago. 2003. Disponível em: <<https://pubmed.ncbi.nlm.nih.gov/12946843/>>. Acesso em: 14 jul. 2020.
- AKERMAN, S. E.; MÜLLER, S. Peroxiredoxin-linked detoxification of hydroperoxides in *Toxoplasma gondii*. **The Journal of biological chemistry**, v. 280, n. 1, p. 564–70, 7 jan. 2005. Disponível em: <<http://www.ncbi.nlm.nih.gov/pubmed/15507457>>. Acesso em: 18 jun. 2018.
- AKOACHERE, M. et al. In vitro assessment of methylene blue on chloroquine-sensitive and -resistant *Plasmodium falciparum* strains reveals synergistic action with artemisinins. **Antimicrobial agents and chemotherapy**, v. 49, n. 11, p. 4592–7, 1 nov. 2005. Disponível em: <<http://www.ncbi.nlm.nih.gov/pubmed/16251300>>. Acesso em: 3 fev. 2019.
- ALINE, F.; BOUT, D.; DIMIER-POISSON, I. Dendritic Cells as Effector Cells: Gamma Interferon Activation of Murine Dendritic Cells Triggers Oxygen-Dependent Inhibition of *Toxoplasma gondii* Replication. **Infection and Immunity**, v. 70, n. 5, p. 2368–2374, 2002. Disponível em: <<https://journals.asm.org/doi/abs/10.1128/IAI.70.5.2368-2374.2002>>. Acesso em: 26 out. 2021.
- ALMAGRO ARMENTEROS, J. J. et al. SignalP 5.0 improves signal peptide predictions using deep neural networks. **Nature Biotechnology**, v. 37, n. 4, p. 420–423, 1 abr. 2019. Disponível em: <<https://doi.org/10.1038/s41587-019-0036-z>>. Acesso em: 23 jul. 2020.
- ALMERÍA, S. et al. Red foxes (*Vulpes vulpes*) are a natural intermediate host of *Neospora caninum*. **Veterinary Parasitology**, v. 107, n. 4, p. 287–294, 22 ago. 2002. . Acesso em: 10 jun. 2020.
- ANDERSON, M. L.; ANDRIANARIVO, A. G.; CONRAD, P. A. Neosporosis in cattle. In: Animal Reproduction Science, **Anais...Elsevier**, 2 jul. 2000. . Acesso em: 11 jun. 2020.
- ANDERSON, M. L.; BARR, B. C.; HOFFMAN, R. L. A survey of causes of bovine abortion occurring in the San Joaquin Valley, California. **Journal of Veterinary Diagnostic Investigation**, v. 2, n. 4, p. 283–287, 1990. . Acesso em: 11 jun. 2020.
- ANGELUCCI, F. et al. Typical 2-Cys peroxiredoxins in human parasites: Several physiological roles for a potential chemotherapy target. **Molecular and Biochemical Parasitology**, v. 206, n. 1–2, p. 2–12, mar. 2016. Disponível em: <<http://www.ncbi.nlm.nih.gov/pubmed/27002228>>. Acesso em: 25 jul. 2018.
- ANVARI, D. et al. **Seroprevalence of Neospora caninum Infection in Dog Population Worldwide: A Systematic Review and Meta-analysis** *Acta Parasitologica* Springer, , 2020. . Acesso em: 11 jun. 2020.
- ARSCOTT, L. D.; THORPE, C.; WILLIAMS, C. H. Glutathione reductase from yeast. Differential reactivity of the nascent thiols in two-electron reduced enzyme and properties of a

monoalkylated derivative. **Biochemistry**, v. 20, n. 6, p. 1513–20, 17 mar. 1981. Disponível em: <<http://www.ncbi.nlm.nih.gov/pubmed/7013796>>. Acesso em: 19 ago. 2018.

ATAMNA, H. et al. Mode of antimalarial effect of methylene blue and some of its analogues on *Plasmodium falciparum* in culture and their inhibition of *P. vinckei petteri* and *P. yoelii nigeriensis* in vivo. **Biochemical Pharmacology**, v. 51, n. 5, p. 693–700, 8 mar. 1996. . Acesso em: 7 fev. 2021.

ATKINSON, R. et al. Seroprevalence of *Neospora caninum* infection following an abortion outbreak in a dairy cattle herd. **Australian Veterinary Journal**, v. 78, n. 4, p. 262–266, 1 abr. 2000. Disponível em: <<https://onlinelibrary.wiley.com/doi/full/10.1111/j.1751-0813.2000.tb11752.x>>. Acesso em: 3 nov. 2021.

BAEK, M. et al. GalaxyHomomer: A web server for protein homo-oligomer structure prediction from a monomer sequence or structure. **Nucleic Acids Research**, v. 45, n. W1, p. W320–W324, 3 jul. 2017. Disponível em: <<https://pubmed.ncbi.nlm.nih.gov/28387820/>>. Acesso em: 28 jan. 2021.

BAHRAMI, S. et al. Sperm quality and hormonal levels in C57BL/6 mice infected with *Neospora caninum*. **Veterinary Parasitology**, v. 273, p. 5–10, 1 set. 2019. . Acesso em: 8 nov. 2021.

BAKER, D. G. et al. Experimental Oral Inoculations in Birds to Evaluate Potential Definitive Hosts of *Neospora caninum*. **The Journal of Parasitology**, v. 81, n. 5, p. 783, out. 1995. . Acesso em: 10 jun. 2020.

BARLING, K. S. et al. Association of serologic status for *Neospora caninum* with postweaning weight gain and carcass measurements in beef calves. **Journal of the American Veterinary Medical Association**, v. 217, n. 9, p. 1356–1360, 1 nov. 2000. . Acesso em: 14 jun. 2020.

BARRANCO-MEDINA, S.; LÁZARO, J. J.; DIETZ, K. J. The oligomeric conformation of peroxiredoxins links redox state to function. **FEBS Letters**, v. 583, n. 12, p. 1809–1816, 18 jun. 2009. . Acesso em: 6 out. 2021.

BELTRAME-BOTELHO, I. T. et al. A Comparative in silico Study of the Antioxidant Defense Gene Repertoire of Distinct Lifestyle Trypanosomatid Species. **Evolutionary Bioinformatics**, v. 12, p. EBO.S40648, 7 jan. 2016. Disponível em: <<http://journals.sagepub.com/doi/10.4137/EBO.S40648>>. Acesso em: 3 jul. 2018.

BERKHOLZ, D. S. et al. Catalytic Cycle of Human Glutathione Reductase Near 1 Å Resolution. **Journal of Molecular Biology**, v. 382, n. 2, p. 371–384, 3 out. 2008. Disponível em: <<https://www.sciencedirect.com/science/article/pii/S0022283608008218?via%3Dihub>>. Acesso em: 18 jul. 2018.

BESTEIRO, S.; DUBREMETZ, J.-F.; LEBRUN, M. The moving junction of apicomplexan parasites: a key structure for invasion. **Cellular Microbiology**, v. 13, n. 6, p. 797–805, 1 jun.

2011. Disponível em: <<https://onlinelibrary.wiley.com/doi/full/10.1111/j.1462-5822.2011.01597.x>>. Acesso em: 3 nov. 2021.

BEYER, R. E. The role of ascorbate in antioxidant protection of biomembranes: Interaction with vitamin E and coenzyme Q. **Journal of Bioenergetics and Biomembranes**, v. 26, n. 4, p. 349–358, ago. 1994. Disponível em: <<https://pubmed.ncbi.nlm.nih.gov/7844109/>>. Acesso em: 27 jul. 2020.

BIDDAU, M. et al. Two essential Thioredoxins mediate apicoplast biogenesis, protein import, and gene expression in *Toxoplasma gondii*. **PLoS pathogens**, v. 14, n. 2, p. e1006836, 2018. Disponível em: <<http://www.ncbi.nlm.nih.gov/pubmed/29470517>>. Acesso em: 22 ago. 2019.

BJERKÅS, I.; MOHN, S. F.; PRESTHUS, J. Unidentified cyst-forming sporozoon causing encephalomyelitis and myositis in dogs. **Zeitschrift für Parasitenkunde**, v. 70, n. 2, p. 271–274, 1984. . Acesso em: 9 jun. 2020.

BJÖRKMAN, C. et al. Neospora species infection in a herd of dairy cattle. **Journal of the American Veterinary Medical Association**, v. 208, n. 9, p. 1441–1444, 1 maio 1996. . Acesso em: 10 jun. 2020.

BJÖRKMAN, C. et al. Application of the *Neospora Caninum* IgG Avidity ELISA in Assessment of Chronic Reproductive Losses after an Outbreak of Neosporosis in a Herd of Beef Cattle. **Journal of Veterinary Diagnostic Investigation**, v. 15, n. 1, p. 3–7, 25 jan. 2003. Disponível em: <<http://journals.sagepub.com/doi/10.1177/104063870301500102>>. Acesso em: 14 jun. 2020.

BÖHME, C. C. et al. Kinetic Characterization of Glutathione Reductase from the Malarial Parasite *Plasmodium falciparum*. **Journal of Biological Chemistry**, v. 275, n. 48, p. 37317–37323, 1 dez. 2000. Disponível em: <<http://www.ncbi.nlm.nih.gov/pubmed/10969088>>. Acesso em: 19 ago. 2018.

BOKOV, A.; CHAUDHURI, A.; RICHARDSON, A. The role of oxidative damage and stress in aging. **Mechanisms of Ageing and Development**, v. 125, n. 10–11, p. 811–826, 1 out. 2004. . Acesso em: 4 nov. 2021.

BOLDUC, J. A. et al. Novel hyperoxidation resistance motifs in 2-Cys peroxiredoxins. **Journal of Biological Chemistry**, v. 293, n. 30, p. 11901–11912, 27 jul. 2018. Disponível em: <<http://www.jbc.org/lookup/doi/10.1074/jbc.RA117.001690>>. Acesso em: 5 maio. 2019.

BOSCH, S. S. et al. Oxidative Stress Control by Apicomplexan Parasites. **BioMed Research International**, v. 2015, p. 1–10, 28 jan. 2015. Disponível em: <<http://www.hindawi.com/journals/bmri/2015/351289/>>. Acesso em: 18 jun. 2018.

BOUCHER, I. W. et al. Structural and biochemical characterization of a mitochondrial peroxiredoxin from *Plasmodium falciparum*. **Molecular Microbiology**, v. 61, n. 4, p. 948–959, 1 ago. 2006. Disponível em: <<https://onlinelibrary.wiley.com/doi/full/10.1111/j.1365-2958.2006.05303.x>>. Acesso em: 26 out. 2021.

BRADFORD, M. M. A rapid and sensitive method for the quantitation of microgram quantities of protein utilizing the principle of protein-dye binding. **Analytical Biochemistry**, v. 72, n. 1–2, p. 248–254, maio 1976. Disponível em: <<http://linkinghub.elsevier.com/retrieve/pii/0003269776905273>>. Acesso em: 27 jun. 2016.

BRADLEY, P. J.; SIBLEY, L. D. Rhoptries: an arsenal of secreted virulence factors. **Current Opinion in Microbiology**, v. 10, n. 6, p. 582–587, 1 dez. 2007. . Acesso em: 3 nov. 2021.

BRANDSTAEDTER, C. et al. Kinetic characterization of wild-type and mutant human thioredoxin glutathione reductase defines its reaction and regulatory mechanisms. **The FEBS journal**, v. 285, n. 3, p. 542–558, fev. 2018. Disponível em: <<http://doi.wiley.com/10.1111/febs.14357>>. Acesso em: 19 jul. 2018.

BRANDSTAEDTER, C. et al. The interactome of 2-Cys peroxiredoxins in Plasmodium falciparum. **Scientific Reports**, v. 9, n. 1, p. 1–15, 1 dez. 2019. Disponível em: <<https://doi.org/10.1038/s41598-019-49841-3>>. Acesso em: 14 jul. 2020.

BRIZUELA, M. et al. Treatment of Erythrocytes with the 2-Cys Peroxiredoxin Inhibitor, Conoidin A, Prevents the Growth of Plasmodium falciparum and Enhances Parasite Sensitivity to Chloroquine. **PLoS ONE**, v. 9, n. 4, p. e92411, 3 abr. 2014. Disponível em: <<https://dx.plos.org/10.1371/journal.pone.0092411>>. Acesso em: 3 fev. 2019.

BUCHHOLZ, K. et al. Interactions of Methylene Blue with Human Disulfide Reductases and Their Orthologues from Plasmodium falciparum. **Antimicrobial Agents and Chemotherapy**, v. 52, n. 1, p. 183–191, 1 jan. 2008. Disponível em: <<http://www.ncbi.nlm.nih.gov/pubmed/17967916>>. Acesso em: 18 jun. 2018.

BURDON, R.; ALLIANGANA, D.; GILL, V. Hydrogen peroxide and the proliferation of BHK-21 cells. **Free radical research**, v. 23, n. 5, p. 471–486, 1995. Disponível em: <<https://pubmed.ncbi.nlm.nih.gov/7581830/>>. Acesso em: 22 jul. 2021.

CAI, H. Hydrogen peroxide regulation of endothelial function: Origins, mechanisms, and consequences. **Cardiovascular Research**, v. 68, n. 1, p. 26–36, 1 out. 2005. Disponível em: <<https://academic.oup.com/cardiovasces/article/68/1/26/287849>>. Acesso em: 24 out. 2021.

CAI, H.; HARRISON, D. G. Endothelial Dysfunction in Cardiovascular Diseases: The Role of Oxidant Stress. **Circulation Research**, v. 87, n. 10, p. 840–844, 10 nov. 2000. Disponível em: <<https://www.ahajournals.org/doi/abs/10.1161/01.RES.87.10.840>>. Acesso em: 4 nov. 2021.

CALABRESE, G. et al. Hyperoxidation of mitochondrial peroxiredoxin limits H₂O₂-induced cell death in yeast. **The EMBO Journal**, v. 38, n. 18, 16 set. 2019. . Acesso em: 2 abr. 2020.

CAMPS, M.; BOOTHROYD, J. C. Toxoplasma gondii: Selective killing of extracellular parasites by oxidation using pyrrolidine dithiocarbamate. **Experimental Parasitology**, v. 98, n. 4, p. 206–214, ago. 2001. Disponível em: <<http://www.ncbi.nlm.nih.gov/pubmed/11560413>>. Acesso em: 2 abr. 2020.

CARLBERG, I.; MANNERVIK, B. Glutathione reductase. **Methods Enzymology**, v. 113, p. 484–490, 1985.

CERQUEIRA-CÉZAR, C. K. et al. All about neosporosis in Brazil. **Revista brasileira de parasitologia veterinária = Brazilian journal of veterinary parasitology : Orgao Oficial do Colegio Brasileiro de Parasitologia Veterinaria**, p. 0, 31 ago. 2017. Disponível em: <<http://www.ncbi.nlm.nih.gov/pubmed/28876360>>. Acesso em: 10 set. 2017.

CHAE, H. Z.; UHM, T. B.; RHEE, S. G. Dimerization of thiol-specific antioxidant and the essential role of cysteine 47. **Proceedings of the National Academy of Sciences of the United States of America**, v. 91, n. 15, p. 7022–7026, 19 jul. 1994. Disponível em: <<http://www.ncbi.nlm.nih.gov/pubmed/8041739>>. Acesso em: 26 jun. 2018.

CHARVAT, R. A.; ARRIZABALAGA, G. Oxidative stress generated during monensin treatment contributes to altered *Toxoplasma gondii* mitochondrial function. **Scientific Reports**, v. 6, n. 1, p. 22997, 15 set. 2016. Disponível em: <<http://www.ncbi.nlm.nih.gov/pubmed/26976749>>. Acesso em: 11 set. 2017.

CHEESEMAN, K. H.; SLATER, T. F. An introduction to free radical biochemistry. **British Medical Bulletin**, v. 49, n. 3, p. 481–493, 1 jan. 1993. Disponível em: <<https://academic.oup.com/bmb/article/49/3/481/299901>>. Acesso em: 4 nov. 2021.

CHO, M.-H. et al. Cloning, expression, and characterization of iron-containing superoxide dismutase from *Neospora caninum*. **Journal of Parasitology**, v. 90, n. 2, p. 278–285, 1 abr. 2004a. . Acesso em: 6 out. 2021.

CHO, M.-H. et al. CLONING, EXPRESSION, AND CHARACTERIZATION OF IRON-CONTAINING SUPEROXIDE DISMUTASE FROM NEOSPORA CANINUM. **Journal of Parasitology**, v. 90, n. 2, p. 278–285, 1 abr. 2004b. . Acesso em: 27 jul. 2021.

COLLINS, J. A. et al. Differential peroxiredoxin hyperoxidation regulates MAP kinase signaling in human articular chondrocytes. **Free Radical Biology and Medicine**, v. 134, p. 139–152, abr. 2019. Disponível em: <<https://linkinghub.elsevier.com/retrieve/pii/S0891584918325243>>. Acesso em: 5 maio. 2019.

COMINI, M. A. Measurement and meaning of cellular thiol:disulfide redox status. **Free Radical Research**, v. 50, n. 2, p. 246–271, 21 fev. 2016. Disponível em: <<http://www.tandfonline.com/doi/full/10.3109/10715762.2015.1110241>>. Acesso em: 27 ago. 2019.

COSTA, K. S. et al. Chickens (*Gallus domesticus*) are natural intermediate hosts of *Neospora caninum*. **International Journal for Parasitology**, v. 38, n. 2, p. 157–159, 1 fev. 2008. . Acesso em: 10 jun. 2020.

COUTO, N.; WOOD, J.; BARBER, J. The role of glutathione reductase and related enzymes on cellular redox homeostasis network. **Free Radical Biology and Medicine**, v. 95, p. 27–42, 1 jun. 2016. Disponível em:

<<https://www.sciencedirect.com/science/article/pii/S0891584916000873>>. Acesso em: 3 jul. 2018.

COX, A.; WINTERBOURN, C.; HAMPTON, M. Measuring the redox state of cellular peroxiredoxins by immunoblotting. **Methods in enzymology**, v. 474, p. 51–66, 1 jan. 2010. Disponível em: <<https://pubmed.ncbi.nlm.nih.gov/20609904/>>. Acesso em: 25 out. 2021.

DAS, K.; ROYCHOUDHURY, A. **Reactive oxygen species (ROS) and response of antioxidants as ROS-scavengers during environmental stress in plants** *Frontiers in Environmental Science* Frontiers Media S.A., , 2 dez. 2014. . Disponível em: <www.frontiersin.org>. Acesso em: 16 mar. 2021.

DAY, A. M. et al. Inactivation of a peroxiredoxin by hydrogen peroxide is critical for thioredoxin-mediated repair of oxidized proteins and cell survival. **Molecular cell**, v. 45, n. 3, p. 398–408, 10 fev. 2012. Disponível em: <<http://www.ncbi.nlm.nih.gov/pubmed/22245228>>. Acesso em: 2 abr. 2020.

DEBACHE, K.; HEMPHILL, A. Effects of miltefosine treatment in fibroblast cell cultures and in mice experimentally infected with *Neospora caninum* tachyzoites. **Parasitology**, v. 139, n. 7, p. 934–944, jun. 2012. Disponível em: <<https://www.cambridge.org/core/journals/parasitology/article/abs/effects-of-miltefosine-treatment-in-fibroblast-cell-cultures-and-in-mice-experimentally-infected-with-neospora-caninum-tachyzoites/DC7B0E1F3BF6C4E5179DE0EC50506320>>. Acesso em: 3 nov. 2021.

DEPONTE, M. Glutathione catalysis and the reaction mechanisms of glutathione-dependent enzymes. **Biochimica et Biophysica Acta (BBA) - General Subjects**, v. 1830, n. 5, p. 3217–3266, 1 maio 2013. Disponível em: <<https://www.sciencedirect.com/science/article/pii/S0304416512002735>>. Acesso em: 16 jul. 2018.

DEY, S.; SIDOR, A.; O’ROURKE, B. Compartment-specific Control of Reactive Oxygen Species Scavenging by Antioxidant Pathway Enzymes. **Journal of Biological Chemistry**, v. 291, n. 21, p. 11185–11197, 20 maio 2016. Disponível em: <<http://www.jbc.org/content/291/21/11185.full>>. Acesso em: 27 ago. 2019.

DIEBOLD, L.; CHANDEL, N. S. **Mitochondrial ROS regulation of proliferating cells** *Free Radical Biology and Medicine* Elsevier Inc., , 1 nov. 2016. . . Acesso em: 2 abr. 2020.

DONNELLY, S. et al. Helminth 2-Cys peroxiredoxin drives Th2 responses through a mechanism involving alternatively activated macrophages. **The FASEB Journal**, v. 22, n. 11, p. 4022–4032, 15 nov. 2008. Disponível em: <<http://www.fasebj.org/doi/10.1096/fj.08-106278>>. Acesso em: 25 jul. 2018.

DOROSTI, H. et al. Designing self-assembled peptide nanovaccine against *Streptococcus pneumoniae*: An in silico strategy. **Molecular and Cellular Probes**, v. 48, 1 dez. 2019. Disponível em: <<https://pubmed.ncbi.nlm.nih.gov/31520715/>>. Acesso em: 28 jan. 2021.

DUARTE, P. O. et al. Serological and molecular detection of *Neospora caninum* and *Toxoplasma gondii* in human umbilical cord blood and placental tissue samples. **Scientific Reports**, v. 10, n. 1, p. 1–8, 1 dez. 2020. Disponível em: <<https://doi.org/10.1038/s41598-020-65991-1>>. Acesso em: 7 out. 2020.

DUBEY, J. P. et al. Newly recognized fatal protozoan disease of dogs. **Journal of the American Veterinary Medical Association**, v. 192, n. 9, p. 1269–85, 1 maio 1988. Disponível em: <<http://www.ncbi.nlm.nih.gov/pubmed/3391851>>. Acesso em: 18 jun. 2018.

DUBEY, J. P. et al. Induced transplacental transmission of *Neospora caninum* in cattle. **Journal of the American Veterinary Medical Association**, v. 201, n. 5, p. 709–713, 1 set. 1992. . Acesso em: 10 jun. 2020.

DUBEY, J. P. Neosporosis—the first decade of research. **International Journal for Parasitology**, v. 29, n. 10, p. 1485–1488, 1 out. 1999. Disponível em: <<https://www.sciencedirect.com/science/article/pii/S0020751999001344>>. Acesso em: 18 jun. 2018.

DUBEY, J. P. et al. Redescription of *Neospora caninum* and its differentiation from related coccidia. **International Journal for Parasitology**, v. 32, n. 8, p. 929–946, 1 jul. 2002. . Acesso em: 2 nov. 2021.

DUBEY, J. P. et al. Gray wolf (*Canis lupus*) is a natural definitive host for *Neospora caninum*. **Veterinary Parasitology**, v. 181, n. 2–4, p. 382–387, 27 set. 2011. . Acesso em: 10 jun. 2020.

DUBEY, J. P.; BUXTON, D.; WOUDA, W. Pathogenesis of Bovine Neosporosis. **Journal of Comparative Pathology**, v. 134, n. 4, p. 267–289, maio 2006. Disponível em: <<http://www.ncbi.nlm.nih.gov/pubmed/16712863>>. Acesso em: 3 fev. 2019.

DUBEY, J. P.; SCHARES, G. Neosporosis in animals—The last five years. **Veterinary Parasitology**, v. 180, n. 1–2, p. 90–108, 4 ago. 2011. Disponível em: <<https://www.sciencedirect.com/science/article/pii/S0304401711003840>>. Acesso em: 18 jun. 2018.

DUBEY, J. P.; SCHARES, G.; ORTEGA-MORA, L. M. Epidemiology and Control of Neosporosis and *Neospora caninum*. **Clinical Microbiology Reviews**, v. 20, n. 2, p. 323–367, abr. 2007. Disponível em: <<https://journals.asm.org/doi/abs/10.1128/CMR.00031-06>>. Acesso em: 2 nov. 2021.

FALL, B. et al. *Plasmodium falciparum* susceptibility to standard and potential anti-malarial drugs in Dakar, Senegal, during the 2013–2014 malaria season. **Malaria Journal**, v. 14, n. 1, p. 60, 6 fev. 2015. Disponível em: <<http://www.ncbi.nlm.nih.gov/pubmed/25849097>>. Acesso em: 14 jan. 2019.

FÄRBER, P. M. et al. Recombinant *Plasmodium falciparum* glutathione reductase is inhibited by the antimalarial dye methylene blue. **FEBS Letters**, v. 422, n. 3, p. 311–314, 1998.

FEREIG, R. M. et al. Immunization with *Toxoplasma gondii* peroxiredoxin 1 induces protective immunity against toxoplasmosis in mice. **PLoS ONE**, v. 12, n. 4, p. 1–22, 27 abr. 2017. Disponível em: <<http://dx.doi.org/10.1371/journal.pone.0176324>>. Acesso em: 12 set. 2017.

FEREIG, R. M.; NISHIKAWA, Y. Peroxiredoxin 3 promotes IL-12 production from macrophages and partially protects mice against infection with *Toxoplasma gondii*. **Parasitology International**, v. 65, n. 6, p. 741–748, 1 dez. 2016. Disponível em: <<http://www.ncbi.nlm.nih.gov/pubmed/27644889>>. Acesso em: 12 set. 2017.

FEREIG, R. M.; NISHIKAWA, Y. From Signaling Pathways to Distinct Immune Responses: Key Factors for Establishing or Combating *Neospora caninum* Infection in Different Susceptible Hosts. **Pathogens**, v. 9, n. 5, p. 384, 16 maio 2020. Disponível em: <<https://www.mdpi.com/2076-0817/9/5/384>>. Acesso em: 10 jun. 2020.

FERNANDEZ-MARCOS, P. J.; NÓBREGA-PEREIRA, S. NADPH: new oxygen for the ROS theory of aging. **Oncotarget**, v. 7, n. 32, p. 50814, 1 ago. 2016. Disponível em: <[labs/pmc/articles/PMC5239434](https://pubmed.ncbi.nlm.nih.gov/27644889)>. Acesso em: 4 nov. 2021.

FERRARI, C. K. B. et al. Oxidative and nitrosative stress on phagocytes' function: From effective defense to immunity evasion mechanisms. **Archivum Immunologiae et Therapiae Experimentalis**, v. 59, n. 6, p. 441–448, dez. 2011. Disponível em: <<https://pubmed.ncbi.nlm.nih.gov/21972015/>>. Acesso em: 27 jul. 2020.

FİDAN, A. F. et al. The levels of antioxidant activity, malondialdehyde and nitric oxide in cows naturally infected with *Neospora caninum*. **Journal of Animal and Veterinary Advances**, v. 9, n. 12, p. 1707–1711, 2010. . Acesso em: 8 nov. 2021.

FINN, R. D. et al. The Pfam protein families database: towards a more sustainable future. **Nucleic Acids Research**, v. 44, n. D1, p. D279–D285, 4 jan. 2016. Disponível em: <<https://academic.oup.com/nar/article-lookup/doi/10.1093/nar/gkv1344>>. Acesso em: 23 jul. 2018.

FISHER, A. B. **The phospholipase A2 activity of peroxiredoxin 6** **Journal of Lipid Research** American Society for Biochemistry and Molecular Biology Inc., , 1 jul. 2018. . Disponível em: <<http://www.jlr.org>>. Acesso em: 16 set. 2020.

FOREMAN, J. et al. Reactive oxygen species produced by NADPH oxidase regulate plant cell growth. **Nature**, v. 422, n. 6930, p. 442–446, 27 mar. 2003. . Acesso em: 2 abr. 2020.

FUJII, J. et al. Unveiling the roles of the glutathione redox system in vivo by analyzing genetically modified mice. **Journal of clinical biochemistry and nutrition**, v. 49, n. 2, p. 70–78, set. 2011. Disponível em: <<https://pubmed.ncbi.nlm.nih.gov/21980221/>>. Acesso em: 2 nov. 2021.

GEISZT, M.; LETO, T. L. **The Nox family of NAD(P)H oxidases: Host defense and beyond***Journal of Biological Chemistry*American Society for Biochemistry and Molecular Biology, , 10 dez. 2004. . . Acesso em: 2 abr. 2020.

GHALMI, F. et al. Study of the risk factors associated with *Neospora caninum* seroprevalence in Algerian cattle populations. **Research in Veterinary Science**, v. 93, n. 2, p. 655–661, 1 out. 2012. . Acesso em: 11 jun. 2020.

GINSBURG, H. et al. Inhibition of glutathione-dependent degradation of heme by chloroquine and amodiaquine as a possible basis for their antimalarial mode of action. **Biochemical Pharmacology**, v. 56, n. 10, p. 1305–1313, 15 nov. 1998. Disponível em: <<https://pubmed.ncbi.nlm.nih.gov/9825729/>>. Acesso em: 26 jul. 2020.

GLOMBOWSKY, P. et al. Oxidative stress in dairy cows seropositives for *Neospora caninum*. **Comparative Immunology, Microbiology and Infectious Diseases**, v. 54, p. 34–37, 1 out. 2017a. . Acesso em: 28 out. 2021.

GLOMBOWSKY, P. et al. Oxidative stress in dairy cows seropositives for *Neospora caninum*. **Comparative Immunology, Microbiology and Infectious Diseases**, v. 54, p. 34–37, 1 out. 2017b. . Acesso em: 28 jul. 2021.

GONDIM, L. F. P. et al. Coyotes (*Canis latrans*) are definitive hosts of *Neospora caninum*. **International Journal for Parasitology**, v. 34, n. 2, p. 159–161, 1 fev. 2004a. . Acesso em: 10 jun. 2020.

GONDIM, L. F. P. et al. TRANSPLACENTAL TRANSMISSION AND ABORTION IN COWS ADMINISTERED NEOSPORA CANINUM OOCYSTS. **Journal of Parasitology**, v. 90, n. 6, p. 1394–1400, 1 dez. 2004b. . Acesso em: 10 jun. 2020.

GONDIM, L. S. Q. et al. *Toxoplasma gondii* and *Neospora caninum* in sparrows (*Passer domesticus*) in the Northeast of Brazil. **Veterinary Parasitology**, v. 168, n. 1–2, p. 121–124, 26 fev. 2010. . Acesso em: 10 jun. 2020.

GRANT, C. M.; DAWES, I. W. Synthesis and role of glutathione in protection against oxidative stress in yeast. **Redox Report**, v. 2, n. 4, p. 223–229, 13 ago. 1996. Disponível em: <<http://www.tandfonline.com/doi/full/10.1080/13510002.1996.11747054>>. Acesso em: 18 jun. 2018.

GUERRIERO, G. et al. Identification of the aquaporin gene family in *Cannabis sativa* and evidence for the accumulation of silicon in its tissues. **Plant Science**, v. 287, p. 110167, 1 out. 2019. . Acesso em: 28 jan. 2021.

GUEVARA-FLORES, A. et al. The Architecture of Thiol Antioxidant Systems among Invertebrate Parasites. **Molecules**, v. 22, n. 2, p. 259, 10 fev. 2017. Disponível em: <<http://www.mdpi.com/1420-3049/22/2/259>>. Acesso em: 18 jun. 2018.

GUPTA, A. et al. Fasciola gigantica thioredoxin glutathione reductase: Biochemical properties and structural modeling. **International Journal of Biological Macromolecules**, v. 89, p. 152–160, 1 ago. 2016. . Acesso em: 29 jan. 2021.

HAI, X. et al. Identification of 2-Cys Peroxiredoxin (BmTPx-2) as antioxidant active molecule from Babesia microti. **Frontiers in Microbiology**, v. 8, n. OCT, p. 1–7, 2017.

HAKIMI, H. et al. Cloning and characterization of Plasmodium vivax thioredoxin peroxidase-1. **Parasitology Research**, v. 111, n. 2, p. 525–529, 6 ago. 2012. Disponível em: <<http://link.springer.com/10.1007/s00436-012-2864-3>>. Acesso em: 1 jul. 2018.

HAKIMI, H. et al. Plasmodium vivax and Plasmodium knowlesi: Cloning, expression and functional analysis of 1-Cys peroxiredoxin. **Experimental Parasitology**, v. 133, n. 1, p. 101–105, 1 jan. 2013. Disponível em: <<https://www.sciencedirect.com/science/article/pii/S0014489412003293>>. Acesso em: 1 jul. 2018.

HASSAN, I. A. et al. Immunoglobulin and cytokine changes induced following immunization with a DNA vaccine encoding Toxoplasma gondii selenium-dependent glutathione reductase protein. **Experimental Parasitology**, v. 146, p. 1–10, 1 nov. 2014. Disponível em: <<https://www.sciencedirect.com/science/article/pii/S001448941400201X>>. Acesso em: 18 jun. 2018.

HECKER, Y. P. et al. Immune response and protection provided by live tachyzoites and native antigens from the NC-6 Argentina strain of Neospora caninum in pregnant heifers. **Veterinary Parasitology**, v. 197, n. 3–4, p. 436–446, 8 out. 2013. . Acesso em: 15 jun. 2020.

HECKER, Y. P. et al. A Neospora caninum vaccine using recombinant proteins fails to prevent foetal infection in pregnant cattle after experimental intravenous challenge. **Veterinary Immunology and Immunopathology**, v. 162, n. 3–4, p. 142–153, 15 dez. 2014. . Acesso em: 16 jun. 2020.

HEMPHILL, A.; AGUADO-MARTÍNEZ, A.; MÜLLER, J. Approaches for the vaccination and treatment of Neospora caninum infections in mice and ruminant models. **Parasitology**, v. 143, n. 03, p. 245–259, 2 mar. 2016. Disponível em: <http://www.journals.cambridge.org/abstract_S0031182015001596>. Acesso em: 3 fev. 2019.

HEO, L.; PARK, H.; SEOK, C. GalaxyRefine: Protein structure refinement driven by side-chain repacking. **Nucleic acids research**, v. 41, n. Web Server issue, p. W384–W388, 1 jul. 2013. Disponível em: <<http://galaxy.seoklab.>>. Acesso em: 28 jan. 2021.

HEO, S.; KIM, S.; KANG, D. The Role of Hydrogen Peroxide and Peroxiredoxins throughout the Cell Cycle. **Antioxidants**, v. 9, n. 4, p. 280, 26 mar. 2020. Disponível em: <<https://www.mdpi.com/2076-3921/9/4/280>>. Acesso em: 16 mar. 2021.

HERNANDEZ, J.; RISCO, C.; DONOVAN, A. Association between exposure to *Neospora caninum* and milk production in dairy cows. **Journal of the American Veterinary Medical Association**, v. 219, n. 5, p. 632–635, 1 set. 2001. . Acesso em: 14 jun. 2020.

HOBSON, J. C. et al. *Neospora caninum* serostatus and milk production of Holstein cattle. **Journal of the American Veterinary Medical Association**, v. 221, n. 8, p. 1160–1164, 15 out. 2002. . Acesso em: 14 jun. 2020.

HORCAJO, P. et al. Vaccines for bovine neosporosis: current status and key aspects for development. **Parasite Immunology**, v. 38, n. 12, p. 709–723, 1 dez. 2016. Disponível em: <<http://doi.wiley.com/10.1111/pim.12342>>. Acesso em: 18 jun. 2018.

IMRE, K. et al. Serological Survey of *Neospora caninum* Infection in Cattle Herds From Western Romania. **Journal of Parasitology**, v. 98, n. 3, p. 683–685, 1 jun. 2012. . Acesso em: 11 jun. 2020.

ISHII, T.; WARABI, E.; YANAGAWA, T. Novel roles of peroxiredoxins in inflammation, cancer and innate immunity. **Journal of clinical biochemistry and nutrition**, v. 50, n. 2, p. 91–105, mar. 2012. Disponível em: <<http://joi.jlc.jst.go.jp/JST.JSTAGE/jcbn/11-109?from=CrossRef>>. Acesso em: 25 jul. 2018.

JENKINS, M. C. et al. Serological investigation of an outbreak of *Neospora caninum*-associated abortion in a dairy herd in southeastern United States. **Veterinary Parasitology**, v. 94, n. 1–2, p. 17–26, 20 dez. 2000. . Acesso em: 14 jun. 2020.

JORTZIK, E.; BECKER, K. Thioredoxin and glutathione systems in *Plasmodium falciparum*. **International Journal of Medical Microbiology**, v. 302, n. 4–5, p. 187–194, out. 2012. Disponível em: <<http://www.ncbi.nlm.nih.gov/pubmed/22939033>>. Acesso em: 19 ago. 2018.

KASOZI, D. et al. Real-Time Imaging of the Intracellular Glutathione Redox Potential in the Malaria Parasite *Plasmodium falciparum*. **PLoS Pathogens**, v. 9, n. 12, p. 1–18, 2013. Disponível em: <<https://pubmed.ncbi.nlm.nih.gov/24348249/>>. Acesso em: 7 fev. 2021.

KAVISHE, R. A.; KOENDERINK, J. B.; ALIFRANGIS, M. Oxidative stress in malaria and artemisinin combination therapy: Pros and Cons. **FEBS Journal**, v. 284, n. 16, p. 2579–2591, 1 ago. 2017. Disponível em: <<https://pubmed.ncbi.nlm.nih.gov/28467668/>>. Acesso em: 27 jul. 2020.

KAWAI, S. et al. Effect of three types of mixed anesthetic agents alternate to ketamine in mice. **Experimental animals**, v. 60, n. 5, p. 481–7, 2011. Disponível em: <<http://www.ncbi.nlm.nih.gov/pubmed/22041285>>. Acesso em: 19 ago. 2018.

KAWAZU, S. et al. Molecular characterization of a 2-Cys peroxiredoxin from the human malaria parasite *Plasmodium falciparum*. **Mol Biochem Parasitol**, v. 116, n. 1, p. 73–79, 1 ago. 2001. Disponível em: <http://www.ncbi.nlm.nih.gov/entrez/query.fcgi?cmd=Retrieve&db=PubMed&dopt=Citation&list_uids=11463468>. Acesso em: 18 jun. 2018.

KAWAZU, S. et al. Expression profiles of peroxiredoxin proteins of the rodent malaria parasite *Plasmodium yoelii*. **International Journal for Parasitology**, v. 33, n. 13, p. 1455–1461, 1 nov. 2003. Disponível em: <<https://www.sciencedirect.com/science/article/pii/S002075190300184X>>. Acesso em: 1 jul. 2018.

KEHR, S. et al. Compartmentation of Redox Metabolism in Malaria Parasites. **PLoS Pathogens**, v. 6, n. 12, p. e1001242, 23 dez. 2010. Disponível em: <<http://dx.plos.org/10.1371/journal.ppat.1001242>>. Acesso em: 22 jul. 2018.

KHAN, A. et al. Neosporosis: An Overview of Its Molecular Epidemiology and Pathogenesis. **Engineering**, v. 6, n. 1, p. 10–19, 1 fev. 2020. . Acesso em: 28 out. 2021.

KIM, J. T. et al. In vitro antiprotozoal effects of artemisinin on *Neospora caninum*. **Veterinary Parasitology**, v. 103, n. 1–2, p. 53–63, 3 jan. 2002. . Acesso em: 15 jun. 2020.

KIM, Y.; JANG, H. H. The Role of Peroxiredoxin Family in Cancer Signaling. **Journal of Cancer Prevention**, v. 24, n. 2, p. 65, 30 jun. 2019. Disponível em: </labs/pmc/articles/PMC6619859/>. Acesso em: 4 nov. 2021.

KIMURA, R. et al. 2-Cys peroxiredoxin of *Plasmodium falciparum* is involved in resistance to heat stress of the parasite. **Parasitology International**, v. 62, n. 2, p. 137–143, 1 abr. 2013. . Acesso em: 4 nov. 2021.

KING, J. S. et al. Australian dingoes are definitive hosts of *Neospora caninum*. **International Journal for Parasitology**, v. 40, n. 8, p. 945–950, 1 jul. 2010. . Acesso em: 10 jun. 2020.

KLEIGER, G.; EISENBERG, D. GXXXG and GXXXA Motifs Stabilize FAD and NAD(P)-binding Rossmann Folds Through C α -H \cdots O Hydrogen Bonds and van der Waals Interactions. **Journal of Molecular Biology**, v. 323, n. 1, p. 69–76, 11 out. 2002. Disponível em: <<https://www.sciencedirect.com/science/article/pii/S0022283602008859>>. Acesso em: 17 ago. 2018.

KOIWAI, M. et al. Nationwide seroprevalence of *Neospora caninum* among dairy cattle in Japan. **Veterinary Parasitology**, v. 135, n. 2, p. 175–179, 30 jan. 2006. . Acesso em: 11 jun. 2020.

KONCAREVIC, S. et al. The malarial parasite *Plasmodium falciparum* imports the human protein peroxiredoxin 2 for peroxide detoxification. **Proceedings of the National Academy of Sciences of the United States of America**, v. 106, n. 32, p. 13323–13328, 11 ago. 2009. Disponível em: <<https://pubmed.ncbi.nlm.nih.gov/19666612/>>. Acesso em: 2 abr. 2020.

KRAFTS, K.; HEMPELMANN, E.; SKÓRSKA-STANIA, A. From methylene blue to chloroquine: a brief review of the development of an antimalarial therapy. **Parasitology Research**, v. 111, n. 1, p. 1–6, 13 jul. 2012. Disponível em: <<http://www.ncbi.nlm.nih.gov/pubmed/22411634>>. Acesso em: 3 fev. 2019.

KRITZNER, S. et al. An explorative study to assess the efficacy of Toltrazuril-sulfone (Ponazuril) in calves experimentally infected with *Neospora caninum*. **Annals of Clinical Microbiology and Antimicrobials** **2002** **1:1**, v. 1, n. 1, p. 1–10, 18 out. 2002. Disponível em: <<https://link.springer.com/articles/10.1186/1476-0711-1-4>>. Acesso em: 3 nov. 2021.

KRNAJSKI, Z. et al. Thioredoxin Reductase Is Essential for the Survival of *Plasmodium falciparum* Erythrocytic Stages. **Journal of Biological Chemistry**, v. 277, n. 29, p. 25970–25975, 19 jul. 2002. . Acesso em: 28 out. 2021.

KUNTZ, A. N. et al. Thioredoxin glutathione reductase from *Schistosoma mansoni*: An essential parasite enzyme and a key drug target. **PLoS Medicine**, v. 4, n. 6, p. 1071–1086, 2007.

LEI, X. G. et al. Paradoxical roles of antioxidant enzymes: Basic mechanisms and health implications. **Physiological Reviews**, v. 96, n. 1, p. 307–364, 16 dez. 2015. Disponível em: <www.prv.org>. Acesso em: 16 mar. 2021.

LI, W. et al. Identification and characterization of a microneme protein (NcMIC6) in *Neospora caninum*. **Parasitology Research** **2015** **114:8**, v. 114, n. 8, p. 2893–2902, 10 maio 2015. Disponível em: <<https://link.springer.com/article/10.1007/s00436-015-4490-3>>. Acesso em: 3 nov. 2021.

LILLIG, C. H.; BERNDT, C.; HOLMGREN, A. Glutaredoxin systems. **Biochimica et Biophysica Acta (BBA) - General Subjects**, v. 1780, n. 11, p. 1304–1317, 1 nov. 2008. . Acesso em: 4 nov. 2021.

LINDSAY, D. S. et al. Prevalence of *Neospora caninum* and *Toxoplasma gondii* Antibodies in Coyotes (*Canis latrans*) and Experimental Infections of Coyotes with *Neospora caninum*. **The Journal of Parasitology**, v. 82, n. 4, p. 657, ago. 1996. . Acesso em: 10 jun. 2020.

LINDSAY, D. S.; UPTON, S. J.; DUBEY, J. P. A structural study of the *Neospora caninum* oocyst. **International Journal for Parasitology**, v. 29, n. 10, p. 1521–1523, 1 out. 1999. . Acesso em: 4 nov. 2021.

LIU, Y.; REICHEL, M. P.; LO, W. C. Combined control evaluation for *Neospora caninum* infection in dairy: Economic point of view coupled with population dynamics. **Veterinary Parasitology**, v. 277, p. 108967, 1 jan. 2020. . Acesso em: 3 nov. 2021.

LLANO, H. A. B. et al. Seroprevalence and risk factors for *Neospora caninum* infection in cattle from the eastern Antioquia, Colombia. **Veterinary and Animal Science**, v. 6, p. 69–74, 1 dez. 2018. . Acesso em: 11 jun. 2020.

LÓPEZ-BAREA, J.; PINTO, M. C. Purification by Affinity Chromatography of Glutathione Reductase (EC 1.6.4.2) from *Escherichia Coli* and Characterization of Such Enzyme. **Zeitschrift fur Naturforschung - Section C Journal of Biosciences**, v. 39, n. 9–10, p. 908–915, 1 out. 1984. Disponível em: <<https://www.degruyter.com/document/doi/10.1515/znc-1984-9-1009/html>>. Acesso em: 10 maio. 2021.

LU, G. et al. Efficacy and safety of methylene blue in the treatment of malaria: a systematic review. **BMC Medicine**, v. 16, n. 1, p. 59, 25 dez. 2018. Disponível em: <<https://bmcmedicine.biomedcentral.com/articles/10.1186/s12916-018-1045-3>>. Acesso em: 3 fev. 2019.

LU, J.; HOLMGREN, A. The thioredoxin antioxidant system. **Free radical biology & medicine**, v. 66, p. 75–87, 8 jan. 2014. Disponível em: <<http://www.ncbi.nlm.nih.gov/pubmed/23899494>>. Acesso em: 26 jun. 2018.

MANDI, G. et al. Safety of the combination of chloroquine and methylene blue in healthy adult men with G6PD deficiency from rural Burkina Faso. **Tropical Medicine and International Health**, v. 10, n. 1, p. 32–38, 1 jan. 2005. Disponível em: <<http://doi.wiley.com/10.1111/j.1365-3156.2004.01356.x>>. Acesso em: 26 jul. 2020.

MANSILLA, F. C. et al. Dose-dependent immunogenicity of a soluble *Neospora caninum* tachyzoite-extract vaccine formulated with a soy lecithin/ β -glucan adjuvant in cattle. **Veterinary Parasitology**, v. 197, n. 1–2, p. 13–21, 18 out. 2013. . Acesso em: 15 jun. 2020.

MANSILLA, F. C. et al. Safety and immunogenicity of a soluble native *Neospora caninum* tachyzoite-extract vaccine formulated with a soy lecithin/ β -glucan adjuvant in pregnant cattle. **Veterinary Immunology and Immunopathology**, v. 165, n. 1–2, p. 75–80, 15 maio 2015. . Acesso em: 15 jun. 2020.

MARBÁN-CASTRO, E.; MATTAR, S.; GONZÁLEZ TOUS, M. Las zoonosis reemergentes bajo el enfoque de “Una salud.” **Revista MVZ Córdoba**, v. 18, n. 1, p. 7280–7284, 9 jul. 2019. . Acesso em: 11 jun. 2020.

MARSHALL, E. S. et al. *Toxoplasma gondii* peroxiredoxin promotes altered macrophage function, caspase-1-dependent IL-1 secretion enhances parasite replication. **Veterinary Research**, v. 42, n. 1, p. 1–9, 27 jun. 2011. Disponível em: <<https://link.springer.com/articles/10.1186/1297-9716-42-80>>. Acesso em: 14 jul. 2020.

MARUGÁN-HERNÁNDEZ, V. et al. Identification of novel rhoptry proteins in *Neospora caninum* by LC/MS-MS analysis of subcellular fractions. **Journal of Proteomics**, v. 74, n. 5, p. 629–642, 1 maio 2011. . Acesso em: 3 nov. 2021.

MARUGAN-HERNANDEZ, V. *Neospora caninum* and Bovine Neosporosis: Current Vaccine Research. **Journal of Comparative Pathology**, v. 157, n. 2–3, p. 193–200, 1 ago. 2017. Disponível em: <<https://pubmed.ncbi.nlm.nih.gov/28942304/>>. Acesso em: 27 jul. 2020.

MASATANI, T. et al. Identification and functional analysis of a novel mitochondria-localized 2-Cys peroxiredoxin, BbTPx-2, from *Babesia bovis*. **Parasitology Research**, v. 115, n. 8, p. 3139–3145, 19 ago. 2016. Disponível em: <<https://link.springer.com/content/pdf/10.1007%2Fs00436-016-5071-9.pdf>>. Acesso em: 1 jul. 2018.

MCALLISTER, M. M. et al. Dogs are definitive hosts of *Neospora caninum*. **International Journal for Parasitology**, v. 28, n. 9, p. 1473–1479, 1 set. 1998. . Acesso em: 10 jun. 2020.

MCALLISTER, M. M. et al. Evidence of point-source exposure to *Neospora caninum* and protective immunity in a herd of beef cows. **Journal of the American Veterinary Medical Association**, v. 217, n. 6, p. 881–887, 15 set. 2000. . Acesso em: 14 jun. 2020.

MCCARTY, S. E. et al. Plasmodium falciparum Thioredoxin Reductase (PfTrxR) and Its Role as a Target for New Antimalarial Discovery. **Molecules** **2015**, Vol. **20**, Pages **11459-11473**, v. 20, n. 6, p. 11459–11473, 22 jun. 2015. Disponível em: <<https://www.mdpi.com/1420-3049/20/6/11459/htm>>. Acesso em: 26 out. 2021.

MOEN, A. R. et al. Increased risk of abortion following *Neospora caninum* abortion outbreaks: A retrospective and prospective cohort study in four dairy herds. **Theriogenology**, v. 49, n. 7, p. 1301–1309, 1 maio 1998. . Acesso em: 14 jun. 2020.

MOHRING, F. et al. The Redox Systems of Plasmodium falciparum and Plasmodium vivax: Comparison, In silico Analyses and Inhibitor Studies. **Current Medicinal Chemistry**, v. 21, n. 15, p. 1728–1756, 5 abr. 2014. Disponível em: <<https://pubmed.ncbi.nlm.nih.gov/24304272/>>. Acesso em: 27 jul. 2020.

MORRIS, G. et al. The Glutathione System: A New Drug Target in Neuroimmune Disorders. **Molecular Neurobiology** **2014** **50:3**, v. 50, n. 3, p. 1059–1084, 22 abr. 2014. Disponível em: <<https://link.springer.com/article/10.1007/s12035-014-8705-x>>. Acesso em: 4 nov. 2021.

MOTA, C. M. et al. Interplay Between Reactive Oxygen Species and the Inflammasome Are Crucial for Restriction of *Neospora caninum* Replication. **Frontiers in Cellular and Infection Microbiology**, v. 0, p. 243, 25 maio 2020. . Acesso em: 24 out. 2021.

MÜLLER, J. et al. Two novel calcium-dependent protein kinase 1 inhibitors interfere with vertical transmission in mice infected with *Neospora caninum* tachyzoites. **Antimicrobial Agents and Chemotherapy**, v. 61, n. 4, 1 abr. 2017. Disponível em: <<https://doi.org/10.1128/AAC.02324-16>>. Acesso em: 7 out. 2020.

MÜLLER, J. et al. In Vitro Activities of MMV Malaria Box Compounds against the Apicomplexan Parasite *Neospora caninum*, the Causative Agent of Neosporosis in Animals. **Molecules**, v. 25, n. 6, p. 1460, 24 mar. 2020. Disponível em: <<https://www.mdpi.com/1420-3049/25/6/1460>>. Acesso em: 7 out. 2020.

MÜLLER, J.; HEMPHILL, A. Drug target identification in protozoan parasites. **Expert Opinion on Drug Discovery**, v. 11, n. 8, p. 815–824, 2 ago. 2016. Disponível em: <<http://www.ncbi.nlm.nih.gov/pubmed/27238605>>. Acesso em: 22 ago. 2019.

MÜLLER, O. et al. How worthwhile is methylene blue as a treatment of malaria? **Expert Review of Anti-Infective Therapy**, v. 17, n. 7, p. 471–473, 3 jul. 2019. Disponível em: <<https://www.tandfonline.com/action/journalInformation?journalCode=ierz20>>. Acesso em: 27 jul. 2020.

MÜLLER, S. et al. Thioredoxin and glutathione system of malaria parasite *Plasmodium falciparum*. **Protoplasma**, v. 217, n. 1–3, p. 43–9, 2001. Disponível em: <<http://www.ncbi.nlm.nih.gov/pubmed/11732337>>. Acesso em: 14 jan. 2019.

MÜLLER, S. et al. Thiol-based redox metabolism of protozoan parasites. **Trends in Parasitology**, v. 19, n. 7, p. 320–328, 1 jul. 2003. Disponível em: <<https://www.sciencedirect.com/science/article/pii/S1471492203001417>>. Acesso em: 27 ago. 2019.

MÜLLER, S. **Redox and antioxidant systems of the malaria parasite Plasmodium falciparum** *Molecular Microbiology* Mol Microbiol, , set. 2004. . Disponível em: <<https://pubmed.ncbi.nlm.nih.gov/15387810/>>. Acesso em: 14 jul. 2020.

MÜLLER, S. Role and Regulation of Glutathione Metabolism in *Plasmodium falciparum*. **Molecules**, v. 20, n. 6, p. 10511–10534, 8 jun. 2015. Disponível em: <<http://www.mdpi.com/1420-3049/20/6/10511>>. Acesso em: 2 abr. 2020.

MWANGI, V. I. et al. Methylene blue inhibits lumefantrine-resistant *Plasmodium berghei*. **The Journal of Infection in Developing Countries**, v. 10, n. 06, p. 635, 30 jun. 2016. Disponível em: <<http://www.ncbi.nlm.nih.gov/pubmed/27367013>>. Acesso em: 14 jan. 2019.

NAGULESWARAN, A. et al. Neospora caninum Microneme Protein NcMIC3: Secretion, Subcellular Localization, and Functional Involvement in Host Cell Interaction. **Infection and Immunity**, v. 69, n. 10, p. 6483–6494, 2001. Disponível em: <<https://journals.asm.org/doi/abs/10.1128/IAI.69.10.6483-6494.2001>>. Acesso em: 3 nov. 2021.

NAGULESWARAN, A. et al. Vero cell surface proteoglycan interaction with the microneme protein NcMIC3 mediates adhesion of *Neospora caninum* tachyzoites to host cells unlike that in *Toxoplasma gondii*. **International Journal for Parasitology**, v. 32, n. 6, p. 695–704, 1 jun. 2002. . Acesso em: 11 jun. 2020.

NAKAMURA, T. et al. Crystal structure of peroxiredoxin from *Aeropyrum pernix* K1 complexed with its substrate, hydrogen peroxide. **Journal of biochemistry**, v. 147, n. 1, p. 109–15, 1 jan. 2010. Disponível em: <<https://academic.oup.com/jb/article-lookup/doi/10.1093/jb/mvp154>>. Acesso em: 19 ago. 2018.

NAZIR, M. M. et al. Effects of Age and Breed on the Prevalence of *Neospora caninum* in Commercial Dairy Cattle from Pakistan . **Journal of Parasitology**, v. 99, n. 2, p. 368–370, 1 abr. 2013. . Acesso em: 11 jun. 2020.

NELSON, K. J. et al. Analysis of the peroxiredoxin family: Using active-site structure and sequence information for global classification and residue analysis. **Proteins: Structure, Function, and Bioinformatics**, v. 79, n. 3, p. 947–964, mar. 2011. Disponível em: <<http://www.ncbi.nlm.nih.gov/pubmed/21287625>>. Acesso em: 17 ago. 2018.

NEVERAUSKAS, C. E.; NASIR, A.; REICHEL, M. P. Prevalence and distribution of *Neospora caninum* in water buffalo (*Bubalus bubalis*) and cattle in the Northern Territory of Australia. **Parasitology International**, v. 64, n. 5, p. 392–396, 1 out. 2015. . Acesso em: 11 jun. 2020.

NICOLINO, R. R. et al. Estimating the abortion risk difference in *Neospora caninum* seropositive dairy cattle in Brazil. **Ciência Rural**, v. 45, n. 9, p. 1629–1633, 30 jun. 2015. Disponível em: <http://www.scielo.br/scielo.php?script=sci_arttext&pid=S0103-84782015000901629&lng=en&tlng=en>. Acesso em: 3 fev. 2019.

NIESEN, F. H.; BERGLUND, H.; VEDADI, M. The use of differential scanning fluorimetry to detect ligand interactions that promote protein stability. **Nature Protocols**, v. 2, n. 9, p. 2212–2221, 13 set. 2007. Disponível em: <<https://www.nature.com/articles/nprot.2007.321>>. Acesso em: 8 mar. 2021.

NISHIMURA, M. et al. Oligomannose-coated liposome-entrapped dense granule protein 7 induces protective immune response to *Neospora caninum* in cattle. **Vaccine**, v. 31, n. 35, p. 3528–3535, 2 ago. 2013. . Acesso em: 16 jun. 2020.

NOGUEIRA, N. P. et al. Proliferation and differentiation of *Trypanosoma cruzi* inside its vector have a new trigger: Redox status. **PLoS ONE**, v. 10, n. 2, 11 fev. 2015. . Acesso em: 2 abr. 2020.

NOICHR, Y. et al. In vivo parameters influencing 2-Cys Prx oligomerization: The role of enzyme sulfinylation. **Redox Biology**, v. 6, p. 326–333, 1 dez. 2015. Disponível em: <<https://www.sciencedirect.com/science/article/pii/S2213231715001019>>. Acesso em: 17 ago. 2018.

NORDBERG, J.; ARNÉR, E. S. J. Reactive oxygen species, antioxidants, and the mammalian thioredoxin system. **Free Radical Biology and Medicine**, v. 31, n. 11, p. 1287–1312, 1 dez. 2001. . Acesso em: 8 nov. 2021.

NORDHOFF, A. et al. Folding of the Four Domains and Dimerization Are Impaired by the Gly446→Glu Exchange in Human Glutathione Reductase. Implications for the Design of Antiparasitic Drugs. **Biochemistry**, v. 32, n. 15, p. 4060–4066, 1 abr. 1993. Disponível em: <<https://pubmed.ncbi.nlm.nih.gov/8097111/>>. Acesso em: 30 jan. 2021.

NOVAES, R. D.; TEIXEIRA, A. L.; DE MIRANDA, A. S. Oxidative stress in microbial diseases: Pathogen, host, and therapeutics. **Oxidative Medicine and Cellular Longevity**, v. 2019, p. 1–3, 2019. Disponível em: <<https://pubmed.ncbi.nlm.nih.gov/30774746/>>. Acesso em: 9 fev. 2021.

OHGURO, N. et al. Concentration dependent effects of hydrogen peroxide on lens epithelial cells. **British Journal of Ophthalmology**, v. 83, n. 9, p. 1064–1068, 1 set. 1999. Disponível em: <<https://bjo.bmj.com/content/83/9/1064>>. Acesso em: 22 jul. 2021.

OLIVEIRA, L. P. de. **Neospora caninum: estudo do secretoma e caracterização molecular de três proteínas com domínios Apple**. 2013. Biblioteca Digital de Teses e Dissertações da Universidade de São Paulo, Ribeirão Preto, 2013. Disponível em: <<http://www.teses.usp.br/teses/disponiveis/60/60135/tde-18122013-155545/>>. Acesso em: 18 jun. 2018.

OSTROVIDOV, S. et al. Effects of H₂O₂ on the growth, secretion, and metabolism of hybridoma cells in culture. **In vitro cellular & developmental biology. Animal**, v. 34, n. 3, p. 259–264, 1998. Disponível em: <<https://pubmed.ncbi.nlm.nih.gov/9557944/>>. Acesso em: 22 jul. 2021.

PADAYATTY, S. J. et al. Vitamin C as an Antioxidant: Evaluation of Its Role in Disease Prevention. **Journal of the American College of Nutrition**, v. 22, n. 1, p. 18–35, 1 fev. 2003. Disponível em: <<https://pubmed.ncbi.nlm.nih.gov/12569111/>>. Acesso em: 27 jul. 2020.

PADÍN-IRIZARRY, V. et al. Glutathione-deficient Plasmodium berghei parasites exhibit growth delay and nuclear DNA damage. **Free Radical Biology and Medicine**, v. 95, p. 43–54, 1 jun. 2016. Disponível em: <<https://www.sciencedirect.com/science/article/pii/S0891584916000915>>. Acesso em: 12 set. 2017.

PÁDUA, R. A. P. et al. ThermoFMN - A thermofluor assay developed for ligand-screening as an alternative strategy for drug discovery. **Journal of the Brazilian Chemical Society**, v. 25, n. 10, p. 1864–1871, 2014. Disponível em: <http://dx.doi.org/10.5935/0103-5053.20140157*>. Acesso em: 8 mar. 2021.

PAIVA, C. N.; BOZZA, M. T. Are reactive oxygen species always detrimental to pathogens? **Antioxidants and Redox Signaling**, v. 20, n. 6, p. 1000–1034, 20 fev. 2014. Disponível em: <<https://pubmed.ncbi.nlm.nih.gov/23992156/>>. Acesso em: 27 jul. 2020.

PAL, C.; BANDYOPADHYAY, U. Redox-active antiparasitic drugs. **Antioxidants and Redox Signaling**, v. 17, n. 4, p. 555–582, 15 ago. 2012. . Acesso em: 27 jul. 2020.

PARÉ, J.; THURMOND, M. C.; HIETALA, S. K. Congenital Neospora caninum infection in dairy cattle and associated calfhoo mortality. **Canadian Journal of Veterinary Research**, v. 60, n. 2, p. 133, 1996. . Acesso em: 10 jun. 2020.

PERCÁRIO, S. et al. Oxidative Stress in Malaria. **International Journal of Molecular Sciences 2012, Vol. 13, Pages 16346-16372**, v. 13, n. 12, p. 16346–16372, 3 dez. 2012. Disponível em: <<https://www.mdpi.com/1422-0067/13/12/16346/htm>>. Acesso em: 28 out. 2021.

PEREIRA, L. M. et al. A new thrombospondin-related anonymous protein homologue in Neospora caninum (NcMIC2-like1). **Parasitology**, v. 138, n. 03, p. 287–297, 30 mar. 2011. Disponível em: <http://www.journals.cambridge.org/abstract_S0031182010001290>. Acesso em: 7 ago. 2018.

PEREIRA, L. M. et al. Evaluation of methylene blue, pyrimethamine and its combination on an in vitro *Neospora caninum* model. **Parasitology**, v. 144, n. 06, p. 827–833, 11 maio 2017. Disponível em: <<http://www.ncbi.nlm.nih.gov/pubmed/28073383>>. Acesso em: 23 jul. 2018.

PEREIRA, L. M. et al. Synergic in vitro combinations of artemisinin, pyrimethamine and methylene blue against *Neospora caninum*. **Veterinary Parasitology**, v. 249, p. 92–97, 15 jan. 2018. Disponível em: <<https://pubmed.ncbi.nlm.nih.gov/29279093/>>. Acesso em: 2 abr. 2020.

PEREIRA, L. M. et al. Inhibitory action of phenothiazinium dyes against *Neospora caninum*. **Scientific Reports**, v. 10, n. 1, p. 1–13, 1 dez. 2020. . Acesso em: 7 jun. 2020.

PEREIRA, L. M.; YATSUDA, A. P. The chloramphenicol acetyltransferase vector as a tool for stable tagging of *Neospora caninum*. **Molecular and Biochemical Parasitology**, v. 196, n. 2, p. 75–81, 1 set. 2014. Disponível em: <<https://www.sciencedirect.com/science/article/pii/S0166685114000929>>. Acesso em: 3 fev. 2019.

PERKINS, A. et al. Peroxiredoxins: guardians against oxidative stress and modulators of peroxide signaling. **Trends in biochemical sciences**, v. 40, n. 8, p. 435–45, ago. 2015. Disponível em: <<http://linkinghub.elsevier.com/retrieve/pii/S0968000415000961>>. Acesso em: 19 ago. 2018.

PIACENZA, L. et al. **Trypanosoma cruzi antioxidant enzymes as virulence factors in chagas disease** *Antioxidants and Redox Signaling* Mary Ann Liebert, Inc. 140 Huguenot Street, 3rd Floor New Rochelle, NY 10801 USA , , 1 set. 2013. . Disponível em: <<https://www.liebertpub.com/doi/abs/10.1089/ars.2012.4618>>. Acesso em: 16 mar. 2021.

PIZZINO, G. et al. Oxidative Stress: Harms and Benefits for Human Health. **Oxid Med Cell Longev**, v. 2017, p. 1–13, 2017. Disponível em: <<https://doi.org/10.1155/2017/8416763>>. Acesso em: 27 jul. 2020.

POOLE, L. B.; NELSON, K. J. **Distribution and features of the six classes of peroxiredoxins** *Molecules and Cells* Korean Society for Molecular and Cellular Biology, , 2016. . Disponível em: <<https://pubmed.ncbi.nlm.nih.gov/27444444/>>. Acesso em: 16 mar. 2021.

POYNTON, R. A.; HAMPTON, M. B. Peroxiredoxins as biomarkers of oxidative stress. **Biochimica et Biophysica Acta (BBA) - General Subjects**, v. 1840, n. 2, p. 906–912, 1 fev. 2014a. Disponível em: <<https://www.sciencedirect.com/science/article/pii/S0304416513003450?via%3DIihub>>. Acesso em: 2 nov. 2019.

POYNTON, R. A.; HAMPTON, M. B. Peroxiredoxins as biomarkers of oxidative stress. **Biochimica et Biophysica Acta (BBA) - General Subjects**, v. 1840, n. 2, p. 906–912, 1 fev. 2014b. . Acesso em: 6 out. 2021.

PRIYATHILAKA, T. T. et al. Identification and molecular characterization of peroxiredoxin 6 from Japanese eel (*Anguilla japonica*) revealing its potent antioxidant properties and putative

immune relevancy. **Fish and Shellfish Immunology**, v. 51, p. 291–302, 1 abr. 2016. . Acesso em: 16 mar. 2021.

PUSHPAMALI, W. A. et al. Comparative study of two thioredoxin peroxidases from disk abalone (*Haliotis discus discus*): Cloning, recombinant protein purification, characterization of antioxidant activities and expression analysis. **Fish & Shellfish Immunology**, v. 24, n. 3, p. 294–307, 1 mar. 2008. Disponível em: <<https://www.sciencedirect.com/science/article/pii/S1050464807002070>>. Acesso em: 6 nov. 2018.

QIAN, W. et al. Activity of several kinds of drugs against *Neospora caninum*. **Parasitology International**, v. 64, n. 6, p. 597–602, 1 dez. 2015. . Acesso em: 14 jun. 2020.

QUINN, J. et al. Distinct Regulatory Proteins Control the Graded Transcriptional Response to Increasing H₂O₂ Levels in Fission Yeast *Schizosaccharomyces pombe*. <https://doi.org/10.1091/mbc.01-06-0288>, v. 13, n. 3, p. 805–816, 7 mar. 2002. Disponível em: <<https://www.molbiolcell.org/doi/abs/10.1091/mbc.01-06-0288>>. Acesso em: 24 out. 2021.

R. BUETTNER, G. Superoxide Dismutase in Redox Biology: The Roles of Superoxide and Hydrogen Peroxide. **Anti-Cancer Agents in Medicinal Chemistry**, v. 11, n. 4, p. 341–346, 3 nov. 2012. . Acesso em: 16 mar. 2021.

RAHBAR, M. R. et al. Pierce into the Native Structure of Ata, a Trimeric Autotransporter of *Acinetobacter baumannii* ATCC 17978. **International Journal of Peptide Research and Therapeutics**, v. 26, n. 3, p. 1269–1282, 1 set. 2020. Disponível em: <<https://doi.org/10.1007/s10989-019-09920-5>>. Acesso em: 28 jan. 2021.

REICHEL, M. P. et al. What is the global economic impact of *Neospora caninum* in cattle - The billion dollar question. **International Journal for Parasitology**, v. 43, n. 2, p. 133–142, 1 fev. 2013. . Acesso em: 8 set. 2020.

REICHEL, M. P. et al. Control options for *Neospora caninum* – is there anything new or are we going backwards? **Parasitology**, v. 141, n. 11, p. 1455–1470, 25 set. 2014. Disponível em: <http://www.journals.cambridge.org/abstract_S0031182014000158>. Acesso em: 18 jun. 2018.

RESCIGNO, M.; PERHAM, R. N. Structure of the NADPH-Binding Motif of Glutathione Reductase: Efficiency Determined by Evolution. **Biochemistry**, v. 33, n. 19, p. 5721–5727, 1 maio 1994. Disponível em: <<https://pubmed.ncbi.nlm.nih.gov/8180198/>>. Acesso em: 28 jan. 2021.

RHEE, S. G. et al. Peroxiredoxin, a Novel Family of Peroxidases. **IUBMB Life (International Union of Biochemistry and Molecular Biology: Life)**, v. 52, n. 1, p. 35–41, 1 jul. 2001. Disponível em: <<http://doi.wiley.com/10.1080/15216540252774748>>. Acesso em: 16 mar. 2021.

RHEE, S. G. et al. Peroxiredoxin Functions as a Peroxidase and a Regulator and Sensor of Local Peroxides *. **Journal of Biological Chemistry**, v. 287, n. 7, p. 4403–4410, 1 fev. 2012a. Disponível em: <<http://www.jbc.org/article/S0021925820480962/fulltext>>. Acesso em: 30 set. 2021.

RHEE, S. G. et al. **Peroxiredoxin functions as a peroxidase and a regulator and sensor of local peroxides** **Journal of Biological Chemistry** Elsevier, , 10 fev. 2012b. . . Acesso em: 16 mar. 2021.

RHEE, S. G.; CHAE, H. Z.; KIM, K. Peroxiredoxins: A historical overview and speculative preview of novel mechanisms and emerging concepts in cell signaling. 2005. Disponível em: <https://ac.els-cdn.com/S0891584905000985/1-s2.0-S0891584905000985-main.pdf?_tid=272c34f6-c338-4921-881a-65ab7d843cd7&acdnat=1530135647_3a6321900557512dc18834af8161b634>. Acesso em: 26 jun. 2018.

RHEE, S. G.; WOO, H. A. **Multiple functions of 2-Cys peroxiredoxins, I and II, and their regulations via post-translational modifications** **Free Radical Biology and Medicine** Elsevier Inc., , 20 maio 2020. . . Acesso em: 16 mar. 2021.

RHEE, S. Goo. Overview on Peroxiredoxin. **Molecules and Cells**, v. 39, n. 1, p. 1–5, 31 jan. 2016. Disponível em: <<http://www.ncbi.nlm.nih.gov/pubmed/26831451>>. Acesso em: 25 jul. 2018.

RIETVELD, P. et al. Reductive and oxidative half-reactions of glutathione reductase from *Escherichia coli*. **Biochemistry**, v. 33, n. 46, p. 13888–95, 22 nov. 1994. Disponível em: <<http://www.ncbi.nlm.nih.gov/pubmed/7947797>>. Acesso em: 18 jul. 2018.

ROBERT, X.; GOUET, P. Deciphering key features in protein structures with the new ENDscript server. **Nucleic Acids Research**, v. 42, 2014. Disponível em: <<http://escript.ibcp.fr>>. Acesso em: 28 jul. 2020.

ROMERO, J. J.; PÉREZ, E.; FRANKENA, K. Effect of a killed whole *Neospora caninum* tachyzoite vaccine on the crude abortion rate of Costa Rican dairy cows under field conditions. **Veterinary Parasitology**, v. 123, n. 3–4, p. 149–159, 2 set. 2004. . Acesso em: 16 jun. 2020.

SABLINA, A. A. et al. The antioxidant function of the p53 tumor suppressor. **Nature Medicine** **2005** **11:12**, v. 11, n. 12, p. 1306–1313, 13 nov. 2005. Disponível em: <<https://www.nature.com/articles/nm1320>>. Acesso em: 24 out. 2021.

SAJIB, A. A. et al. Interaction of rs316019 variants of SLC22A2 with metformin and other drugs- an in silico analysis. **Journal of Genetic Engineering and Biotechnology**, v. 16, n. 2, p. 769–775, 1 dez. 2018. . Acesso em: 28 jan. 2021.

ŠALI, A.; BLUNDELL, T. L. Comparative protein modelling by satisfaction of spatial restraints. **Journal of Molecular Biology**, v. 234, n. 3, p. 779–815, 5 dez. 1993. Disponível em: <<https://pubmed.ncbi.nlm.nih.gov/8254673/>>. Acesso em: 28 jul. 2020.

SÁNCHEZ-SÁNCHEZ, R. et al. Treatment of Toxoplasmosis and Neosporosis in Farm Ruminants: State of Knowledge and Future Trends. **Current Topics in Medicinal Chemistry**, v. 18, n. 15, p. 1304–1323, 2 out. 2018. Disponível em: <<https://pubmed.ncbi.nlm.nih.gov/30277158/>>. Acesso em: 27 jul. 2020.

SARMA, G. N. N. et al. Glutathione reductase of the malarial parasite Plasmodium falciparum: Crystal structure and inhibitor development. **Journal of Molecular Biology**, v. 328, n. 4, p. 893–907, 9 maio 2003. Disponível em: <<https://www.sciencedirect.com/science/article/pii/S0022283603003474>>. Acesso em: 18 jun. 2018.

SAURI, H. et al. Antioxidant function of recombinant human natural killer enhancing factor. **Biochemical and biophysical research communications**, v. 208, n. 3, p. 964–9, 28 mar. 1995. Disponível em: <<http://www.ncbi.nlm.nih.gov/pubmed/7702627>>. Acesso em: 1 jul. 2018.

SCHARES, G. et al. The efficiency of vertical transmission of Neospora caninum in dairy cattle analysed by serological techniques. **Veterinary Parasitology**, v. 80, n. 2, p. 87–98, 31 dez. 1998. . Acesso em: 10 jun. 2020.

SCHARES, G.; CONRATHS, F. J.; REICHEL, M. P. Bovine neosporosis: Comparison of serological methods using outbreak sera from a dairy herd in New Zealand. **International Journal for Parasitology**, v. 29, n. 10, p. 1659–1667, 1 out. 1999. . Acesso em: 14 jun. 2020.

SCHIRMER, R. H. et al. Methylene blue as an antimalarial agent. **Redox Report**, v. 8, n. 5, p. 272–275, 19 out. 2003. Disponível em: <<https://pubmed.ncbi.nlm.nih.gov/14962363/>>. Acesso em: 3 fev. 2019.

SCHIRMER, R. H. et al. “Lest we forget you - methylene blue...” **Neurobiology of Aging**, v. 32, n. 12, p. 2325.e7-2325.e16, 2011. Disponível em: <<https://pubmed.ncbi.nlm.nih.gov/21316815/>>. Acesso em: 27 jul. 2020.

SCHULZ, G. E. et al. The structure of the flavoenzyme glutathione reductase. **Nature**, v. 273, n. 5658, p. 120–124, 11 maio 1978. Disponível em: <<http://www.nature.com/doifinder/10.1038/273120a0>>. Acesso em: 16 jul. 2018.

SCRUTTON, N. S.; BERRY, A.; PERHAM, R. N. Purification and characterization of glutathione reductase encoded by a cloned and over-expressed gene in Escherichia coli. **The Biochemical journal**, v. 245, n. 3, p. 875–80, 1 ago. 1987. Disponível em: <<http://www.ncbi.nlm.nih.gov/pubmed/3311037>>. Acesso em: 18 jun. 2018.

SEAVER, L. C.; IMLAY, J. A. Alkyl hydroperoxide reductase is the primary scavenger of endogenous hydrogen peroxide in Escherichia coli. **Journal of bacteriology**, v. 183, n. 24, p. 7173–81, 15 dez. 2001. Disponível em: <<http://www.ncbi.nlm.nih.gov/pubmed/11717276>>. Acesso em: 27 jun. 2018.

SEMANGO, G. et al. The Sero-epidemiology of *Neospora caninum* in Cattle in Northern Tanzania. **Frontiers in Veterinary Science**, v. 6, n. SEP, p. 327, 26 set. 2019. Disponível em: <<https://www.frontiersin.org/article/10.3389/fvets.2019.00327/full>>. Acesso em: 11 jun. 2020.

SEN, A. et al. The 29-kilodalton thiol-dependent peroxidase of *Entamoeba histolytica* is a factor involved in pathogenesis and survival of the parasite during oxidative stress. **Eukaryotic cell**, v. 6, n. 4, p. 664–73, abr. 2007. Disponível em: <<http://www.ncbi.nlm.nih.gov/pubmed/17307964>>. Acesso em: 2 abr. 2020.

SHRESTHA, S. P. et al. Proliferation of *Toxoplasma gondii* in inflammatory macrophages in vivo is associated with diminished oxygen radical production in the host cell. **International Journal for Parasitology**, v. 36, n. 4, p. 433–441, 1 abr. 2006. . Acesso em: 28 jul. 2021.

SIEMS, W.; SOMMERBURG, O.; GRUNE, T. Erythrocyte free radical and energy metabolism. **Clinical Nephrology**, v. 53, n. 1 Suppl, p. S9-17, 1 fev. 2000. Disponível em: <<https://europepmc.org/article/med/10746800>>. Acesso em: 20 jul. 2021.

SIES, H. Oxidative stress: oxidants and antioxidants. **Experimental Physiology**, v. 82, n. 2, p. 291–295, 1 mar. 1997. Disponível em: <<https://onlinelibrary.wiley.com/doi/full/10.1113/expphysiol.1997.sp004024>>. Acesso em: 4 nov. 2021.

SIKANYIKA, M. et al. The structure and activity of the glutathione reductase from *Streptococcus pneumoniae*. **Acta Crystallographica Section F: Structural Biology Communications**, v. 75, n. 1, p. 54–61, 1 jan. 2019. Disponível em: <<http://scripts.iucr.org/cgi-bin/paper?cb5109>>. Acesso em: 10 maio. 2021.

SOBOTTA, M. C. et al. Peroxiredoxin-2 and STAT3 form a redox relay for H₂O₂ signaling. **Nature Chemical Biology** 2014 11:1, v. 11, n. 1, p. 64–70, 24 nov. 2014. Disponível em: <<https://www.nature.com/articles/nchembio.1695>>. Acesso em: 19 out. 2021.

SOHN, C. S. et al. Identification of novel proteins in *Neospora caninum* using an organelle purification and monoclonal antibody approach. **PloS one**, v. 6, n. 4, p. e18383, 4 abr. 2011. Disponível em: <<http://www.ncbi.nlm.nih.gov/pubmed/21483743>>. Acesso em: 1 jul. 2018.

SOITO, L. et al. PREX: PeroxiRedoxin classification indEX, a database of subfamily assignments across the diverse peroxiredoxin family. **Nucleic Acids Research**, v. 39, n. SUPPL. 1, p. D332–D337, 1 jan. 2011. Disponível em: <<http://peroxibase.toulouse.inra.fr/>>. Acesso em: 16 mar. 2021.

SOLDATI, D.; DUBREMETZ, J. F.; LEBRUN, M. **Microneme proteins: Structural and functional requirements to promote adhesion and invasion by the apicomplexan parasite *Toxoplasma gondii*** *International Journal for Parasitology* Pergamon, , 1 out. 2001. . . Acesso em: 7 mar. 2020.

SON, E. S. et al. Molecular cloning and characterization of peroxiredoxin from *Toxoplasma gondii*. **The Korean journal of parasitology**, v. 39, n. 2, p. 133–141, 2001. Disponível em: <<https://pubmed.ncbi.nlm.nih.gov/11511111/>>. Acesso em: 14 jul. 2020.

SONG, L. et al. Thioredoxin Glutathione Reductase as a Novel Drug Target: Evidence from *Schistosoma japonicum*. **PLoS ONE**, v. 7, n. 2, p. e31456, 22 fev. 2012. Disponível em: <<https://dx.plos.org/10.1371/journal.pone.0031456>>. Acesso em: 29 jan. 2021.

SONG, X. et al. Glutaredoxin 1 Deficiency Leads to Microneme Protein-Mediated Growth Defects in *Neospora caninum*. **Frontiers in Microbiology**, v. 0, p. 2152, 31 ago. 2020. . Acesso em: 28 out. 2021.

SONG, X. et al. Identification and Function of Apicoplast Glutaredoxins in *Neospora caninum*. **International Journal of Molecular Sciences** **2021**, Vol. **22**, Page **11946**, v. 22, n. 21, p. 11946, 4 nov. 2021. Disponível em: <<https://www.mdpi.com/1422-0067/22/21/11946/htm>>. Acesso em: 8 nov. 2021.

SORDILLO, L. M.; AITKEN, S. L. Impact of oxidative stress on the health and immune function of dairy cattle. **Veterinary Immunology and Immunopathology**, v. 128, n. 1–3, p. 104–109, 15 mar. 2009. . Acesso em: 8 nov. 2021.

SUSSMANN, R. A. C. et al. *Plasmodium falciparum* uses vitamin e to avoid oxidative stress. **Parasites and Vectors**, v. 10, n. 1, 10 out. 2017. Disponível em: <<https://pubmed.ncbi.nlm.nih.gov/29017543/>>. Acesso em: 27 jul. 2020.

SUZUKI, Y.; FORMAN, H.; SEVANIAN, A. Oxidants as stimulators of signal transduction. **Free radical biology & medicine**, v. 22, n. 1–2, p. 269–285, 1997. Disponível em: <<https://pubmed.ncbi.nlm.nih.gov/8958153/>>. Acesso em: 22 jul. 2021.

SYED-HUSSAIN, S. S. et al. Study on the use of toltrazuril to eliminate *Neospora caninum* in congenitally infected lambs born from experimentally infected ewes. **Veterinary Parasitology**, v. 210, n. 3–4, p. 141–144, 15 jun. 2015. . Acesso em: 14 jun. 2020.

SZEWCZYK-GOLEC, K. et al. Oxidative Stress as a Possible Target in the Treatment of Toxoplasmosis: Perspectives and Ambiguities. **International Journal of Molecular Sciences** **2021**, Vol. **22**, Page **5705**, v. 22, n. 11, p. 5705, 27 maio 2021. Disponível em: <<https://www.mdpi.com/1422-0067/22/11/5705/htm>>. Acesso em: 28 out. 2021.

TANAKA, M. et al. Cloning and characterization of peroxiredoxin in *Babesia bovis*. **Parasitology Research**, v. 105, n. 5, p. 1473–1477, 13 out. 2009. Disponível em: <<http://link.springer.com/10.1007/s00436-009-1587-6>>. Acesso em: 1 jul. 2018.

TEIXEIRA, F. et al. Chaperone activation and client binding of a 2-cysteine peroxiredoxin. **Nature Communications**, v. 10, n. 1, p. 659, 8 dez. 2019. Disponível em: <<http://www.ncbi.nlm.nih.gov/pubmed/30737390>>. Acesso em: 5 maio. 2019.

THURMOND, M. C.; HIETALA, S. K. Culling associated with *Neospora caninum* infection in dairy cows. **American Journal of Veterinary Research**, v. 57, n. 11, p. 1559–1562, 1 nov. 1996. . Acesso em: 14 jun. 2020.

TONIN, A. A. et al. Oxidative Stress in Brain Tissue of Gerbils Experimentally Infected with *Neospora caninum*. **Journal of Parasitology**, v. 100, n. 1, p. 154–156, 1 fev. 2014a. . Acesso em: 28 out. 2021.

TONIN, A. A. et al. Oxidative Stress in Brain Tissue of Gerbils Experimentally Infected with *Neospora caninum*. **Journal of Parasitology**, v. 100, n. 1, p. 154–156, 1 fev. 2014b. . Acesso em: 28 jul. 2021.

TONIN, A. A. et al. Serum levels of nitric oxide and protein oxidation in goats seropositive for *Toxoplasma gondii* and *Neospora caninum*. **Comparative Immunology, Microbiology and Infectious Diseases**, v. 41, p. 55–58, 1 ago. 2015. . Acesso em: 8 nov. 2021.

TRANAS, J. et al. Serological Evidence of Human Infection with the Protozoan *Neospora caninum*. **Clinical Diagnostic Laboratory Immunology**, v. 6, n. 5, p. 765–767, 1999. Disponível em: <<https://journals.asm.org/doi/abs/10.1128/CDLI.6.5.765-767.1999>>. Acesso em: 2 nov. 2021.

TREES, A. J.; WILLIAMS, D. J. L. Endogenous and exogenous transplacental infection in *Neospora caninum* and *Toxoplasma gondii*. **Trends in Parasitology**, v. 21, n. 12, p. 558–561, 1 dez. 2005. . Acesso em: 10 jun. 2020.

UGGLA, A. et al. Oral *Neospora caninum* inoculation of neonatal calves. **International Journal for Parasitology**, v. 28, n. 9, p. 1467–1472, 1 set. 1998. . Acesso em: 10 jun. 2020.

VANLEEUEWEN, J. A. et al. Monensin use against *Neospora caninum* challenge in dairy cattle. **Veterinary Parasitology**, v. 175, n. 3–4, p. 372–376, 10 fev. 2011. . Acesso em: 14 jun. 2020.

VEAL, E. A.; DAY, A. M.; MORGAN, B. A. Hydrogen Peroxide Sensing and Signaling. **Molecular Cell**, v. 26, n. 1, p. 1–14, 13 abr. 2007. . Acesso em: 24 out. 2021.

VENANCIO-BROCHI, J. C. et al. Glutathione reductase: A cytoplasmic antioxidant enzyme and a potential target for phenothiazinium dyes in *Neospora caninum*. **International Journal of Biological Macromolecules**, v. 187, p. 964–975, 30 set. 2021. . Acesso em: 6 out. 2021.

VENNERSTROM, J. L. et al. Antimalarial dyes revisited: xanthenes, azines, oxazines, and thiazines. **Antimicrobial agents and chemotherapy**, v. 39, n. 12, p. 2671–7, 1 dez. 1995. Disponível em: <<http://www.ncbi.nlm.nih.gov/pubmed/8593000>>. Acesso em: 14 jan. 2019.

VIANNA, M. C. B. et al. Isolation of *Neospora caninum* from naturally infected white-tailed deer (*Odocoileus virginianus*). **Veterinary Parasitology**, v. 129, n. 3–4, p. 253–257, 15 maio 2005. . Acesso em: 10 jun. 2020.

VONLAUFEN, N. et al. Exogenous nitric oxide triggers *Neospora caninum* tachyzoite-to-bradyzoite stage conversion in murine epidermal keratinocyte cell cultures. **International Journal for Parasitology**, v. 32, n. 10, p. 1253–1265, 1 set. 2002. . Acesso em: 8 nov. 2021.

WAINWRIGHT, M. Methylene blue derivatives--suitable photoantimicrobials for blood product disinfection? **International journal of antimicrobial agents**, v. 16, n. 4, p. 381–94, dez. 2000. Disponível em: <<http://www.ncbi.nlm.nih.gov/pubmed/11118846>>. Acesso em: 3 fev. 2019.

WAINWRIGHT, M.; AMARAL, L. Review: The phenothiazinium chromophore and the evolution of antimalarial drugs. **Tropical Medicine and International Health**, v. 10, n. 6, p. 501–511, 1 jun. 2005. Disponível em: <<http://doi.wiley.com/10.1111/j.1365-3156.2005.01417.x>>. Acesso em: 3 fev. 2019.

WALDNER, C. L. et al. Outbreak of abortion associated with *Neospora caninum* infection in a beef herd. **Journal of the American Veterinary Medical Association**, v. 215, n. 10, p. 1485–90, 1448, 1 nov. 1999. . Acesso em: 14 jun. 2020.

WANG, X. et al. Microneme Protein 6 Is Involved in Invasion and Egress by *Neospora caninum*. **Pathogens 2021, Vol. 10, Page 201**, v. 10, n. 2, p. 201, 13 fev. 2021. Disponível em: <<https://www.mdpi.com/2076-0817/10/2/201/htm>>. Acesso em: 3 nov. 2021.

WANG, Y. et al. **Superoxide dismutases: Dual roles in controlling ROS damage and regulating ROS signaling** **Journal of Cell Biology** Rockefeller University Press, , 1 jun. 2018. . Disponível em: <<https://pubmed.ncbi.nlm.nih.gov/29669742/>>. Acesso em: 15 jul. 2020.

WEBER, F. H. et al. On the efficacy and safety of vaccination with live tachyzoites of *Neospora caninum* for prevention of *Neospora*-associated fetal loss in cattle. **Clinical and Vaccine Immunology**, v. 20, n. 1, p. 99–105, 1 jan. 2013. . Acesso em: 15 jun. 2020.

WEIDINGER, A.; KOZLOV, A. Biological Activities of Reactive Oxygen and Nitrogen Species: Oxidative Stress versus Signal Transduction. **Biomolecules**, v. 5, n. 2, p. 472–484, 15 abr. 2015. Disponível em: <<http://www.ncbi.nlm.nih.gov/pubmed/25884116>>. Acesso em: 18 jun. 2018.

WESTON, J. F.; HEUER, C.; WILLIAMSON, N. B. Efficacy of a *Neospora caninum* killed tachyzoite vaccine in preventing abortion and vertical transmission in dairy cattle. **Preventive veterinary medicine**, v. 103, n. 2–3, p. 136–44, 1 fev. 2012. Disponível em: <<http://www.ncbi.nlm.nih.gov/pubmed/21925752>>. Acesso em: 16 jun. 2020.

WEZENA, C. A. et al. Growth inhibitory effects of standard pro- and antioxidants on the human malaria parasite *Plasmodium falciparum*. **Experimental Parasitology**, v. 180, p. 64–70, 1 set. 2017. . Acesso em: 2 abr. 2020.

WILLIAMS, C. J. et al. MolProbity: More and better reference data for improved all-atom structure validation. **Protein Science**, v. 27, n. 1, p. 293–315, 1 jan. 2018. Disponível em: <pmc/articles/PMC5734394/?report=abstract>. Acesso em: 28 jul. 2020.

WILSON, D. J. et al. Neospora caninum is the leading cause of bovine fetal loss in British Columbia, Canada. **Veterinary Parasitology**, v. 218, p. 46–51, 15 mar. 2016. . Acesso em: 11 jun. 2020.

WOOD, Z. et al. Structure, mechanism, and regulation of peroxiredoxins. **Trends Biochemistry Science**, v. 28, n. 1, p. 32–40, jan. 2003. Disponível em: <<http://www.ncbi.nlm.nih.gov/pubmed/12517450>>. Acesso em: 18 jun. 2018.

WOOD, Z. A. et al. Dimers to doughnuts: redox-sensitive oligomerization of 2-cysteine peroxiredoxins. **Biochemistry**, v. 41, n. 17, p. 5493–504, 30 abr. 2002. Disponível em: <<http://www.ncbi.nlm.nih.gov/pubmed/11969410>>. Acesso em: 26 jun. 2018.

XIAO, Z. et al. Molecular Mechanisms of Glutaredoxin Enzymes: Versatile Hubs for Thiol–Disulfide Exchange between Protein Thiols and Glutathione. **Journal of Molecular Biology**, v. 431, n. 2, p. 158–177, 18 jan. 2019. . Acesso em: 4 nov. 2021.

XIE, S. C.; RALPH, S. A.; TILLEY, L. K13, the Cytostome, and Artemisinin Resistance. **Trends in Parasitology**, v. 36, n. 6, p. 533–544, 1 jun. 2020. . Acesso em: 27 jul. 2020.

XUE, J. et al. Thioredoxin reductase from *Toxoplasma gondii*: An essential virulence effector with antioxidant function. **FASEB Journal**, v. 31, n. 10, p. 4447–4457, 2017.

ZHANG, L. bin; FENG, M. G. **Antioxidant enzymes and their contributions to biological control potential of fungal insect pathogens** *Applied Microbiology and Biotechnology* Springer Verlag, , 1 jun. 2018. . Disponível em: <<https://doi.org/10.1007/s00253-018-9033-2>>. Acesso em: 16 mar. 2021.

6. ANEXO

ANEXO A – Autorização do Comitê de Ética no Uso de Animais.



UNIVERSIDADE DE SÃO PAULO
Faculdade de Ciências Farmacêuticas de Ribeirão Preto
COMISSÃO DE ÉTICA NO USO DE ANIMAIS

AUTORIZAÇÃO

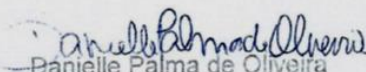
Certificamos que a proposta intitulada "Controle redox em *Neospora caninum*: investigação de enzimas do sistema antioxidante", registrada sob nº 17.5.278.60.8, sob a responsabilidade de Jade Cabestre Verancio e Ana Patricia Yatsuda Natsui, que envolve a manutenção e utilização de animais pertencentes ao filo Chordata, subfilo Vertebrata (exceto o homem) para fins de pesquisa científica encontra-se de acordo com os preceitos da Lei nº 11.794, de 8 de outubro de 2008, do Decreto nº 6.899, de 15 de julho de 2009, e com as normas editadas pelo Conselho Nacional de Controle da Experimentação Animal (CONCEA), foi aprovada *ad referendum* em 14/03/2018 pela Comissão de Ética no Uso de Animais da Faculdade de Ciências Farmacêuticas de Ribeirão Preto (CEUA FCFRP).

Lembramos da obrigatoriedade de apresentação do relatório de atividades, em modelo da CEUA, para emissão do certificado como disposto nas Resoluções Normativas do CONCEA.

Colaborador: Luiz Miguel Pereira.

Finalidade	() Ensino (x) Pesquisa Científica
Vigência da Autorização	03/04/2018 a 19/11/2018
Espécie/Linhagem/Raça	Camundongo isogênico BALB/c
Nº de animais	40
Sexo	Macho
Peso/Idade	20-30g/ 6-8 semanas
Origem	Biotério I da FCFRP.

Ribeirão Preto, 21 de maio de 2018.


Danielle Palma de Oliveira
Vice-Coordenador da CEUA-FCFRP

